

RCA REVIEW

a technical journal

**RADIO AND ELECTRONICS
RESEARCH • ENGINEERING**

VOLUME XVII

MARCH 1956

NO. 1

RADIO CORPORATION OF AMERICA

DAVID SARNOFF, *Chairman of the Board*

FRANK M. FOLSOM, *President*

E. W. ENGSTROM, *Senior Executive Vice President*

JOHN Q. CANNON, *Secretary*

ERNEST B. GORIN, *Vice President and Treasurer*

RCA LABORATORIES

D. H. EWING, *Vice President*

RCA REVIEW

C. C. FOSTER, *Manager*

CHARLES H. VOSE, *Business Manager*

PRINTED IN U.S.A.

RCA REVIEW, published quarterly in March, June, September, and December by RCA Laboratories, Radio Corporation of America, Princeton, New Jersey. Entered as second class matter July 3, 1950 at the Post Office at Princeton, New Jersey, under the act of March 3, 1879. Subscription price in the United States and Canada; one year \$2.00, two years \$3.50 three years \$4.50; in other countries: one year \$2.40, two years \$4.30, three years \$5.70. Single copies in the United States, \$.75; in other countries, \$.85.

RCA REVIEW

a technical journal

RADIO AND ELECTRONICS
RESEARCH • ENGINEERING

Published quarterly by

RCA LABORATORIES

in cooperation with all subsidiaries and divisions of

RADIO CORPORATION OF AMERICA

VOLUME XVII

MARCH, 1956

NUMBER 1

CONTENTS

	PAGE
In Memoriam — Robert E. Shelby	3
Surface Treatment of Silicon for Low Recombination Velocity	5
H. NELSON AND A. R. MOORE	
The Omniguide Antenna — An Omnidirectional Waveguide Array for UHF-Television Broadcasting	13
O. M. WOODWARD, JR. AND J. J. GIBSON	
P-N-P Transistors Using High-Emitter-Efficiency Alloy Materials ..	37
L. D. ARMSTRONG, C. L. CARLSON AND M. BENTIVEGNA	
Uniform Planar Alloy Junctions for Germanium Transistors	46
C. W. MUELLER AND N. H. DITRICK	
Miniature Loudspeakers for Personal Radio Receivers	57
J. C. BLEAZEY, J. PRESTON AND E. G. MAY	
A Variable-Capacitance Germanium Junction Diode for UHF	68
J. H. O'CONNELL AND L. J. GIACOLETTO	
Phase Angle Distortion in Traveling-Wave Tubes	86
W. R. BEAM AND D. J. BLATTNER	
The Electron-Voltaic Effect in Germanium and Silicon P-N Junctions	100
P. RAPPAPORT, J. J. LOFERSKI AND E. G. LINDER	
RCA TECHNICAL PAPERS	129
CORRECTION	134
AUTHORS	135

© 1956 by Radio Corporation of America
All rights reserved

RCA REVIEW is regularly abstracted and indexed by *Industrial Arts Index*, *Science Abstracts* (I.E.E.-Brit.), *Electronic Engineering Master Index*, *Chemical Abstracts*, *Proc. I.R.E.*, and *Wireless Engineer*.

RCA REVIEW

BOARD OF EDITORS

Chairman

R. S. HOLMES
RCA Laboratories

M. C. BATSEL
Engineering Products Division

G. L. BEERS
Radio Corporation of America

H. H. BEVERAGE
RCA Laboratories

G. H. BROWN
RCA Laboratories

I. F. BYRNES
Radiomarine Corporation of America

D. D. COLE
RCA Victor Television Division

O. E. DUNLAP, JR.
Radio Corporation of America

E. W. ENGSTROM
Radio Corporation of America

D. H. EWING
RCA Laboratories

A. N. GOLDSMITH
Consulting Engineer, RCA

A. L. HAMMERSCHMIDT
National Broadcasting Company, Inc.

O. B. HANSON
Radio Corporation of America

E. W. HEROLD
RCA Laboratories

R. F. HOLTZ
RCA International Division

C. B. JOLLIFFE
Radio Corporation of America

E. A. LAPORT
Radio Corporation of America

C. W. LATIMER
RCA Communications, Inc.

H. W. LEVERENZ
RCA Laboratories

G. F. MAEDEL
RCA Institutes, Inc.

H. B. MARTIN
Radiomarine Corporation of America

H. F. OLSON
RCA Laboratories

D. S. RAU
RCA Communications, Inc.

D. F. SCHMIT
Radio Corporation of America

S. W. SEELEY
RCA Laboratories

G. R. SHAW
Tube Division

A. W. VANCE
RCA Laboratories

A. F. VAN DYCK
Radio Corporation of America

I. WOLFF
RCA Laboratories

Secretary

C. C. FOSTER
RCA Laboratories

REPUBLICATION AND TRANSLATION

Original papers published herein may be referenced or abstracted without further authorization provided proper notation concerning authors and source is included. All rights of republication, including translation into foreign languages, are reserved by RCA Review. Requests for republication and translation privileges should be addressed to *The Manager*.

IN MEMORIAM

ROBERT E. SHELBY

On December 8, 1955, Robert E. Shelby died unexpectedly of a heart attack. Although death came at the young age of 49, Mr. Shelby had a close interest in radio for 35 years, and was actively engaged in television work for 24 years. He joined the National Broadcasting Company in



1929 after graduation from the University of Texas. In 1931 he was placed in charge of NBC's first experimental television installation atop the Empire State Building. Among the positions he subsequently held with NBC were Director of Technical Development and Director of Technical Operations for the television network, and Director of Color Television Systems Development. In

July 1954, he was made Vice President and Chief Engineer of NBC.

In the early days of black-and-white television, Mr. Shelby devoted much of his time to working with various industry committees. This work eventually led to the adoption of the present signal specifications for commercial television. Similarly, Mr. Shelby played an important role in the formulation of the signal specifications for compatible color television which were eventually adopted by the Federal Communications Commission. He was a Fellow of the Institute of Radio Engineers, a Fellow of the American Institute of Electrical Engineers, and a member of the Society of Motion Picture and Television Engineers, Tau Beta Pi, Phi Beta Kappa, Eta Kappa Nu, and Sigma Xi.

Mr. Shelby has made substantial contributions to *RCA Review* both as an author and as a member of the Board of Editors. His loss will be keenly felt by all who knew him.

SURFACE TREATMENT OF SILICON FOR LOW RECOMBINATION VELOCITY†

BY

A. R. MOORE AND HERBERT NELSON

RCA Laboratories,
Princeton, N. J.

Summary—The surface recombination velocity ordinarily attained on silicon surfaces as a result of common etches is of the order of 10⁴ centimeters per second. This high value is a serious limitation in the performance of silicon transistor devices due to the loss of minority carriers at the surface. Films of aniline-like aromatic liquids and films of sodium dichromate-like salts have been found which dramatically reduce the recombination velocity by two orders of magnitude. Surface recombination velocities similar to those commonly obtained on germanium (100 centimeters per second) can be obtained for p-type silicon. In case of n-p-n alloy type silicon transistors, surface treatment with sodium dichromate commonly leads to values of the current amplification factor, α_{cb} , which are four times larger than the values observed before the treatment. The surface treatments also eliminate "channeling leakage" at p-n junctions. This is consistent with the view that the films produce their effects by causing the energy bands (in p-type silicon) to curve upwards at the surface.

A tentative hypothesis is proposed to account for the behavior of the surface films.

INTRODUCTION

THE electrical characteristics of semiconductor devices are greatly affected by surface recombination of minority carriers. It is well known that the base-to-collector current amplification factor, α_{cb} , of transistors decreases¹ and the junction saturation current increases² with an increase in the surface recombination velocity, s . With germanium, conventional electrolytic and chemical etches lead to rather low values of s (50-200 centimeters per second). High values of α_{cb} may be obtained with conventional etches, since only a very small fraction of the current carriers injected by the emitter is lost at the surface. In silicon, however, s remains high (5,000-10,000 centimeters per second) after etching with the common etches. Consequently it is more difficult to obtain high values of α_{cb} in the case of silicon devices. It is particularly important, therefore, in the case of silicon to consider other means than etching for the reduction of s .

† Presented at the I.R.E.-A.I.E.E. Conference on Semiconductor Research, Philadelphia, Pa., June 22, 1955.

¹ A. R. Moore and J. I. Pankove, "Effect of Junction Shape and Surface Recombination on Transistor Current Gain," *Proc. I.R.E.*, Vol. 42, pp. 907-913, June, 1954.

² W. M. Webster, "The Saturation Current in Alloy Junctions," *Proc. I.R.E.*, Vol. 43, pp. 277-280, March, 1955.

Considerations by A. Moore and W. Webster,³ for instance, lead to the conclusion that an increase in the doping impurity concentration at the surface of a semiconductor will tend to inhibit surface recombination. Under these conditions, the minority carriers are prevented from reaching the surface by an internal electric field associated with the variation in doping impurity concentration. In p-type silicon, therefore, a surface treatment which causes the energy bands to curve upwards at the surface should similarly cause a reduction in s . It was thought that this effect may be produced by a chemical treatment which leads to a surface film containing ionic components of high electron affinity. Attempts to produce films of this type on silicon surfaces have achieved a dramatic reduction of s . Surface recombination velocities similar to those commonly obtained on germanium are achieved on p-type silicon by these treatments. A description of the techniques used and the results obtained constitute the subject matter of the present report.

MATERIALS AND PROCESSING TECHNIQUES

Two groups of chemical compounds have been found to produce surface films on silicon which greatly reduce the surface recombination velocity. One is a group of strongly ionic salts which are oxidizing agents. Sodium dichromate is a typical example. The other is a group of aniline-like aromatic liquids. The conditions under which the two groups of compounds produce the desired effect differ considerably and consequently each case will be discussed separately.

The practices involved in the use of sodium dichromate-like salts for the reduction of s on p-type silicon are extremely simple. A solution of the salt in distilled water is prepared and a droplet applied to the area to be treated. The water evaporates and leaves a strongly adsorbed salt film on the surface which leads to an immediate and permanent reduction of s . The concentration of the salt in solution is not critical; values on the order of 1 per cent by weight are normally used. The silicon specimen must be freshly etched before the application of the salt. A hot sodium hydroxide solution is normally used as the etch and good results are obtained with a solution of 7 grams of the hydroxide in 100 cubic centimeters of water heated to 80°C.

When aromatic liquids are used, the practices involved are more complicated. The vapor pressure of the liquid is high so that lasting

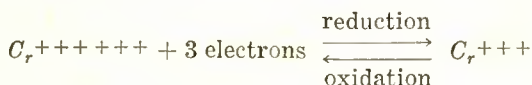
³ A. R. Moore and W. M. Webster, "The Effective Surface Recombination of a Germanium Surface with a Floating Barrier," *Proc. I.R.E.*, Vol. 43, pp. 427-435, April, 1955.

reductions of s are obtained only when the silicon specimens are hermetically sealed in containers filled with these liquids. The aromatic liquids inhibit surface recombination only in the presence of an electric field. The difference in potential between the emitter dot and the adjacent surface of the silicon often is sufficient to establish the requisite electrical gradient in a transistor device but in some cases auxiliary electrodes are essential for optimum results. Before immersion in the aromatic liquid, the silicon specimens are etched in the hot sodium hydroxide solution described above.

TENTATIVE HYPOTHESIS OF FILM BEHAVIOR

The exact behavior of the inorganic salts which reduce surface recombination on p-type silicon is not completely understood. Nevertheless, it is of interest to consider a tentative hypothesis based on the observation that these salts are relatively strong oxidizing agents and belong to reversible systems of oxidation-reduction reactions. It is proposed that the oxidation-reduction potential developed in such systems modifies the surface potential in such a manner that minority carriers are inhibited from reaching the surface. It is this effect which reduces the effective recombination rate. Other systems for creating such a barrier within the semiconductor to achieve similar results have been discussed by Moore and Webster.³

The terms oxidation and reduction are used in their general sense, i.e., an oxidation reaction is one in which an element loses electrons and thus increases in valence. Oxygen may or may not be involved. Conversely, in a reducing reaction an element gains electrons to decrease its valence. Thus the dichromate-chromic system (e.g., sodium dichromate) has been found effective in the reduction of surface recombination velocity, and



where the reduction and oxidation directions refer to the chromium.

In a reversible system, both the oxidized and reduced components may be present simultaneously and an equilibrium will be reached between them and the electrons. An inert metallic electrode immersed in a solution of oxidized and reduced components will give up or abstract electrons according to the inclination towards reduction or oxidation, respectively. In our example, the strongly oxidizing dichromate inclines the reaction to reduction (of $C_{r,+++++}$) and in so doing abstracts electrons from the electrode. The potential of the electrode is thereby

raised with respect to the solution. This potential, measured under standard conditions, determines the equilibrium state and, in electrochemistry, is the "standard oxidation-reduction potential." For our example, the standard potential E_0 is 1.3 volts.

It is characteristic of the salts found effective for the reduction of surface recombination on p-type silicon that they have relatively large positive standard potentials (> 0.3 volt). Thus the following systems have been found effective for possible practical use:

System	E_0
$\text{MnO}_4:\text{MnO}_2$	1.6
$\text{ClO}^-:\text{Cl}^-$.9
$\text{Cr}_2\text{O}_7:\text{Cr}^{+++}$	1.3

In addition many other oxidation-reduction systems, some of a particularly simple type, have been found equally effective in reducing s . Many of these are not suitable for practical use because of chemical instability, excessive moisture effects and the like. However, it is characteristic of all that their standard oxidation-reduction potentials exceed 0.3 volt.

In the case of a metallic electrode, the oxidation-reduction potential is supported in a narrow region of the solution adjacent to the electrode. It cannot be supported in the electrode itself since the electrode is a good conductor. If a semiconductor is substituted for the metallic electrode, the situation is entirely different. With a semiconducting electrode the fixed charge concentration (impurity density) in the semiconductor is generally much lower than the ionic concentration in ordinary electrolytes. Under these conditions it is much easier to support the potential in the semiconductor than in the solution. Thus, we arrive at the conclusion that the surface of a chemically inert semiconductor immersed in an oxidation-reduction solution will charge up to the appropriate standard electrode potential while the interior of the semiconductor will remain unaffected. In the case of a positive electrode (or surface) potential, this creates just under the surface the type of barrier described by Moore and Webster to inhibit surface recombination on p-type material. That is, the surface is effectively more p-type (through the loss of electrons) than the interior. The resultant internal electrostatic field prevents minority carriers from reaching the surface and consequently the effective surface recombination rate is lowered.

It has also been suggested that s may be a function of surface potential because of its effect on the population of surface traps. What-

ever the detailed reasoning it does not seem improbable that adjustment of the surface potential can have a drastic influence on surface recombination.

It is recognized that in the experimental evidence described earlier we do not have the "standard" solutions so that the actual potential will be somewhat different from the standard potential. Moreover in the absence of definite information to the contrary the possibility of a chemical reaction with the silicon has been neglected. However in the present hypothesis, it is suggested that these effects would modify the magnitude of the potential but not alter the general argument.

The above argument has been derived solely from observations on inorganic oxidation-reduction systems. If this hypothesis is a general one it should also explain the action of the aromatic liquids; these are equally effective in reducing s but require a small electrolyzing voltage. The chemistry of these materials is complicated and very little is known about their reaction with silicon. However, nitrobenzene forms many intermediate products during electrolytic reduction to aniline and one of these products is quinone. It is suggested that this intermediate product might be the active ingredient. Quinone and hydroquinone form a well-known oxidation-reduction system with a standard electrode potential of 0.718 volt. A mixture of quinone and hydroquinone (quinhydrone) in water solution was tried on p-type silicon (without an electrolyzing potential). This solution was found to be fully as effective as either aniline or nitrobenzene for the reduction of s . The function of the polarizing voltage required for the latter compounds, according to this view, is simply to provide for anodic oxidation or cathodic reduction to the active intermediates at the semiconductor surface.

EXPERIMENTAL PROCEDURES AND RESULTS

The effect of the surface treatments on the recombination velocity was determined either directly by measurements of the s of a particular silicon surface before and after application of the film or indirectly by measurements of the α_{cb} of a silicon transistor before and after application of the film to the emitter area.

The light-pulse photoconductivity technique was used for the direct measurements. Thin wafers of silicon (about 5 mils thick) were prepared for the test by an initial etch in CP4 and a final etch in a hot sodium hydroxide solution. To minimize the contribution of volume recombination to the loss of current carriers, silicon of good bulk lifetime (> 20 microseconds) was used for the direct measurements.

Direct measurements were made on the sodium dichromate, aniline, and nitrobenzene systems with p-type silicon.

In case of the sodium dichromate-p-type silicon system, a permanent reduction of s from a value of about 5,000 centimeters per second to a value less than 100 centimeters per second was found to occur as a direct result of application of the film.

In case of the aniline and the nitrobenzene-p-type silicon system, the silicon specimen was inserted between two condenser plates with films of the aromatic liquid occupying the space between the major surfaces of the silicon specimen and the condenser plates. When aniline was used, the surface recombination velocity was reduced from an approximate value of 5,000 to a value of 100 centimeters per second. This reduction of s , however, was contingent upon the application of a *negative* voltage of about one volt to the condenser plates with respect to the silicon specimen. In the absence of this voltage no reduction of s was observed. When nitrobenzene was used, the value of s decreased

Table I—n-p-n Silicon Transistor Performance Before and After Sodium Dichromate Treatment

Transistor	4 kc Current Amplification Factor (α_{cb})		4 kc Power Gain db		Effective Lifetime (τ_e) μ sec.	
	Before	After	Before	After	Before	After
A No. 1	8.2	29.5	33.0	40.5	.75	1.0
No. 2	7.4	30.0	33.0	38.6	.7	1.1
No. 3	8.4	29.1	33.1	40.2	.7	.9
No. 4	8.5	27.2	30.3	35.3	.7	1.1
B No. 1	4.6	13.2	29.5	37.6	.35	.55
No. 2	5.7	14.0	30.5	36.0	.5	.75
No. 3	4.0	11.5	30.5	36.7	.5	.7
No. 4	5.3	13.3	31.0	36.1	.45	.6

All values of gain measured at $V_c = 6$ volts, $I_E = 1$ milliampere. Power gain measured with resistive input and conjugate matched output.

from 5,000 to 220 centimeters per second as a result of the application of a *positive* voltage of one volt to the condenser plates.

Many of the tests carried out to determine the effect of the surface treatments have involved measurements of α_{cb} before and after applying the film to the emitter area of an alloy type n-p-n silicon transistor. Since the use of sodium dichromate films has shown the most promise for practical applications, a large number of tests have involved this salt. Table I is a summary of the results obtained.

The large increases of α_{cb} observed for the transistors of group A are typical of results obtained with units made from silicon of relatively high bulk lifetime. The transistors of group B were made with base widths equal to those of group A but with silicon of low bulk lifetime. Since bulk recombination contributes materially to the loss

of minority carriers in these units, smaller increases in α_{cb} were obtained. The effective lifetime, τ_e , which is determined by bulk as well as surface recombination was measured by a pulse injection technique.⁴

Similar indirect measurements were used to determine the effects of various other surface films. The results obtained indicate that for silicon of equal bulk lifetime and for transistors of equal base widths, roughly equal increases in α_{cb} are obtained when other strongly ionic salts are substituted for sodium dichromate. This is true, for instance, in the case of magnesium chromate, calcium dichromate, calcium hypochlorite, lithium dichromate and potassium permanganate.

Indirect measurement showed that results similar to those obtained with aniline could also be achieved with pyridine, nitrocyclohexane, 0-nitrotoluene, 2, 4 dinitrofluorobenzene and α -100 naphthalene. In these cases, maximum increases in the current amplification factors were obtained with those aromatic liquids which required an applied negative potential for their "activation." This is consistent with the fact that n-p-n transistors require a negative emitter-to-base bias during operation. Thus with aniline, which direct measurements showed to require a negative potential, the increase in α_{cb} was equal to that with sodium dichromate. On the other hand, the increase was smaller with nitrobenzene, which direct measurements showed to require a positive potential.

A few tests were carried out with n-type germanium and silicon. Sodium dichromate showed no effect while immersion in aniline did increase the current-gain factors of p-n-p transistors.

The effects of the surface films on p-type silicon appear permanent. This observation is based largely on experimental data for transistors using sodium dichromate films. A relatively large number of hermetically sealed n-p-n silicon transistors made with the sodium dichromate film have shown no decrease in current amplification factor on shelf life. A few of these transistors have also been exposed to a temperature ambient of 150°C for as long as 48 hours. A decrease in the current amplification factor occurs as a result of the heating. The rate of decrease is appreciable, however, only during the first hours of heating and in all cases the transistors after baking have shown values of α_{cb} substantially higher than those observed before the application of the film.

OTHER EFFECTS OF SURFACE FILMS

In the course of these investigations, other effects have been observed which are consistent with the view that the films cause the

⁴L. R. Lederhandler and L. J. Giacoletto, "Measurement of Minority Carrier Lifetime and Surface Effects in Junction Devices," *Proc. I.R.E.*, Vol. 34, pp. 477-483, April, 1955.

energy bands (in p-type silicon) to curve upwards at the surface. The presence of the films at the p-n junctions was found to cause an improvement of the reverse junction characteristics. This effect is illustrated by the curves A and B of Figure 1. Curve A was obtained before and curve B after application of a sodium dichromate film to the silicon surface adjacent to a p-n junction. "Roundhouse" reverse character-

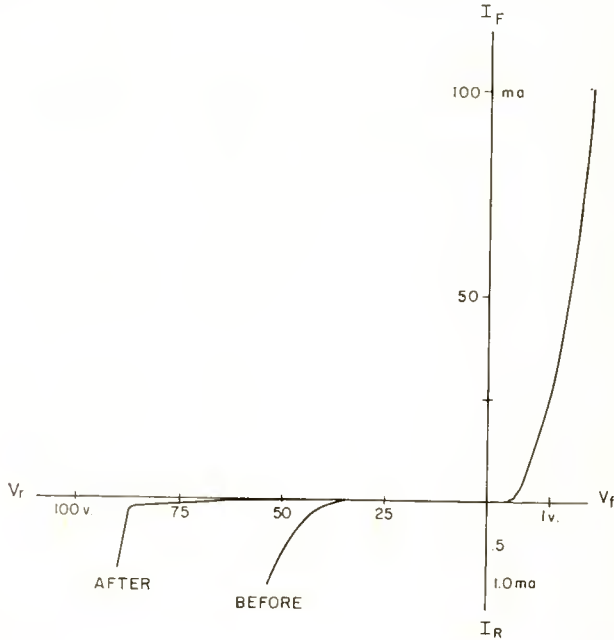


Fig. 1—Diode characteristics of p-n junction on p-type silicon before and after application of sodium dichromate to junction area.

istics of the type shown by curve A are often ascribed to "channeling leakage" at the p-n junction due to the fact that the energy bands normally tend to curve downwards at the surface (in p-type semiconductors). The elimination of the "roundhouse" characteristic in curve B may thus be considered evidence that the application of the surface film has reversed the curvature of the energy bands at the surface.

THE OMNIGUIDE ANTENNA — AN OMNIDIRECTIONAL WAVEGUIDE ARRAY FOR UHF-TELEVISION BROADCASTING

BY

O. M. WOODWARD, JR.[†] AND JAMES GIBSON*

Summary—The “Omniguide” antenna is a new type of high-gain antenna developed for UHF-television broadcasting. Waveguide components are employed in the design instead of coaxial-line elements in order to increase the power-handling capacity. Separate picture and sound inputs are provided which are decoupled over a wide frequency band, thus eliminating the need for a frequency-selective combining filter. A reflection-absorbing circuit increases the picture input bandwidth with very small sacrifice of power.

Experimental measurements taken on an antenna of this type constructed for Channel 72 (818-824 megacycles) are described. Considerations are given to several alternative versions of the system to cover the entire UHF range.

INTRODUCTION

WITH the opening of the UHF television band ranging from 470 to 890 megacycles, the need arose for suitable horizontally polarized, omnidirectional, transmitting antennas. Considerably more gain was required for the UHF antennas as compared to VHF antennas, not only because of the limited power available at the time from the UHF transmitters, but also due to the increased propagation losses at UHF. A simple solution could not be obtained satisfactorily by a scaled reduction in physical size of the present VHF antennas because of the resulting low power-handling capacity. Problems associated with the power distribution and omnidirectional azimuth radiation required a new approach in the antenna design.

As in the previous VHF practice, it is desirable for economic and mechanical reasons to diplex the signals from the picture and sound transmitters into a single antenna. This can be accomplished by either of two methods.

In the first system, the two signals are combined by a frequency-selective filter into a single feed line leading to the transmitting an-

[†] RCA Laboratories, Princeton, N. J.

* Formerly, RCA Laboratories, Princeton, N. J.; now with the Division of Radio Engineering, Royal Institute of Technology, Stockholm, Sweden.

tenna. A practical advantage of this method is that only a single transmission line from the transmitters to the antenna is needed.

In the second system, the antenna employs two separate inputs. These inputs energize the circumferential radiating elements with in-phase and progressively phased voltages, respectively, and are inherently decoupled over a wide frequency band. Therefore, the double-line input permits the use of a reflection-absorbing circuit which increases the bandwidth of one of the inputs.

With future requirements of color transmission and higher input power in view, a program was initiated in 1952. This work resulted in the development of a versatile antenna usable with either the double-input or single-input system and employing wave guides for both power distribution and mechanical support.

Much of the preliminary work was done with small-scale microwave models. A full-scale model was constructed for Channel 72 (818-824 megacycles) during the Summer of 1953. After successful tests were completed on this antenna, further work was continued in improving several of the component parts.

This paper describes the operation and results of field tests on the constructed antenna, and also the general theory and design for the various components.

DESCRIPTION

The antenna (Figure 1) consists of a cylindrical wave guide assembly which converts the energy flowing inside to a radiating, cylindrical current sheet on its outer surface. The symmetry of the wave guide permits propagation of the picture and sound energy as decoupled modes of transmission. This inner wave guide was made in the form of an octagon instead of a circle in order to simplify the mechanical construction.

A number of smaller wave guides containing spaced slots as radiators are grouped around the octagonal wave guide to function as the radiating, cylindrical surface as well as the distribution system supplying power from the inner wave guide to the individual slot radiators. Because of the large over-all diameter, eight surrounding wave guides are required to obtain a circular radiation pattern in the azimuth plane. Each of these wave guides contain a longitudinal ridge which permits operation in the ordinary rectangular wave guide mode.

The coupling of the slots to the wave guide is controlled by the relative offset positioning of the slots with respect to the center line of the ridge wave guide. The number and spacing of the slots are

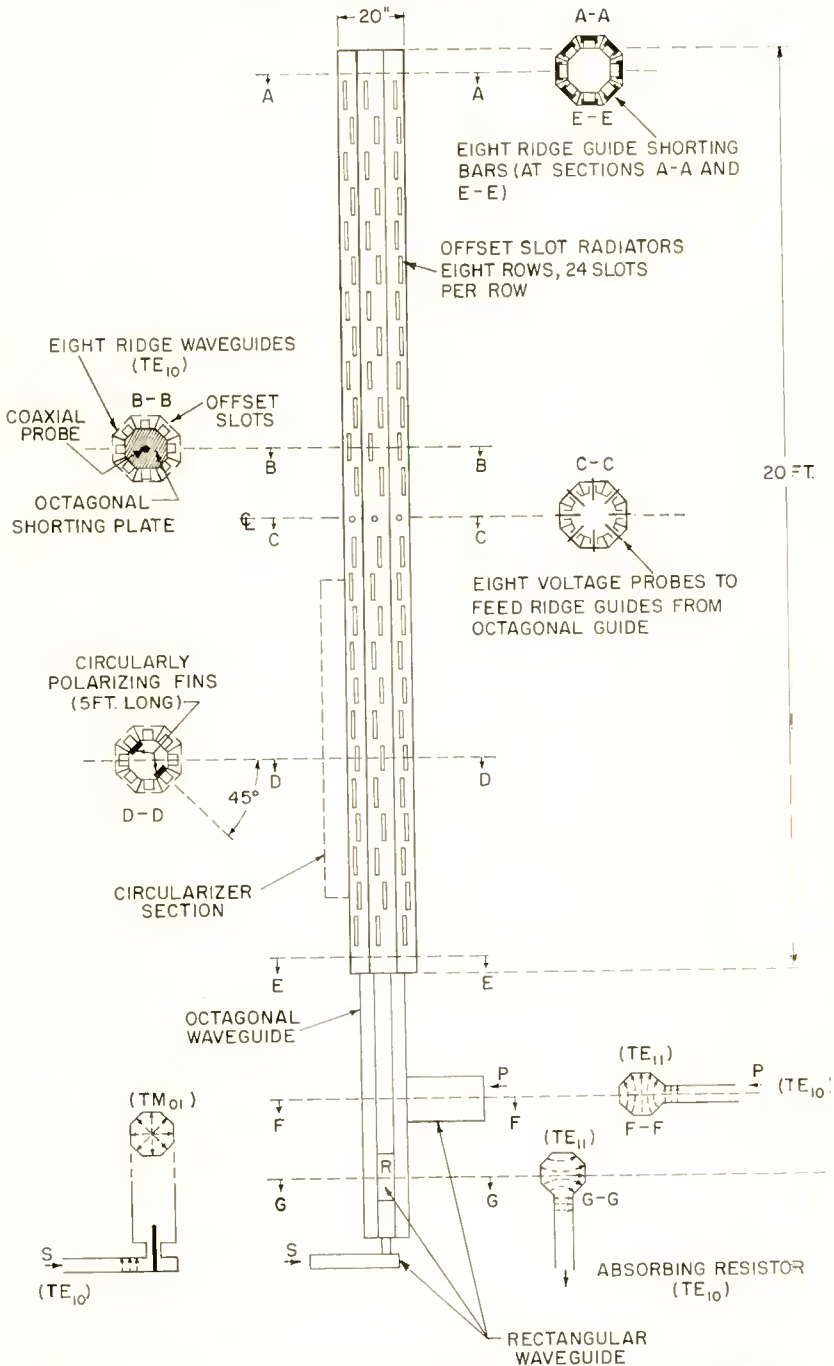


Fig. 1—Descriptive drawing of the Omniguide antenna constructed for Channel 72.

designed to produce the highly directive elevation pattern required for high power gain.

Each ridge wave guide is energized at its center by probe excitation from the octagonal wave guide (section C-C), and is terminated at its ends with shorting plungers at sections A-A and E-E. The symmetry and size of the central octagonal wave guide permits three modes of energy transmission to operate independently.

The signal from the picture transmitter is fed from a rectangular wave guide into the lower end of the octagonal wave guide as a linearly polarized TE_{11} wave (section F-F). Progressing upward, the wave is converted to a circularly polarized wave by a quarter-wave plate or circularizer section. This circularizer consists of two parallel metal fins attached to the inner wall of the octagonal wave guide and lying in a plane making a 45° angle with the direction of polarization of the incoming wave (section D-D).

For purposes of analysis, the incoming wave to this section may be separated into two linearly polarized waves with equal amplitude and phase, one polarized in the plane through the fins and one perpendicular to this plane. These two components propagate with different phase velocities because of the capacitive loading of the fins. With a proper length of the fins, the two components will be in time quadrature as they leave the fin section. Due to the field configuration of the TE_{11} wave, these components add to produce a circularly polarized wave.

This symmetrical wave continues to the voltage probes at section C-C and energizes the ridge wave guides at their centers with equal power and progressive phasing, resulting in essentially omnidirectional radiation in the azimuth plane.

In a reversed procedure, any reflected wave from the radiating section is reconverted by the circularizer to a linearly polarized wave polarized at right angles with respect to the picture input wave. Continuing downward, this reflected wave is coupled to another rectangular waveguide (section G-G) leading to an absorbing resistor. The reflected wave is thus decoupled from the picture input line and is transferred by the diplexer to an absorbing load.

The impedance seen by the picture input line is therefore independent of the impedance properties of the radiating system. This means a considerable improvement in the picture input bandwidth, secured at a very small sacrifice of picture power being dissipated in the absorbing resistor.

As the orientation of the rectangular wave guides to the octagonal wave guide represents a shunt "tee" junction, the centers of the two rectangular wave guides are located an odd multiple of one-quarter

wavelength from the shorting base plate at the lower end of the octagonal wave guide. The two rectangular wave guides are also offset vertically one wavelength to reduce the direct cross feed between the picture input line and absorbing resistor line caused by higher mode excitation in the vicinity of the junctions.

The signal from the sound transmitter, injected through the base of the diplexer, excites the second higher, or TM_{01} , mode in the octagonal wave guide. Due to the geometric symmetry of the system and to the field configuration of the TM_{01} mode, no sound signal is fed into either the picture input line or the absorbing resistor line. The circularizer has only a transformer effect on this mode. Continuing upward

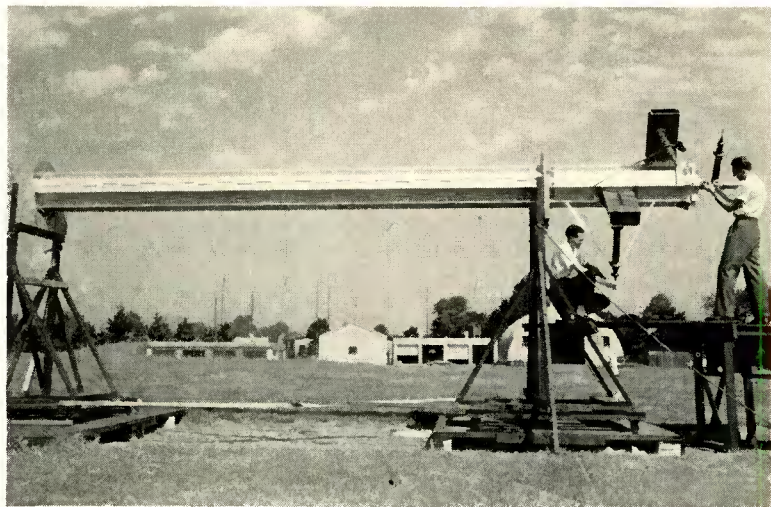


Fig. 2—General view of the Omniguide antenna without fiberglass cover.

to the voltage probes, the wave energizes the eight ridge wave guides with equal, in-phase voltages, which results in essentially omnidirectional radiation in the azimuth plane.

The TM_{01} probe is the extended inner conductor of a coaxial line which, depending on the power requirements, either may continue all of the way down to the sound transmitter or be coupled to a rectangular wave guide leading to this transmitter.

MECHANICAL CONSTRUCTION OF CHANNEL 72 OMNIGUIDE ANTENNA

The complete Omniguide antenna is shown mounted horizontally for testing in Figure 2. A thin-wall, cylindrical covering of fiberglass material (not shown in the photograph) is provided for weather protection. By fabricating the entire antenna from sheets of aluminum

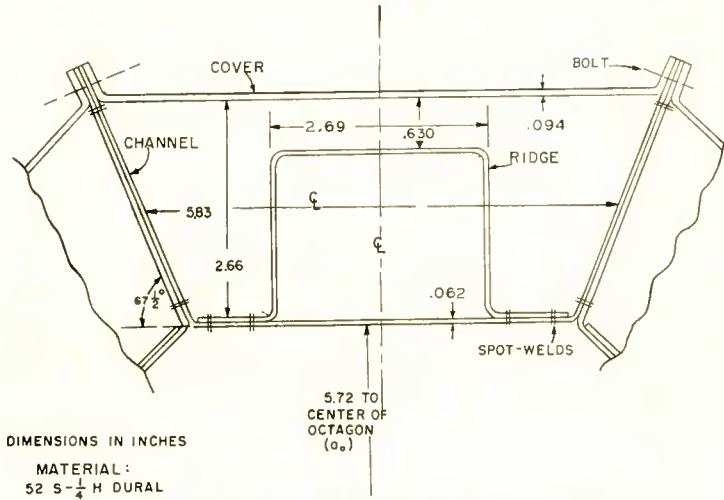


Fig. 3—Cross section of the ridge wave guide.

alloy instead of steel, galvanizing or plating processes were unnecessary and a great saving in weight was possible. The basic structure formed by the ridges and U-shaped channel sections was assembled by electric spot welding.

The cross section of Figure 3 gives details of the ridge wave guide construction. The outer cover plates containing the offset slots are removable, permitting several different sets to be used with a single, basic antenna structure.

The photograph of Figure 4 shows a cross section of the antenna

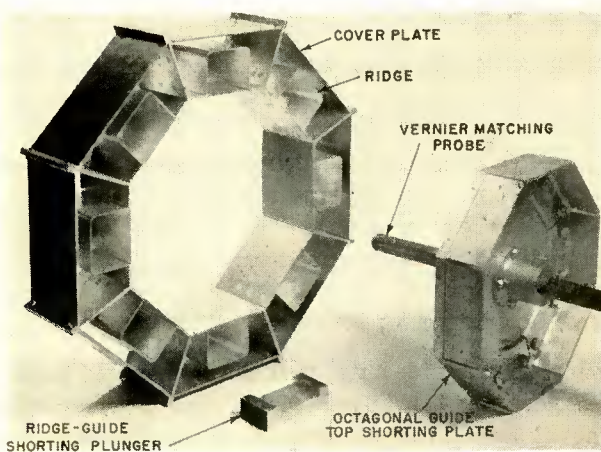


Fig. 4—Cross section of the Omniguide antenna and shorting plungers.

and the shorting plungers for the ridge wave guide and octagonal wave guide. Details of the coupling means between the octagonal and ridge wave guides are illustrated in Figure 5. As the probe is connected to the outer cover plate, external adjustments of its extension into the octagonal wave guide are easily made. The space inside of the ridges may be used for carrying the wiring to the tower lights.

ELECTRICAL MEASUREMENTS

The field tests on the Omniguide antenna showed that the radiation characteristics conformed very closely to theoretical calculations for Channel 72. Measured relative field patterns in both the azimuth and elevation planes over the frequency range of 810 to 830 megacycles

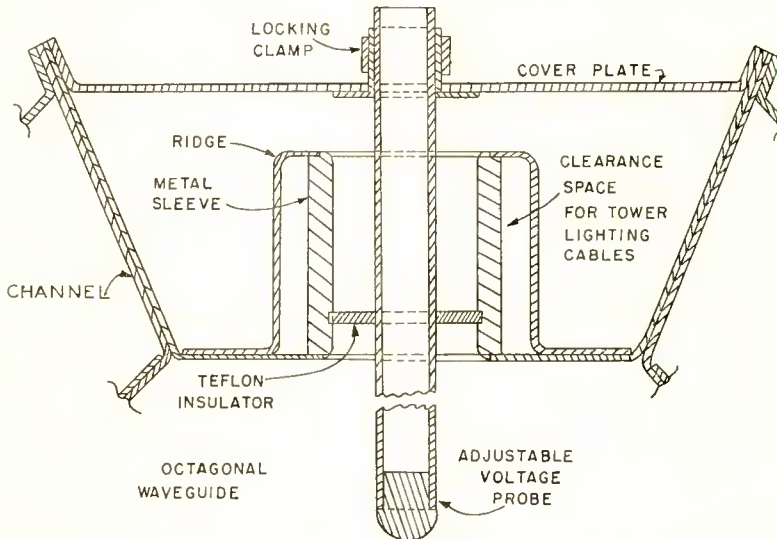


Fig. 5—Cross section of the ridge wave guide showing details of the voltage probe coupling.

are plotted in Figures 6 and 7, respectively. The calculated elevation pattern (dashed curve) at the design frequency of 820 megacycles is compared with the measured pattern in Figure 7.

The elevation pattern beamwidths and relative side-lobe data measured over a wide frequency range versus both frequency and the channel numbers are summarized in Figures 8 and 9. The beamwidth at half field remains fairly constant over a wide band. The increase in side lobes as the frequency departs from the design frequency imposes a fundamental bandwidth limitation on this particular array design of 24 co-phased slots at half-wave spacing.

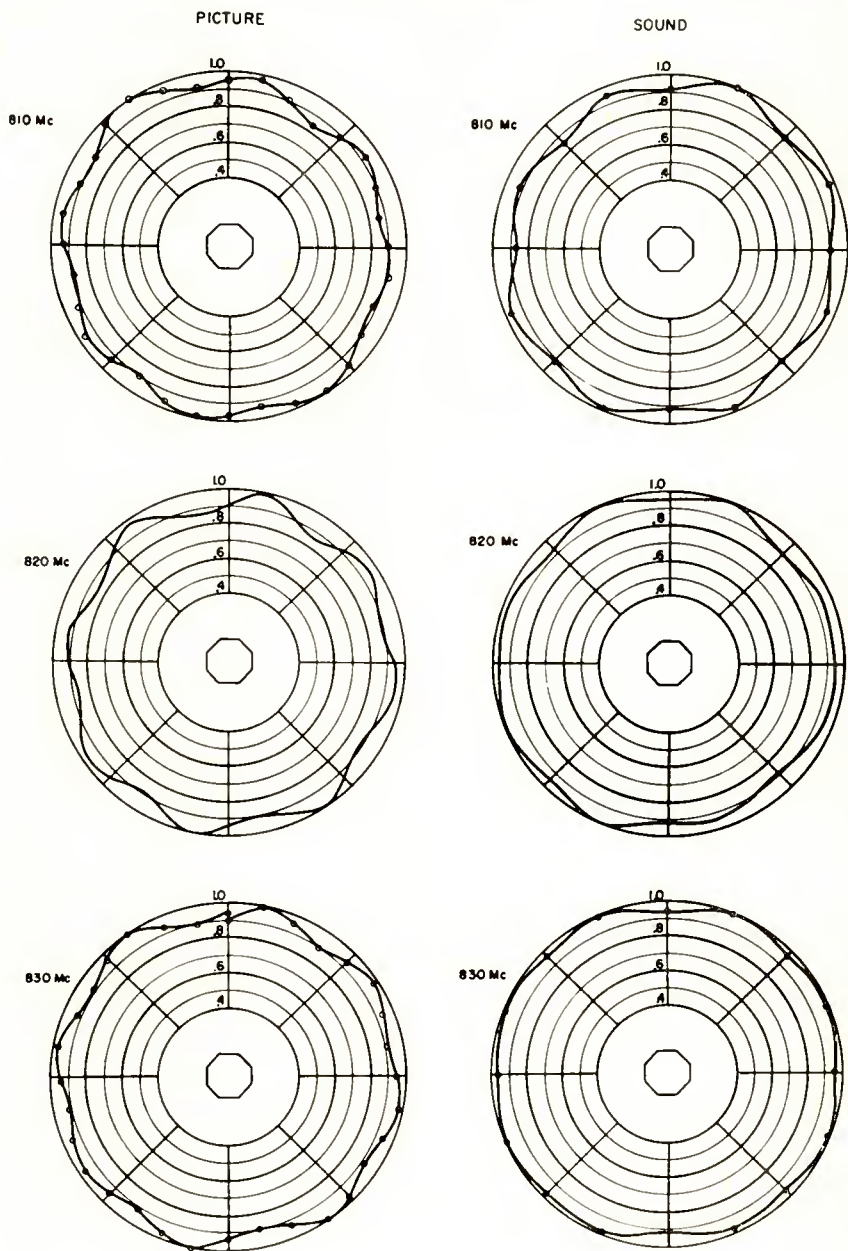


Fig. 6—Azimuth field patterns.

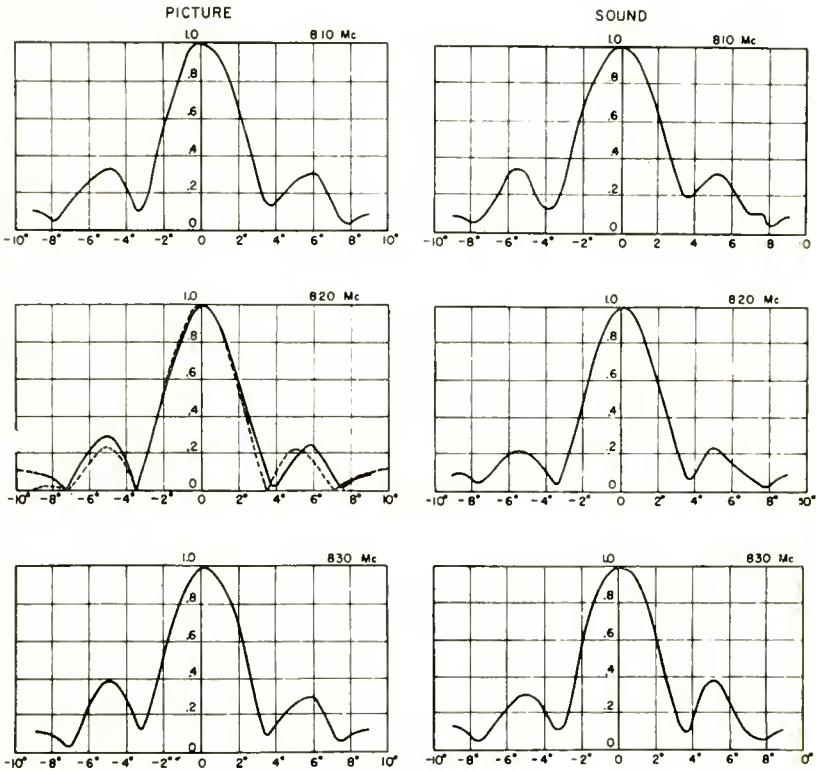


Fig. 7—Elevation field patterns.

The measured power gain, in decibels, versus frequency is plotted as the solid curve in Figure 10. For Channel 72, the average gain variation due to azimuth pattern change is ± 0.5 decibel and the maximum variation is ± 1.0 decibel. This measurement was made with only the frequency being changed. The dashed curve is calculated on the basis of rematching the antenna at each frequency. The useful

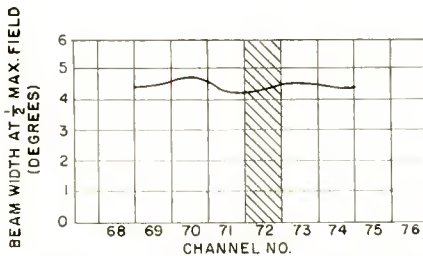


Fig. 8—Measured elevation pattern beamwidth at one-half field versus frequency.

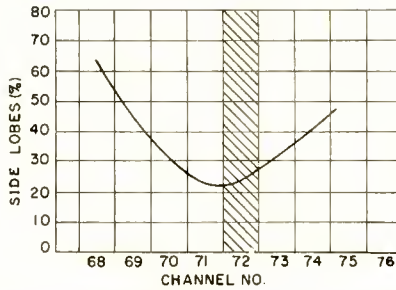


Fig. 9—Measured side-lobe intensity versus frequency.

bandwidth is essentially limited by the increase in side lobes as the frequency departs from the design frequency.

The voltage-standing-wave ratio on the rectangular wave guide leading to the picture transmitter is plotted in Figure 11 over a wide range of frequencies. The voltage-standing-wave ratio characteristic on the sound input line is plotted in Figure 12 on an expanded frequency scale. The picture power lost in the absorbing resistor was less than 0.01 decibel for Channel 72.

The cross coupling between the picture and sound inputs is a function only of the symmetry, and is independent of frequency over a very wide range. From 790 to 850 megacycles, the average cross-feed attenuation was found to be 40 decibels.

Determination of the maximum power-handling capacity of the Omniguide antenna on the basis of existing theory is not accurate because of the many simplifying approximations necessitated by the unusual configurations of the wave guides and the wave guide transi-

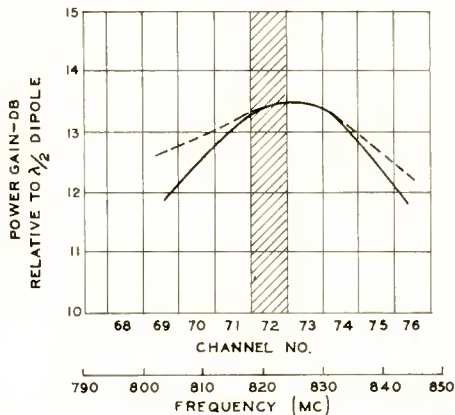


Fig. 10—Power gain in decibels relative to a half-wave dipole versus frequency. The solid curve shows the data obtained without altering the matching adjustments. The dashed curve would obtain if the antenna components were rematched at each test frequency.

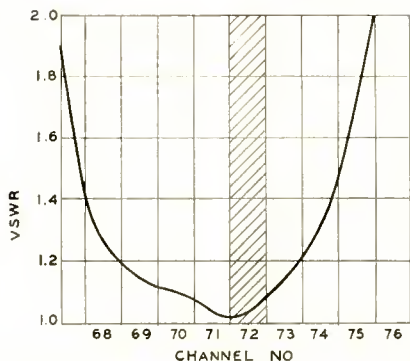


Fig. 11—Measured voltage-standing-wave ratio on the picture input line versus frequency.

tions. However, one test has been made on only a portion of the antenna with 10-kilowatt continuous-wave transmitter.

For this experiment, an end-fed ridge wave guide array containing twelve offset slots was coupled to the transmitter with no voltage breakdown or overheating. On the basis of this arrangement, representing one-sixteenth of the total number of slots, it is concluded that the complete radiating portion of the Omniguide antenna (the ridge wave guides and slots) would safely handle at least 160 kilowatts total average power. Because of the limited available power, no experimental tests could be made on the diplexer assembly.

GENERAL DESIGN

Azimuth Patterns

The number of ridge wave guides surrounding the central wave

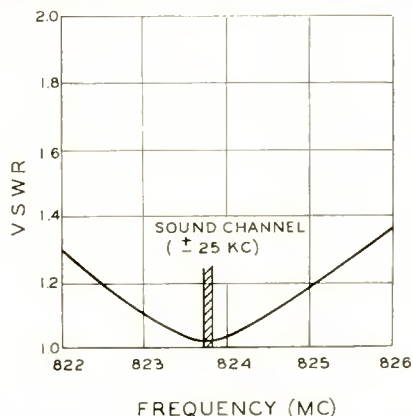


Fig. 12—Measured voltage-standing-wave ratio on the sound input line versus frequency.

guide are determined by the circularity requirements of the azimuth pattern. Any number of wave guides arranged in a regular polygon may be fed in phase progression by a circularly polarized wave simultaneously with, and decoupled from, a TM_{01} wave. However, the symmetry requirements for the two orthogonal modes require that the central wave guide cross section be invariant under rotation of 90° . Among the regular polygons, those having the number of sides equal to a multiple of four satisfy this condition. The inner wave guide formed by such an arrangement will permit propagation of two orthogonal, decoupled TE_{11} waves with similar field configurations and equal phase velocities.

The curves of Figure 13 show the theoretical variations in the azimuth field pattern circularity versus the radius of a cylindrical surface containing equally spaced, axial slot radiators. Because of the

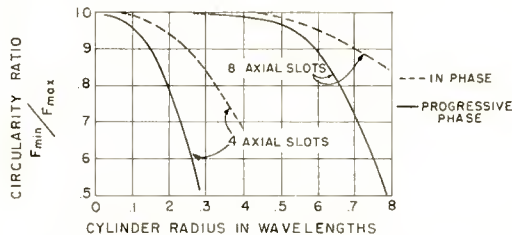


Fig. 13—Azimuth pattern circularity ratio versus the cylinder radius in wavelengths.

advantages in choosing the number of loads to be an integral multiple of four, calculations are given only for two cases of four and eight slots. The solid curves show the circularity ratio for progressively phased slots, and the dashed curves are plotted for in-phase feed. It is noted that, for a given cylinder diameter and number of slots, the in-phase slot excitation always gives a more circular pattern.

Octagonal Wave Guide Design

The cutoff wavelength, λ_c , of the first three modes in a hollow, circular wave guide is related to the radius, a , as follows:

$$\lambda_{c(TE_{11})} = 3.413 a, \quad (1)$$

$$\lambda_{c(TM_{01})} = 2.613 a, \quad (2)$$

$$\lambda_{c(TE_{21})} = 2.057 a. \quad (3)$$

Experimental measurements on the octagonal wave guide showed the corresponding cutoff wavelengths to be:

$$\lambda_{c(TE_{11})} = 3.50 a_0, \quad (4)$$

$$\lambda_{c(TM_{01})} = 2.68 a_0, \quad (5)$$

$$\lambda_{c(TE_{21})} = 2.11 a_0, \quad (6)$$

where a_0 is the radius of an inscribed circle in the octagon.

On substituting these constants in the general phase velocity relation,

$$\lambda_g/\lambda = \frac{1}{\sqrt{1 - (\lambda/\lambda_c)^2}}, \quad (7)$$

where λ is the free-space wavelength and λ_g is the wavelength in the guide, the relative phase velocities of the various modes may be obtained.

An interesting point was observed in comparing the octagonal and circular wave-guide dimensions. For equal cutoff frequencies, the octagonal and circular wave guides were found experimentally to have identical areas.

For useful operation of the octagonal wave-guide modes, the minimum wave-guide radius must be in the neighborhood of 0.4 wavelengths or larger. The maximum wave-guide size is limited by the undesired TE_{21} mode. In the Omniguide antenna, the radius of the outer surface containing the radiating slots is greater than the central wave guide radius by the narrow wall dimension of the outer wave guide. Hence, referring to Figure 13, it is seen that a minimum number of eight outer wave guides are required for an azimuth pattern circularity better than 0.8.

The antenna design curves of Figure 14 give the relative phase velocities of the octagonal-wave-guide modes versus the wave-guide radius in wavelengths as calculated from the measured cutoff values. Also plotted versus the same abscissa is a family of curves showing the azimuth pattern circularity for various shapes of trapezoidal wave guides. The parameter b_1/a_1 is the ratio of height to the average width of the trapezoidal wave guide. The wall thickness of the sheet metal structure was neglected in the calculation of these curves.

In the Omniguide antenna constructed for Channel 72, the octagonal radius was chosen to be 0.397 wavelength, giving a relative phase velocity at 820 megacycles of 1.44 for the TE_{11} mode and 2.98 for the TM_{01} mode.

With the use of this design data, a compromise choice may be made between the inner and outer octagonal sizes for a given trapezoidal

height. However, for such a design using the minimum number of eight outer wave guides, the width, a_1 , of the trapezoidal wave guide is too small to permit propagation of the TE_{10} mode. A simple means of lowering the cutoff frequency is by the use of a longitudinal ridge in the trapezoidal wave guide.

Ridge Wave Guide Design

Ramo and Whinnery¹ describe a method of "foreshortening" the transverse dimension of a rectangular wave guide by the use of a

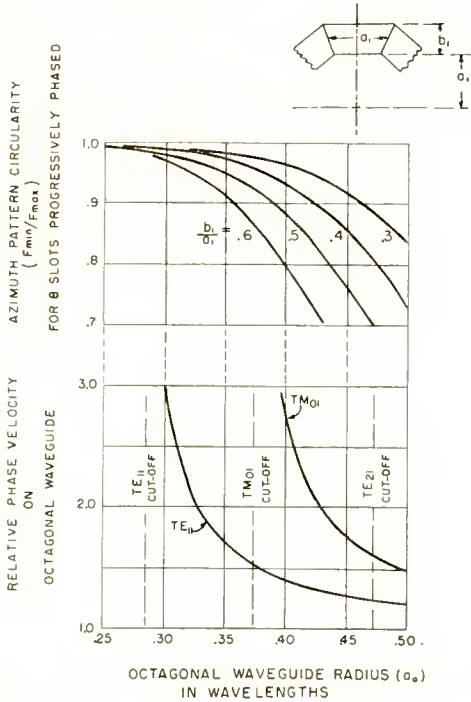


Fig. 14—Omniguide cross section design curves.

ridge in order to lower the cutoff frequency. A more complete analysis presenting design equations and curves is given by Cohn.²

The ridge in a rectangular wave guide may be considered as a capacity in shunt with the inductive regions on either side. Hence, the resonant (or cutoff) frequency may be changed without altering the wave-guide width by adjusting the ridge height.

¹ S. Ramo and J. R. Whinnery, *Fields and Waves in Modern Radio*, John Wiley and Sons, N. Y., 1944; p. 363.

² Seymour B. Cohn, "Properties of Ridge Wave Guide," *Proc. I.R.E.*, Vol. 35, p. 783, August, 1947.

Experimental measurements have shown that the data given by Cohn may also be used for approximate design of a ridged trapezoidal wave guide having a mean width, a_1 , equal to the rectangular-waveguide width. With the dimensions given in Figure 3, the calculated relative phase velocity at 820 megacycles was 1.27 as compared to a measured value of 1.31.

Slot Radiators

The laterally displaced, longitudinal slot was used as the basic radiating element because of the following advantages:

- (1) Simplicity of construction,
- (2) No auxiliary probe or loop coupling required,
- (3) Greater control of the slot impedance and radiation coefficient,
- (4) Elimination of dipole elements protruding outside of the octagonal antenna structure.

Slots of this type have been used extensively in the past for radar and other applications.^{3,4} In general, a narrow slot radiator, operated near its first resonance (approximately one-half wavelength long) and coupled to a rectangular wave guide by lateral displacement, may be considered as essentially equivalent to a single admittance in shunt with the transmission line at the midpoint of the slot, provided that the field distortion in the slotted section is small. Both the slot coupling to the wave guide and the resonant slot length are functions of the slot offset distance.

In the first model of the Omniguide antenna, the 20-foot aperture was uniformly illuminated by a center-fed array of 24 identical slots equally spaced at one-half guide wavelength intervals. Adjacent slots on each half of the array are staggered on opposite sides of the ridge wave guide center line to compensate for the 180° phase reversal at half-wave intervals on the line.

The first array design consisted of slots having a normalized conductance of 1/12 so that the input to each half of the 24-slot array would be matched. However, calculations of impedance versus frequency showed that considerable bandwidth improvement could be obtained by increasing or "overloading"⁵ the slot coupling to the ridge wave guide.

³ R. J. Stegen, "Slot Radiators and Arrays at X-Band," *Transactions of the I.R.E.*, PGAP-1, p. 62, February, 1952.

⁴ R. J. Stegen, "UHF-TV Radiators Using Slot Arrays," *Electronics*, p. 152, July, 1953.

⁵ *Microwave Antenna Theory and Design*, M.I.T. Radiation Laboratory Series, McGraw-Hill Book Co., Inc., N. Y., 1949; p. 324.

Mechanical details and frequency characteristics of the final slot design are given in Figure 15. Measured admittance values versus frequency are plotted on the Smith chart of Figure 16 for a single row of 12 slots. Curves are shown both with and without the fiberglass protective covering. It was found on the test model that a slight final impedance adjustment was desirable by shifting the position of the ridge shorting bars at the top and bottom of the ridge guides.

All measurements on the Omnidirect antenna were made without the fiberglass covering. It is seen from Figure 16 that a slight re-

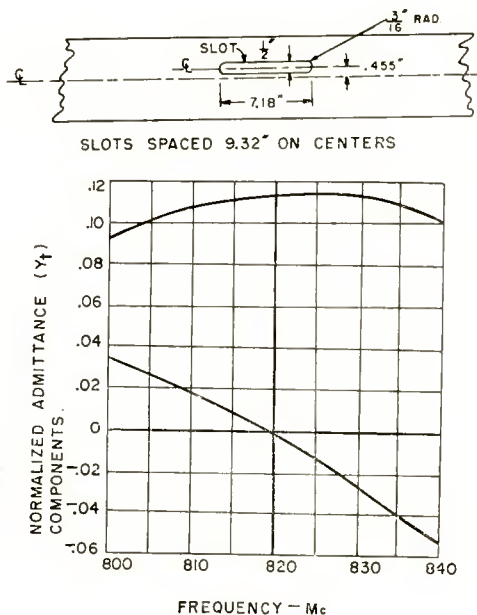


Fig. 15—Design and frequency characteristic of the slot used in the Omnidirect antenna constructed for Channel 72.

matching of the octagonal guide is required after the covering is in place. The fiberglass cylinders are constructed in approximately three-foot lengths for ease of assembly. Hence the final matching adjustment may be made by separating the center cylinders to expose the voltage probe extensions.

The Circularizer

Circular polarization was obtained by a method described by Fox⁶

⁶ A. Gardner Fox, "An Adjustable Wave Guide Phase Changer," *Proc. I.R.E.*, Vol. 35, p. 1489, December, 1947.

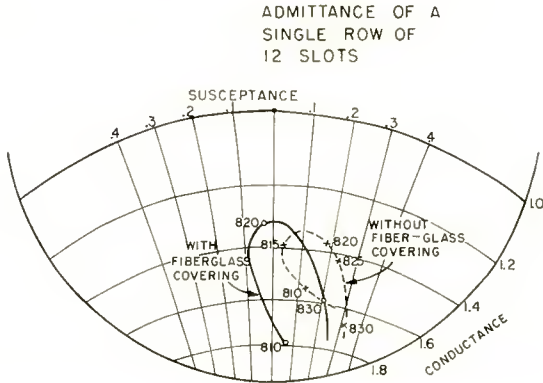


Fig. 16—Normalized admittance data measured on a single row of twelve slots.

which utilizes capacitive fins or ridges to obtain a relative phase difference between orthogonal mode components. A cross section of the octagonal wave guide with a pair of fins attached to the opposite inner walls is shown in Figure 17. The input TE_{11} wave, polarized in

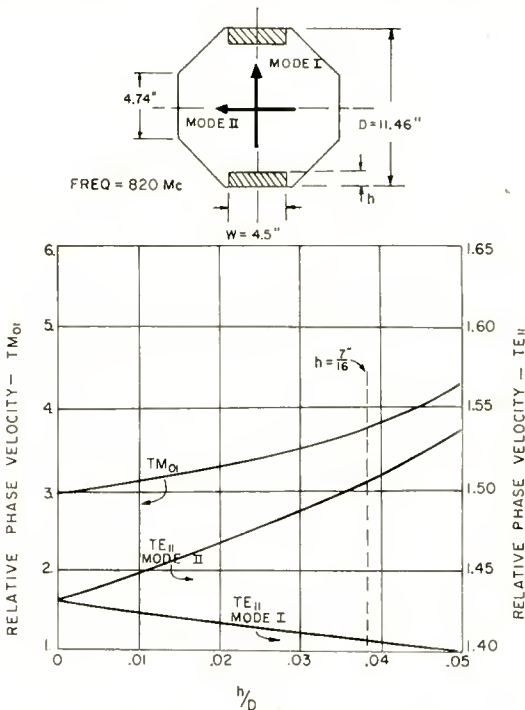


Fig. 17—Measured relative phase velocities of the TE_{11} and TM_{01} modes versus the relative ridge height.

a plane oriented at 45° with respect to the plane of the fins, may be resolved into two equal, orthogonal components, modes I and II. Mode I has a lower phase velocity than mode II because of the capacitive loading.

The relative phase velocity for the two component modes was measured at 820 megacycles for various fin heights and plotted in Figure 17. The measured TM_{01} phase velocity in the finned section was also plotted on the same chart. Since the TM_{01} cutoff is rapidly approached as the fin height is increased, a relatively low fin height of 7/16 inch was chosen for the design.

For this particular size of fin, the relative phase shift difference, ψ , between the two TE_{11} modes in a given line length, L , may be computed as follows:

$$\psi = (\beta_1 - \beta_2)L, \quad (8)$$

where β_1 and β_2 are the phase constants of modes I and II, respectively. This may be expressed in terms of the relative phase velocities, v_1 and v_2 , of the two modes as

$$\psi = \frac{2\pi L}{\lambda} (1/v_1 - 1/v_2). \quad (9)$$

Knowing the relative phase difference per unit length in terms of the fin height, the complete circularizer section may be designed to produce quadrature phase relationship. The final design as used in the Omniguide antenna for Channel 72 is drawn in Figure 18. Quarter-wave steps are provided at the ends of the fins to reduce the reflections from the transition discontinuity.

Figure 19 shows the bandwidth characteristic of this circularizer versus frequency. For this test, the circularizer was inserted in a matched, octagonal wave guide and the axial ratio of the elliptically polarized wave measured as the frequency was changed. It is seen that this fin design covers a wide range of frequencies.

TEM MODE SOUND EXCITATION

The dominant TE_{11} mode transmission in the hollow cylindrical wave guide is followed in order by the TM_{01} and TE_{21} modes as the frequency is increased. A variation of the Omniguide antenna is made possible by adding a coaxial inner conductor to the octagonal wave guide. This conductor may be considered as an extension of the coaxial probe in the octagonal shorting plate (section B-B of Figure 1) downward to the sound excitation probe in the diplexer section. Installing

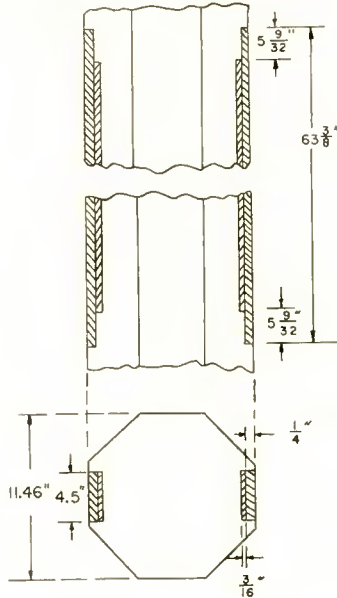


Fig. 18—Dimensions of the circularizer design for Channel 72.

the inner conductor in the wave guide changes the hollow tube to a coaxial line carrying the principal, or *TEM*, wave. In this case, the next higher modes propagated are the *TE*₁₁ and then the *TE*₂₁ modes as the frequency is increased.

With respect to the picture signal, the previous description of the

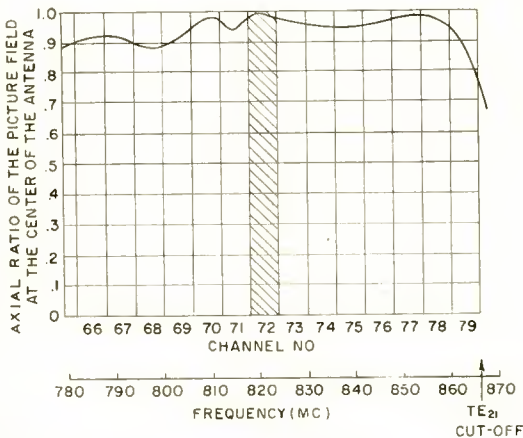


Fig. 19—Bandwidth of the circularly polarizing fins. The measured axial ratio of the picture field at the center of the antenna is plotted versus frequency.

antenna operation also applies to this case. The sound signal, however, is fed upward on the coaxial line as a TEM mode instead of the TM_{01} mode. Although this variation of the antenna is more complicated mechanically, the frequency band over which the octagonal wave guide can operate with decoupled picture and sound modes is increased considerably.

This is illustrated graphically by the drawing of Figure 20, in which the TM_{01} mode in the hollow guide is shown as degenerating into the TEM mode in the coaxial guide, thus increasing the useful range several times. In both cases, the upper limit is chosen near the threshold of the undesired TE_{21} mode.

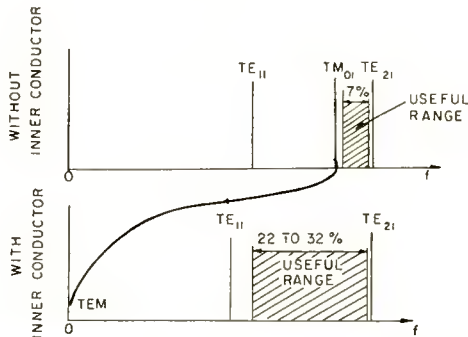


Fig. 20—Diagram showing the increase in useful range secured by employing an inner conductor in the octagonal wave guide.

An increase in the TE_{11} and TE_{21} cutoff wavelengths results as the inner conductor is made larger for a given outer conductor.⁷ Tests made on the Omniguide antenna showed that the addition of a 2-inch inner conductor changed the relative phase velocity from 1.44 to 1.36.

END-FED DIPLEXER

In the previously described diplexer, the lower portion of the octagonal wave guide forms a shorted stub in shunt with the picture input line. The length of this stub at picture carrier frequency is $1\frac{3}{4}$ wavelengths because of the necessary line offsets to prevent cross coupling. As a result, the picture input bandwidth is limited due to the rapid variation of the stub reactance with change in frequency. This bandwidth limitation has been overcome with an end-fed diplexer developed after the first model of the Omniguide antenna was constructed.

⁷ Theodore Moreno, *Microwave Transmission Design Data*, McGraw-Hill Book Co., Inc., N. Y., 1948; p. 71.

In this improved version, shown in Figure 21, the rectangular wave guide from the picture transmitter joins the bottom of the octagonal wave guide by means of a flared or tapered section. This end-fed, tapered section provides a broad-band transition between the rectangular and octagonal wave guides as well as eliminating the shunting stub.

The picture signal reflected from the radiating system is bypassed to the absorbing resistor through a rectangular wave guide joined to the side of the octagonal wave guide. The center of this rectangular

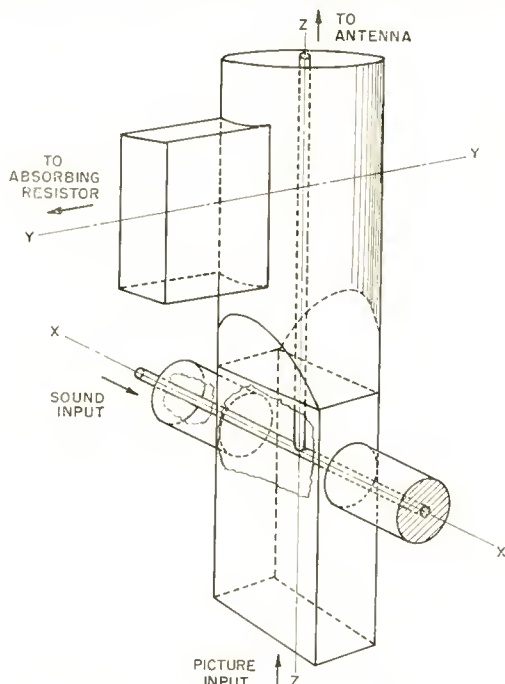


Fig. 21—Details of the end-fed diplexer.

wave guide is positioned vertically an odd multiple of quarter wavelengths from the effective short presented by the tapered section to the reflected wave.

The sound coaxial line is injected through the narrow wall of the picture input rectangular wave guide. The inner conductor of this line extends horizontally through the neutral plane of the rectangular wave guide to a short-circuited stub on the opposite narrow wall. This latter line functions as a mechanical support as well as a tuning means.

Another coaxial conductor extends vertically from the mid-point of the horizontal inner conductor in the rectangular wave guide to propagate the sound signal as either a TM_{01} mode or a TEM mode in

the octagonal wave guide. There will be no cross coupling between the sound and picture lines because of the symmetry of the arrangement.

The bandwidth advantage of this arrangement is demonstrated in Figure 22, which gives a comparison of the voltage-standing-wave ratio characteristics on the picture input line for the two types of diplexers.

TRANSMISSION LINES

At present, there are two standard sizes of rectangular wave guide transmission line commercially available for UHF television applications. The smaller of these, type WR-1150, with inside dimensions of $5\frac{3}{4}$ inches by $11\frac{1}{2}$ inches, was used in the constructed Omniguide antenna for the picture input and absorbing resistor lines. The rectangular wave guides were energized from 3-inch coaxial lines by an

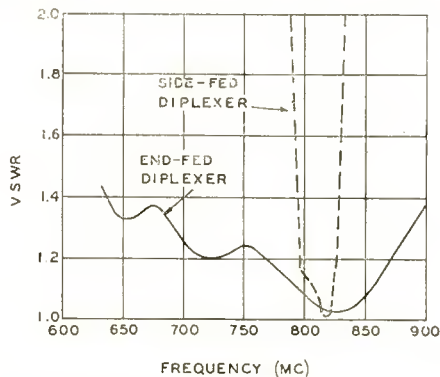


Fig. 22—A comparison of the voltage-standing-wave ratio characteristics of the side-fed diplexer and the end-fed diplexer as measured on the picture input line to the Omniguide antenna.

offset probing system described by Mumford.⁸ Although a 3-inch coaxial line was used for the sound input, a rectangular wave guide could be easily adapted for this purpose.

In actual installations employing the twin line feed system, two 3-inch or 6-inch coaxial transmission lines could be used for energizing the Omniguide antenna if the power and line-loss limits were not exceeded. For higher power transmitters and long-line applications, however, it might be necessary to use two rectangular wave guides. In this case, the economic and mechanical considerations form a major factor in the practical design of the system.

An alternative feed method is the possibility of using a single

⁸ W. W. Mumford, "The Optimum Piston Position for Wide-Band Coaxial-to-Waveguide Transducers," *Proc. I.R.E.*, Vol. 41, p. 256, February, 1953.

circular wave guide as a dual-purpose transmission line for feeding the Omniguide antenna. Both the picture and sound signals could be launched on the circular wave guide as cross-polarized TE_{11} waves, theoretically decoupled independent of frequency change. Additional inherent advantages are very high power-handling capacity and lowered wind loading.

No experiments have been made to date to determine the extent of cross coupling between the two modes in long runs of wave guide caused by mechanical irregularities or unsymmetrical discontinuities. It is believed, however, that if cross coupling did occur in a mechanically stable system, suitable balancing means could be provided at the terminals to decouple the signals.

Another transmission system on which experiments have been conducted is a dual-mode wave guide made by passing a continuous metal septum through the center of a circular wave guide. By transmitting the picture and sound signals separately in the two semicircular wave guides formed by this septum, the cross-coupling problem is solved regardless of possible discontinuities. This is accompanied, however, by increased losses due to current flow in the metal septum.

The dominant mode in the semicircular wave guide corresponds to the TE_{11} mode in circular wave guide, and also has the same cutoff wavelength in terms of the radius. However, no mode corresponding to the TM_{01} mode in circular wave guide can be propagated in the semicircular wave guide. The first higher mode in the latter line corresponds to the TE_{21} mode of circular wave guide and has a cutoff frequency which is 65.9 per cent higher than the dominant mode cutoff frequency. In the circular wave guide, the TM_{01} mode has a cutoff frequency which is 30.6 per cent higher than that of the TE_{11} mode. Hence, the semicircular wave guide has a considerable larger frequency range of operation than the circular wave guide.

An interesting comparison may be made between the split circular wave guide and the dual rectangular wave guide system formed by passing a septum through a square wave guide. For the same cutoff frequency, it is found that the split circular wave guide has slightly less attenuation than the split square wave guide and requires 3 per cent less material. The maximum cross-sectional dimension (and hence the wind load) of the split circular line is 17 per cent less than that of the split square line.

COMPLETE UHF BAND COVERAGE

For the previously described system as constructed for Channel 72, several television channels may be covered by only rematching the

picture and sound inputs and the antenna load to the octagonal wave guide. Using other sets of redesigned slotted cover plates, a bandwidth of approximately 7 per cent may be covered without change in the circularizer or absorbing resistor. This is also the useful range of the octagonal wave guide using the TM_{01} mode for the sound feed.

On the basis of the data obtained on the constructed antenna, the entire UHF band may be covered with nine different scaled sizes of the basic octagonal and trapezoidal structure. For this design, the maximum values of the relative phase velocities for each of the nine sizes are 3.7 and 1.5 for the TM_{01} and TE_{11} modes, respectively.

A second alternative exists if it is desired to combine the picture and sound signals with a frequency-selective filter. For this case, the sound input to the antenna is removed, and the single transmission line joins to the picture input of the antenna. Since the TM_{01} mode is not used, the lower limit of operation may be extended considerably so that the entire UHF band could be covered with only three basic sizes of antenna structures. Under this condition, the TE_{11} phase velocity would not exceed a maximum value of 1.9. For each size, the component requirements would be: 7 to 10 sets of slotted cover plates, at least three different circularizer designs, and 5 to 10 readjustments on the absorbing resistor. In addition, it would be necessary to rematch the octagonal wave guide and signal input lines for each channel.

With the use of an inner conductor in the octagonal wave guide, the bandwidth may be increased considerably while still retaining the advantage of diplexed picture and sound feeds. The same number of component shapes and adjustments as in the second alternative would be needed to cover the UHF range in three basic structure sizes. The maximum value of the TE_{11} relative phase velocity in this case would be 1.7.

P-N-P TRANSISTORS USING HIGH-EMITTER-EFFICIENCY ALLOY MATERIALS†

BY

L. D. ARMSTRONG,‡ C. L. CARLSON,‡ AND M. BENTIVEGNA#

Summary—In the past, the performance of p-n-p alloy transistors at high currents has been limited by the decrease of emitter efficiency with current level. The addition of small percentages of gallium or aluminum to indium, for use as the emitter alloy, produces greatly improved high-current characteristics. As compared with pure indium, the use of gallium alloys improves emitter efficiency by about 3.5 times, and the use of aluminum-bearing alloys by about 10 times. Techniques for preparation of the alloys and results of tests on transistors using the various emitters are described. Volume lifetime is measured as a function of injection level to permit comparison with the theoretical equations for current amplification factor. These measurements are discussed briefly, and a revised equation for current amplification factor at high currents is given.

INTRODUCTION

ONE of the most common methods used in making rectifying p-n junctions in semiconductors is the alloy process.^{1,2} In this technique a metal is alloyed into the semiconductor. When cooling takes place, some of the metal atoms remain in the recrystallized material. Depending on the choice of metal used for alloying, the recrystallized zone may be either "n" or "p" type.

A metal must have certain characteristics to be suitable for alloying into a semiconductor to form rectifying junctions and transistors. It should have low vapor pressure at the alloying temperature so that it will not evaporate and thus spread over the entire surface of the device. It should be soft to minimize mechanical strain during freezing and cooling. It should readily wet the surface of the semiconductor in a controllable fashion. Electrically, the junctions so formed should have low saturation currents, high reverse impedances, and low forward

† Presented at the *I.R.E.-A.I.E.E. Conference on Semiconductor Device Research*, Philadelphia, Pa., June 20, 1955.

‡ RCA Semiconductor Division, Harrison, N. J.

Formerly RCA Semiconductor Division, Harrison, N. J.; now with CBS Hytron, Danvers, Mass.

¹ R. R. Law, C. W. Mueller, J. I. Pankove, and L. D. Armstrong, "A Developmental Germanium P-N-P Junction Transistor," *Proc. I.R.E.*, Vol. 40, p. 1352, November, 1952.

² R. N. Hall, "Power Rectifiers and Transistors," *Proc. I.R.E.*, Vol. 40, p. 1512, November, 1952.

resistance. The breakdown voltage should be high. If the alloy is intended for use as the emitter of a transistor, the injection efficiency of the junction, γ , should be high.³

Because indium satisfies these requirements well, it has been widely used in the familiar p-n-p transistor. At high current levels, however, the injection efficiency of the emitter junction decreases, causing a reduction in current amplification factor.⁴ In addition, the current amplification factor varies from unit to unit when indium emitters are used, indicating possible variations in emitter efficiency.

Shockley³ has pointed out that emitter efficiency depends on the ratio of majority-carrier concentration on the two sides of the emitter junction. The emitter efficiency and, hence, current amplification factor are higher in transistors having high-conductivity emitter regions. In a p-n-p alloy transistor, the critical region is the p-type layer formed during the recrystallization process. A possible method of improving emitter efficiency involves the use of alloying materials having higher segregation coefficients, i.e., metals which are more soluble in solid germanium. When recrystallization occurs, a higher concentration of these metals remains in the recrystallized germanium, and the desired higher conductivity results.

EXPERIMENTAL WORK WITH GALLIUM AND ALUMINUM ALLOYS

Both gallium and aluminum have the desired characteristics for use as possible p-type "doping" agents. Their segregation coefficients at the melting point of germanium are 100 times greater than that of indium. It is reasonable to expect that they will also be more soluble than indium in solid germanium at the lower temperatures used in alloying. However, the physical properties of both metals have limitations. Gallium, for example, is molten at room temperature and cannot be used for mechanical support of connections. It is also difficult to alloy appreciable quantities of gallium with most other soft metals. Many three-component alloys containing gallium and other soft metals become hard and very brittle, frequently breaking into powder during subsequent processing. Aluminum, on the other hand, quickly forms an oxide surface which makes alloying difficult. When alloyed with germanium, it also forms a hard and brittle eutectic which makes penetration control difficult and causes severe mechanical strains.

Fortunately, it has been found that the advantages of both gallium

³ W. Shockley, *Electrons and Holes in Semiconductors*, D. Van Nostrand & Co., New York, N. Y., 1950; pp. 90-91.

⁴ W. M. Webster, "On the Variation of Junction-Transistor Current Amplification Factor with Emitter Current," *Proc. I.R.E.*, Vol. 42, p. 914, June, 1954.

and aluminum as "doping" agents may be retained when only small percentages of these metals are combined with one or more other components.* With these low concentrations, some of the mechanical difficulties can be minimized.

Reproducible gallium-bearing alloys have been made using indium as a major element, with small percentages of gallium and gold or silver added. The third constituent, gold or silver, acts as a carrier agent for the gallium, and insures that the gallium content is reproducible and consistent. In addition, the use of gold or silver favorably modifies the surface tension of the alloy, improves its wetting properties, and results in more consistent and uniform alloy penetration.

These gallium-bearing alloys exhibit alloying and recrystallization properties similar to those of pure indium. The depth of penetration or alloying depends on the relative amounts of the three materials. In general, the percentages of gallium and carrier metal are not critical. Satisfactory results have been obtained with alloys having gallium concentrations between 0.1 and 0.5 per cent, and gold or silver concentrations between 2 and 10 per cent.

It is more difficult to obtain consistent wetting and alloying of alloys containing 0.5 to 2.0 per cent aluminum in indium. Three methods have produced fairly satisfactory results, although each has disadvantages. In the first method, a dot of indium is first soldered or alloyed to germanium at a relatively low temperature. Another indium dot containing a small percentage of aluminum is then placed on top of the first dot and the combination is fired at a higher temperature. During firing, the aluminum from the second dot mixes with the first, or pre-wetted, dot. In the second method, an aluminum-bearing dot is soldered to germanium with the aid of a chemical flux. Metallic (zinc-chloride) fluxes tend to leach out the aluminum and produce low emitter efficiency. Satisfactory results have been obtained with some organic fluxes. The third method involves the preparation of special alloying dots in which the aluminum-bearing portion is surrounded by or sandwiched between layers of a "good-wetting" indium alloy or pure indium. The external layers wet the germanium at a fairly low temperature, but the aluminum becomes uniformly distributed only at higher alloying temperatures.

Junctions made with gallium or aluminum alloys exhibit essentially the same rectification properties as those made with pure indium. Because the emitter efficiency is higher, the current amplification factor

* A power transistor using gallium in the emitter was described by the Philips Company at Hamburg, Germany, in September, 1954. See also L. J. Tummers, "The Influence of Minority Carrier Injection on Power Transistors," N.T.F., Beiheft No. 1, pp. 31-32, 1955.

is greater at normal currents and decreases at a slower rate with increasing current. If desired, germanium having a lower resistivity may be used with these alloys without significant reduction of current amplification factor. Consequently, more freedom is allowed in the choice of one of the important transistor-design parameters.

ELECTRICAL CHARACTERISTICS

Figure 1 shows typical curves of small-signal common-emitter current amplification factor, α_{cb} , as a function of emitter-current density for transistors using emitters made of (1) indium, (2) indium-silver-gallium alloy and (3) indium-aluminum alloy. These units are identical except for emitter material. The emitter diameter is 0.015 inch and the junction spacing, W , is 0.0013 inch. The data shown in Figure 1 was measured on what is termed a "raw" surface, i.e., a condition of low surface-recombination velocity, s , which is obtained by electrolytic etching. Similar curves are shown in Figure 2 for the same three transistors with the surface modified to increase s to a relatively high value. This modification reduces the current amplification factor greatly at low currents and to a smaller degree at high currents.

It can be seen that the value of α_{cb} is considerably increased by the addition of gallium or aluminum and that this higher value is maintained to much higher emitter currents than is possible with pure indium emitters. Some transistors using aluminum alloy emitters have exhibited α_{cb} values greater than 100 at emitter-current densities of 1,000 amperes per square centimeter. It has also been found that the variation of small-signal current amplification factor (measured at low currents) between transistors is less when gallium-bearing alloys are used than when pure indium emitters are used. The reason for this improved uniformity may be simply that variations in emitter efficiency contribute to the spread of low-current α_{cb} when the emitter efficiency is low. Although transistors using aluminum-bearing alloys are even more variable at present than those using pure indium, the variation is probably due to the processing problems mentioned previously.

THEORETICAL DISCUSSION

As mentioned above, the current amplification factor of a transistor is limited by three factors: (a) surface recombination, (b) volume recombination, and (c) emitter efficiency. In most p-n-p alloy transistors, surface recombination is the major limitation at low current levels, as discussed by Moore and Pankove.⁵ However, all three factors may vary

⁵ A. Moore and J. I. Pankove, "Effect of Junction Shape and Surface Recombination on Transistor Current Gain," *Proc. I.R.E.*, Vol. 42, p. 907, June, 1954.

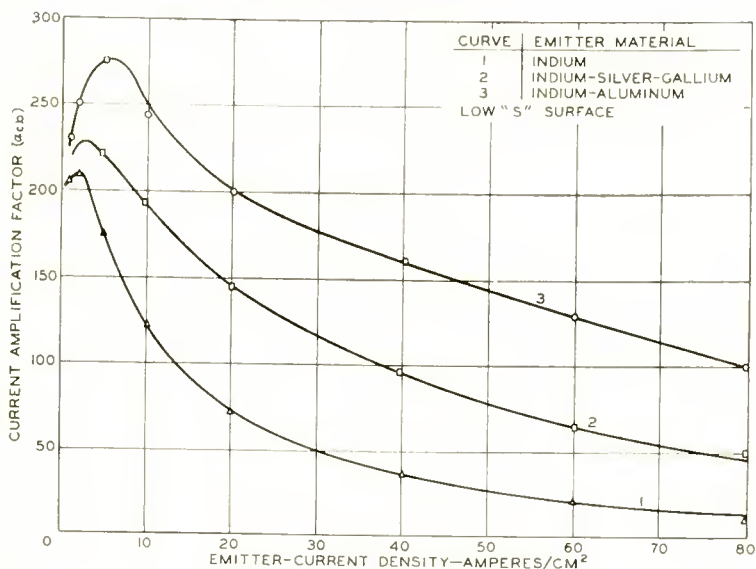


Fig. 1—Variation of small-signal current amplification factor, α_{cb} , with emitter-current density for (1) pure indium, (2) gallium-indium, and (3) aluminum-indium emitters. Surface-recombination velocity, s , is low.

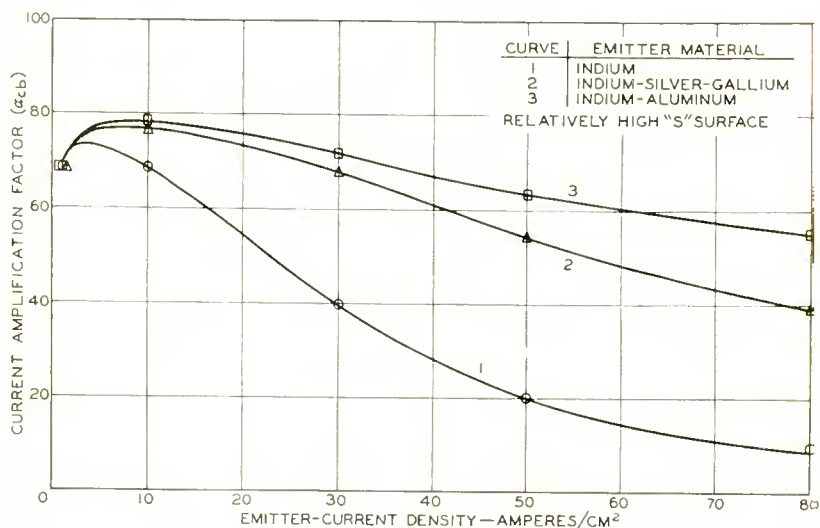


Fig. 2—Variation of small-signal current amplification factor, α_{cb} , with emitter current density for (1) pure indium, (2) gallium-indium, and (3) aluminum-indium emitters. Surface-recombination velocity, s , is high.

with emitter current, as shown by Webster,⁴ Rittner,⁶ and Misawa.⁷ At higher currents, the relative importance of the three factors changes. The percentage of carriers lost from the base by surface recombination decreases by a factor of two due to the development of a small electric field in the base region which aids the flow of these carriers to the collector. Emitter efficiency decreases with increasing emitter current and eventually becomes more important than surface recombination in limiting the current amplification factor, α_{cb} .

It was assumed by Webster that volume lifetime would also decrease with increasing emitter current. This assumption was a consequence of treating volume recombination as a bimolecular process (i.e., the rate of recombination is proportional to the product of hole and electron densities). Recent experiments indicate that this theory is incorrect. Effective lifetime measurements were made on alloy junction diodes in the manner described by Lederhandler and Giacoletto.⁸ The effects of surface recombination were minimized by making the diodes on thick slabs of n-type germanium having a resistivity of 1.5 ohm-centimeters. The diodes were etched in such a way that surface-recombination velocity was very low. Figure 3 shows the volume lifetime of two such diodes as a function of the ratio p/n_0 , where p is the injected density of holes and n_0 is the equilibrium density of electrons in the base material. It can be seen that the lifetime is fairly constant at low injection levels, increases somewhat as the injection level is increased, and then remains essentially constant to quite high injection levels. This data has been confirmed by W. P. Senett of the RCA Semiconductor Division who has measured volume and surface recombination as functions of injection level by a different method in which pulsed light is used as a minority-carrier source. The behavior shown in Figure 3 is qualitatively consistent with the Shockley-Read theory of recombination.⁹ As a point of reference, when the emitter-current density is about 270 amperes per square centimeter, the injection level, p/n_0 , is equal to 50 for a transistor in which the base region has a resistivity of 1.5 ohm-centimeters and a width of 0.0013 inch.

These measurements indicate that the equation given by Webster for small-signal current amplification factor as a function of emitter

⁶ E. S. Rittner, "Extension of the Theory of the Junction Transistor," *Phys. Rev.*, Vol. 94, p. 1161, June, 1954.

⁷ T. Misawa, "Emitter Efficiency of Junction Transistors," *Jour. Phys. Soc. Japan*, Vol. 10, p. 362, May, 1955.

⁸ S. Lederhandler and L. J. Giacoletto, "Measurement of Minority-Carrier Lifetime and Surface Effects in Junction Devices," *Proc. I.R.E.*, Vol. 43, p. 477, April, 1955.

⁹ W. Shockley and W. T. Read, Jr., "Statistics of the Recombinations of Holes and Electrons," *Phys. Rev.*, Vol. 87, p. 835, September, 1952.

current should be revised. Experiments have shown that surface-recombination velocity, s , as well as volume lifetime, is fairly constant at higher injection levels (at least for the surface treatment described above). Only emitter efficiency, therefore, changes appreciably with current, causing the observed reduction in current amplification factor. At high currents ($p/n_0 \gg 1$), the equation for current amplification factor in a p-n-p transistor is given by*

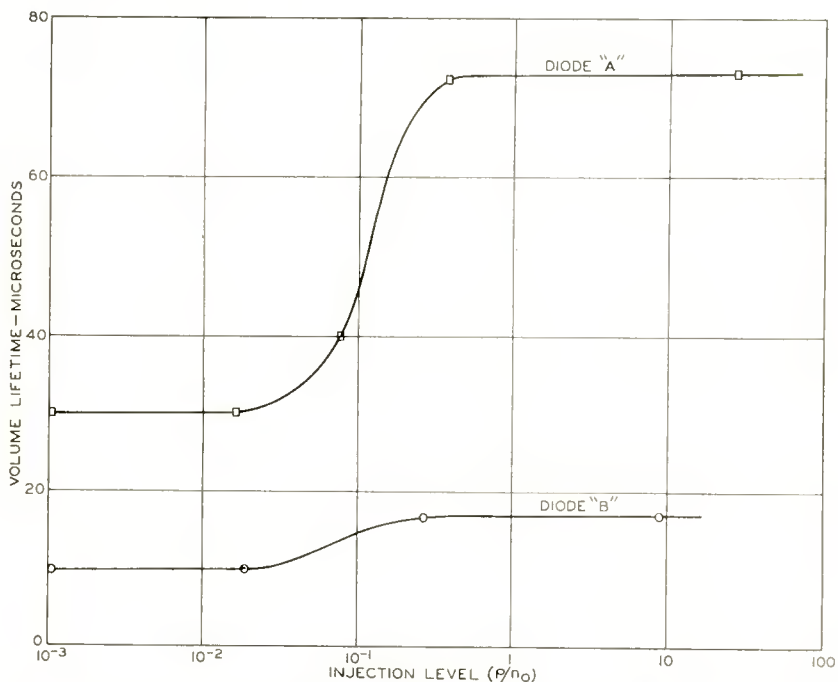


Fig. 3—Variation of volume lifetime with injection level for two alloy-junction diodes.

$$\frac{1}{\alpha_{cb}} = \frac{s A_s W}{2 D_p A} + \frac{W^2}{4 D_p \tau} + \frac{1}{2} \frac{W^2 \mu_c}{A \sigma_e L_e D_p} I_E, \tag{1}$$

where α_{cb} is the small-signal a-c collector-to-base current amplification factor, W is the effective junction spacing, s is the surface recombination velocity, A_s is the area over which surface recombination takes

* Equation (1) supplied by W. M. Webster. The factor 1/2 which appears in the third term does not appear in Reference (4), but is the result of a more rigorous derivation^{6, 7} which states that $\sigma_b W / \sigma_e L_e$ should be multiplied by $(1 + p/n_0)$ rather than $(1 + Z)$. At high currents, $(1 + p/n_0)$ approaches $Z/2$.

place, D_p is the diffusion constant for holes in the base region, A is the area of the emitter, σ_e is the conductivity of the emitter region adjacent to the junction, L_e is the diffusion length for electrons in the emitter region, τ is the volume lifetime at high injection levels, μ_e is the electron mobility, and I_E is the d-c emitter current.

The first term in Equation (1) represents the effects of carrier loss due to recombination at the surface. As Moore and Pankove⁵ have shown, this loss occurs mainly in a circular region around the emitter having a width approximately equal to the junction spacing, W . The second term gives the loss of carriers in the base region due to volume recombination, and the third term gives the effect of injection efficiency.

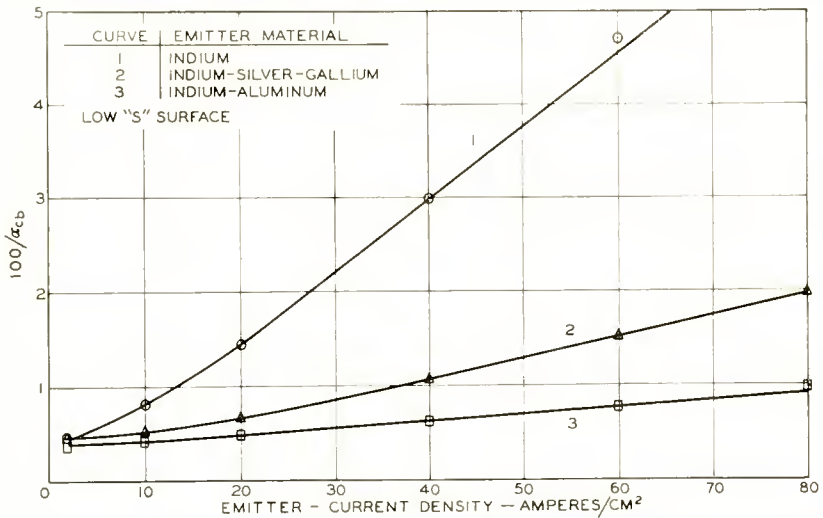


Fig. 4—Curves of $100/\alpha_{cb}$ versus emitter-current density for (1) pure indium, (2) gallium-indium, and (3) aluminum-indium emitters. The value of $\sigma_e L_e$ can be obtained from these curves.

Equation (1) indicates that the product $\sigma_e L_e$ can be computed from the slope of a curve showing $1/\alpha_{cb}$ as a function of I_E provided the emitter area and the junction spacing are known. The data shown in Figure 1 is replotted in Figure 4 to show $100/\alpha_{cb}$ as a function of emitter-current density. The curves in Figure 4 illustrate the difference between the units. The values of $\sigma_e L_e$ obtained from these curves were approximately 0.6 mho for pure indium, 2 mhos when gallium is added, and 6 mhos for aluminum alloys. The values for indium and gallium alloys are relatively consistent, having a spread of about two to one, but wider variations are observed in aluminum alloys. Although values of $\sigma_e L_e$ as high as 30 mhos have been observed, it is felt that 6 mhos is a fairly typical figure.

DISCUSSION

The use of these alloys permits a given p-n-p geometry to be used at much higher currents than previously considered practical. The alloys are very useful, therefore, in power transistors for audio output stages, switching service, and the like. Because high current amplification factor values are maintained to high current levels, high-level operation with good sensitivity and low distortion is possible. With these alloys, it is also possible to make good emitters on low-resistivity base layers, and thus to improve high-frequency devices. A less obvious advantage concerns p-n-p and n-p-n transistors which are symmetrical in electrical characteristics. If two devices are identical in all respects (dimensions, conductivities, etc.) except that one is n-p-n and the other p-n-p, current amplification factor will decrease less rapidly with increasing emitter current in the n-p-n unit by the square of the ratio of electron mobility to hole mobility (4 in germanium).⁴ It is desirable, therefore, to use a higher value of $\sigma_e L_e$ in the p-n-p transistor than in the n-p-n unit so that true complementary symmetry will be maintained at high currents. The flexibility introduced by the new p-type alloys permits closer matching of characteristics.

ACKNOWLEDGMENT

In conclusion, the authors would like to express their appreciation to W. M. Webster, both for valuable discussion and suggestions concerning the problems, and for editorial assistance in the composition of the paper.

UNIFORM PLANAR ALLOY JUNCTIONS FOR GERMANIUM TRANSISTORS*

BY

C. W. MUELLER† AND N. H. DITRICK‡

Summary—In the alloying process previously used, for example in germanium p-n-p junction transistors, wetting and alloying proceed simultaneously. This often produces a rounded junction whose shape, area and penetration are not adequately controlled for close-spaced transistor devices. Techniques are described which, by separating the wetting from the alloying steps, achieve a control over junction geometry not heretofore realized. These techniques permit the alloy transistor to be economically exploited to considerably higher frequencies and constitute a major advance in junction preparation.

Uniform wetted areas are obtained in a low-temperature soldering operation using a small amount of zinc in the indium dot material and a liquid flux. Control of the dot material volume, alloying temperature, and crystal orientations provide for uniform penetration during the alloying process in an atmosphere chosen to restrict further spreading. The dense (111) plane of the germanium wafer is used to provide a planar junction front. By this means an inherent structural property of the crystal is utilized to provide a flat junction front independent of minor variations in the physical environment. With these techniques junctions can be made that are flat to within $\frac{1}{2}$ micron (0.02 mil) over 90 per cent of their diameter.

A slow cooling rate provides for uniform recrystallization of the dissolved germanium. The uniform recrystallized region requires less etching and gives improved electrical performance.

INTRODUCTION

THE alloy junction has been widely used in audio transistors where a rounded junction shape can be accepted without serious undesirable effects. However, for many reasons, flat parallel junctions would be preferred. Flat parallel junctions are especially important to improve the uniformity of characteristics and to facilitate construction of transistors with small base widths. This paper describes new techniques which are believed to constitute a major advance in the alloy junction art and which achieve a control over the junction geometry not heretofore realized by the alloy process. By the use of these new techniques, junctions can be made that are flat within $\frac{1}{2}$ micron (0.02 mil) over 90 per cent of their diameter.

At present, the method most generally used for making alloy junc-

* Presented at the I.R.E.-A.I.E.E. Conference on Semiconductor Research, Philadelphia, Pa., June 22, 1955.

† RCA Laboratories, Princeton, N. J.

‡ RCA Semiconductor Division, Harrison, N. J.

tions¹ is to position an impurity dot on the base wafer and fire the assembly in a reducing atmosphere. In this process, the dot material first wets at one point from which point alloying and wetting progress simultaneously. Thus, the dot penetrates and spreads out at the same time and a curved junction front as shown in cross section in Figure 1 results. The final shape of the junction front can be altered somewhat by changing the temperature during the process cycle or applying weights to the dots. However, as long as alloying and wetting take place at the same time, it is extremely difficult, if not impossible, to make a truly flat junction. The important feature of the new technique is that the present one-step process is separated into a three-step process: (1) the dot material is caused to wet a certain area of the

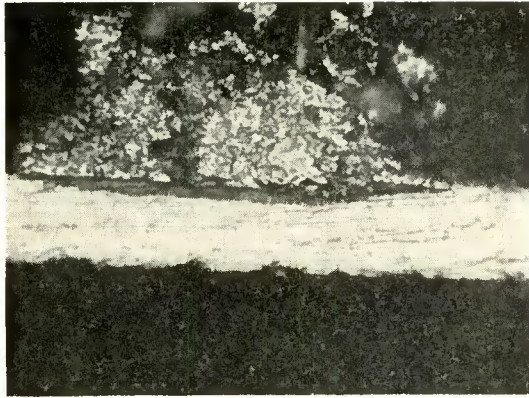


Fig. 1—Cross-section of p-n alloy junction diode.

base wafer; (2) the dot material is alloyed into the base wafer without further wetting; (3) the dissolved germanium with a small amount of dot material is recrystallized upon the base wafer. Each of these steps is important and will be discussed in order. The new technique has been applied to p (indium-rich) dot material on n germanium with about 10,000 edge dislocations per square centimeter, and the description that follows is applicable thereto. Similar techniques to those to be described can be employed for other types of dot materials and semiconductors.

WETTING AND SOLDERING

Good wetting over the entire dot area is a prerequisite for obtaining uniform planar junctions. To prevent appreciable alloy penetration

¹R. R. Law, C. W. Mueller, J. I. Pankove, and L. D. Armstrong, "A Developmental Germanium P-N-P Junction Transistor," *Proc. I.R.E.*, Vol. 40, pp. 1352-1357, November, 1952.

from taking place during the wetting process, this operation must be carried out at a low temperature, say 300° to 350° C, for an indium-rich material. At these low temperatures, hydrogen is no longer useful as a flux and other fluxes must be used. The flux must clean the surface to permit wetting and also reduce the molten liquid surface tension. The dot material then flows out over a well-defined reproducible area. Any residual products of the flux must be either removed by subsequent cleaning or must produce no deleterious effects in the final junction. Wetting is also dependent upon the dot material, and alloys of indium with certain others metals have been found to be superior to pure indium. Although the art of soldering is old, adequate theories or data are not available to explain the various wetting properties. This subject has been surveyed by Bondi.²

A liquid flux containing zinc chloride, similar to that used by tin-smiths for decades, was employed with some success in wetting indium to germanium. It has good wetting properties, but dissolves a considerable amount of indium when heated. The dissolved indium is then deposited as a thin spotty layer around the dot periphery. This condition, aptly called "measles," can cause death or crippling illness to the junction and in any event causes penetration over an uncontrollable area during the subsequent alloying step. One possible solution to the problem is to use a different flux, but no flux other than those containing ZnCl₂ has been found which will cause pure indium to wet germanium satisfactorily at about 300° C. However, if 1 per cent zinc is added to the indium, the wetting properties are improved. Zinc is a p-type impurity and does not change the electrical characteristics of the junction. However, the better wetting properties permit the use of a weak flux to obtain satisfactory wetting at 300° C. A suitable nonmetallic flux is the following:

Ammonium chloride	— NH ₄ Cl	2 grams
Hydrazine monohydrobromide	— N ₂ H ₄ ·HBr	2 grams
Methanol	— CH ₃ CH	10 cc
Water	— H ₂ O	5 cc
Glycerin	— C ₃ H ₅ (OH) ₃	1 cc

This flux dissolves less indium and avoids the difficulties mentioned above when zinc chloride is used. Some of the commercial fluxes as for instance Diveco 521* also work reasonably well in this respect.

² A. Bondi, "The Spreading of Liquid Metals on Solid Surfaces," *Chemical Review*, Vol. 52, pp. 417-458, 1953.

* Product of Division Lead Company, Chicago, Illinois.

The details of the wetting or soldering operation are as follows:

(1) The 1 per cent zinc-indium alloy is made into balls of the desired volume.

(2) The balls are etched in a 1 per cent HCl solution for three minutes, then washed in deionized water. Rinsed in methanol and dried.

(3) The balls are placed in the previously described nonmetallic flux, the excess flux drained off and then placed on the germanium wafer in an anodized aluminum jig. (Jigs are used only during the soldering operation.)

(4) The assembly is placed in a furnace with a pure dry hydrogen atmosphere, heated rapidly to 340° C and held there for 3 minutes. (This firing may also be done in air with reasonable success.)

(5) The germanium wafer is now washed in a 10 per cent HCl solution and then rinsed in a deionized water solution containing a few drops of Triton X-102* wetting agent.

With the above processing, the dots are firmly soldered to the germanium, and by a process of alloying, a small amount of germanium is taken into solution by the zinc-indium. The initial penetration is about 0.1 mil.

It is important to have some means of evaluating the wetting-soldering operation. The standard technique for doing this is to remove the dot material from the germanium by dissolving the dot with hydrochloric acid. (This does not attack the germanium.) The exposed surface structure is then examined microscopically for unwetted areas. This technique is tedious and difficult to interpret exactly. A refinement of this technique using preferential crystallization of germanium makes the interpretation and absolute evaluation more definite. A germanium wafer with its face about 10 degrees off the (111) crystal plane is used for these tests. The recrystallized germanium surfaces follow the (111) faces so there will be a 10-degree difference between the surface planes of the recrystallized area and the unwetted area. Thus, if vertical illumination is used for the examination and if the surface is adjusted so light is reflected into the lens from the germanium wafer surface, all unwetted areas will be bright and easily detected. Figure 2 shows the application of this technique to accentuate an unwetted area.

ALLOYING

In the alloying operation, the dot material penetrates the germanium wafer. It is generally desirable to arrange the alloying

* Product of Rohm and Haas Resinous Products Division, Phila., Pa.

condition so that it is an equilibrium process in which case the depth of penetration is independent of time of alloying. The depth of penetration is determined by alloying temperature, dot volume, and wetted area with the aid of standard phase diagrams. The dot volume and wetted area are so chosen that the wetting angle between the dot and germanium surfaces is such that further spreading due to liquid forces is minimized. To prevent further wetting during alloying, a neutral or slightly oxidizing atmosphere is desirable.

Indium alloying into germanium is a dissolving process similar in many respects to etching of germanium by acid. The rate of penetration is different for the various crystal planes so that the crystallographic orientation of the germanium wafer is important. The (111) crystallographic plane (see Figure 3) is most densely populated and



Fig. 2—Recrystallized region on an off-axis crystal.

the atoms in these planes are tied together by 3 bonds. The single bond (pointing upward in Figure 3) is most easily removed, thus giving penetration principally by the peeling off of layers. The (111) plane, therefore, acts as a natural leveling means to flatten out the alloying front. Better leveling action is obtained if near-equilibrium conditions prevail. For this reason, a gradual increase in temperature is desirable; 20° C per minute from 300° C to the final temperature is satisfactory.

In a germanium crystal there are other (111) planes that can act to resist alloy penetration. These planes can be located by remembering that the 4 bonds of each atom of Figure 3 point in a [111] direction and the location of the planes are then perpendicular to these directions. A set of planes will then intersect to form a truncated pyramid

as sketched in Figure 4a. Figure 4b shows the top view of a junction in which the triangular shape is evident. If a junction is sectioned along the place indicated in Figure 4a, it should intersect the bottom plane and be perpendicular to the right (111) plane. The line of intersection should include a 110-degree angle. Figure 4c shows such a cross-section with the correct angle of 110 degrees. The left intersection is rounded because the original round liquid front and the sharp angle of the (111) planes are incompatible.

The highly restrictive action of the (111) plane is shown in Figure 5a with a corresponding pictorial sketch in Figure 5b. Here the alloy-

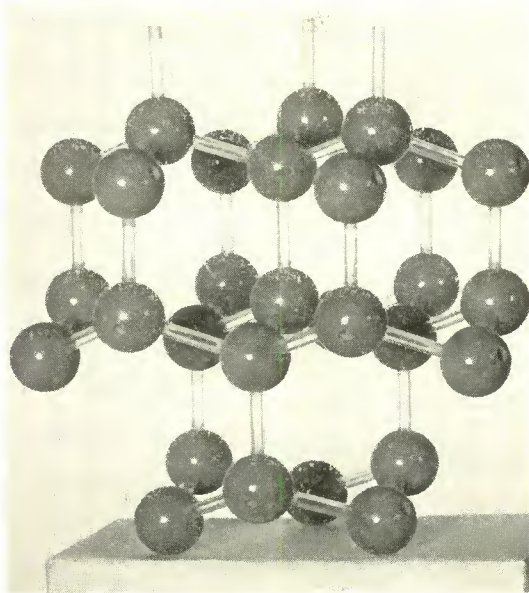
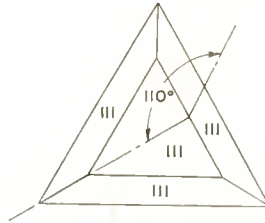


Fig. 3—Model of germanium crystal lattice.

ing was done on a crystal 9 degrees off axis. The resulting junction was flat but at the corresponding 9-degree angle with the surface.

The restrictive influences of the side (111) planes have a deleterious effect if there are unwetted spots. Where the (111) planes are well defined, they tend to prevent the undercutting of an unwetted section on the triangular sides and cause the unwetted region to propagate itself. Such an unwetted spot is shown in Figure 6. Note that the junction is flat on both sides of the unwetted area.

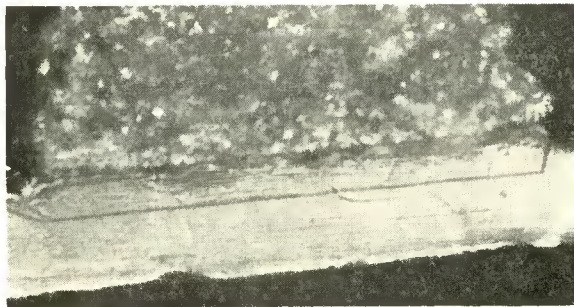
The success of this new technique in obtaining flat junctions can be seen in Figure 4c. No deviations can be detected in the bottom of the junction when compared with the microscope cross hair at a mag-



a. Sketch of (111) planes in solid.



b. Top view of indium dot showing triangular shape.



c. Cross section of p-n junction.

Fig. 4—Influence of (111) planes on wetting.

nification of 480 times. This degree of flatness is convincing evidence that the junction surface is determined by a crystal plane. In experimental lots of six units, flat junctions have been made that showed a variation of ± 0.025 mil in the location of the junction. Thus, not only do these new techniques provide for microscopically flat junctions, but also for precise control of their location.

Junction sectioning as shown in Figure 4 was very useful in evaluating the new alloying process. The major requirement of a cross-

sectioning method in addition to showing a true high-definition picture is that the method be fast so that a large number of samples can be readily examined. An improved method for rapidly exposing junctions was developed and proved to be an important tool. Details are given in the Appendix.

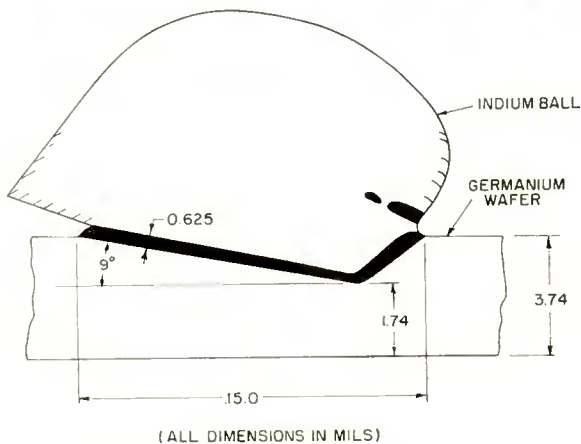


Fig. 5—Effect of crystal orientation.

RECRYSTALLIZATION

Recrystallization of the dissolved germanium back upon the base wafer as a good single crystal is the final step in the formation of a junction. For greater uniformity and crystal perfection, recrystallization should proceed on a near equilibrium basis. A gradual decrease in temperature is required; a 20°C reduction per minute has been satisfactory.

When the temperature is decreased gradually, substantially all the dissolved germanium is redeposited on the base and a uniformly thick recrystallized region as shown in Figure 4c is obtained. Dendritic growth, a potential source of noise, is also eliminated. The thin recrystallized end regions obtained in the single step alloying process (see Figure 1) are not present. The usual heavy etching used to remove these thin regions is no longer required. Another result of the gradual decrease in temperature is the absence of germanium crystallites scattered through the resolidified indium. This makes the connection of wire leads to the dots considerably easier.

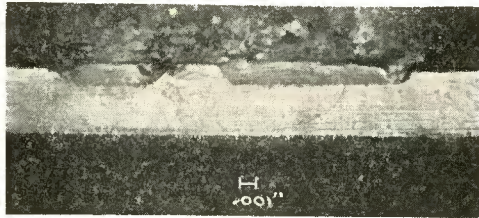


Fig. 6—p-n junction showing an unwetted area.

CONCLUSIONS

Junctions made by the three-step process outlined have the following desirable characteristics:

- (1) Flat bottom surface.
- (2) Exactly defined depth and area.
- (3) Uniformly thick recrystallized regions.
- (4) Absence of thin end regions and dendritic growth.
- (5) Absence of germanium crystallites in the dots.

The net result of these characteristics is a uniform well-defined junction with considerably improved electrical properties. Thus, the upper frequency limit to which the alloy transistor can be economically exploited is considerably extended.

ACKNOWLEDGMENT

Contributions by L. Pensak, especially to the soldering technique, are gratefully acknowledged. Discussions with H. Kettering on chemical problems were very valuable. The skill of Mrs. E. Moonan in preparing and sectioning a great many samples expedited the progress of the work.

Appendix — JUNCTION SECTIONING TECHNIQUE

To prepare a germanium junction for sectioning, it is firmly mounted on a suitable stem and lead wires are attached to the indium dots. No encapsulant or potting material is necessary, thus speeding up the process greatly.

The mounted pellet assembly is then clamped in the sectioning jig, Figure 7, with the free end of the germanium crystal down through the slot in the jig. A piece of No. 1 metallographic paper is placed on a smooth flat surface with the abrasive side up. Two paper strips are placed on the paper with their edges parallel and about $\frac{1}{2}$ inch apart. The jig is then placed on the paper strips so that the jig body itself is on the paper strips, but the slot is over the abrasive between the

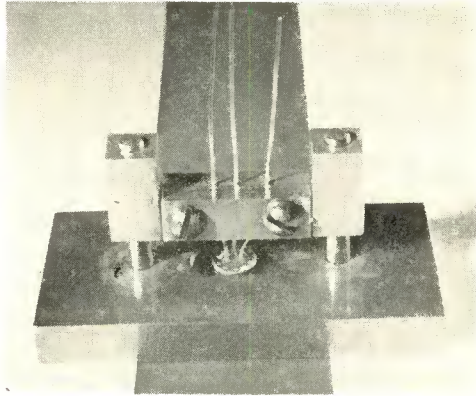


Fig. 7—Sectioning jig.

paper strips. The jig is then moved along the paper strips with the weight of the jig slide holding the germanium down against the abrasive in one direction of travel and with the slide raised as the jig is moved in the other direction. The cutting is done in one direction only in order to obtain a plane surface over the germanium wafer. When the germanium wafer is ground down to within 5 or 6 mils of the point where the junction shapes are to be examined, the No. 1 metallographic paper is replaced by No. 0 emery and the grinding procedure continued through successively finer paper down to 4/0. The final polish is done on a glass plate using Linde* A aluminum oxide powder mixed with water. The jig is used directly on glass with no paper strips this time. The polishing strokes must be in the same direction as was used for grinding. A highly polished surface is not

* Trademark of Linde Air Products Co., New York, N. Y.

necessary if the copper plating technique described below is used to increase contrast.

When the polishing is completed, the transistor is removed from the jig and washed thoroughly with water. It is then etched for about one second in a mixture of 5 parts nitric acid, 5 parts hydrofluoric acid and 2 parts water. After rinsing with water, it is connected in the circuit shown in Figure 8 and immersed in a solution of $\text{Cu}(\text{NH}_3)_4(\text{OH})_2$ (with just enough NH_4OH to clear the solution) contained in a copper cup.² Copper is selectively plated on the p-type germanium regions by depressing the push button for a total of about three seconds. This is normally done by using three one-second pulses separated by an

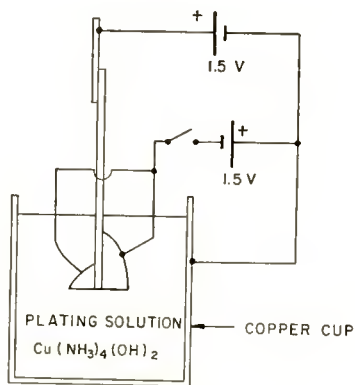


Fig. 8—Plating circuit.

interval of a few seconds to prevent depletion of the electrolyte near the germanium.

The unit is then washed with water and dried. The junction contours can now be seen by viewing the transistor through a microscope having vertical illumination. The junction locations may be seen both as a color difference and as a fine line caused by selective electrolytic etching at the junction interface.

By use of the described procedure, a satisfactory sample can be prepared in about 15 minutes. Multiple jigs that hold three units may also be used.

* The resistivity of the plating solution is 600 to 800 ohm centimeters.

MINIATURE LOUDSPEAKERS FOR PERSONAL RADIO RECEIVERS

BY

JOHN C. BLEAZEY, JOHN PRESTON, AND EVERETT G. MAY

RCA Laboratories, Princeton, N.J.

Summary—This paper presents two small experimental loudspeakers of the same general design, suitable for use in personal radio receivers. The design of the magnetic structure is unconventional in that the loudspeaker cone housing and the magnet occupy the same space, and the over-all loudspeaker depth is thereby reduced. The vibrating system of the loudspeaker is conventional so that the directional characteristics, distortion, and frequency response are, in general, similar to a completely conventional loudspeaker of the same diameter.

Some general design considerations applicable to this type loudspeaker are discussed, together with a chart summarizing these design considerations.

INTRODUCTION

WITH the present trend toward personal radio receivers of smaller size and weight, and with the use of transistors in such receivers, the size and weight of the loudspeaker becomes increasingly important. The major design problem in this type loudspeaker is that of balancing cubical content against sensitivity; of a secondary order, within reasonable limits, are frequency response, distortion, weight, etc. The loudspeaker designs presented in this paper result in a minimum dimension in depth, and use an internal magnet well shielded by the magnetic structure, so that the possibility of saturating the ferrite core of the receiver antenna by the magnetic field of the loudspeaker should be reduced.

Two experimental loudspeakers of the same general design are presented: one, $2\frac{1}{2}$ inches in diameter; the other, $2\frac{1}{8}$ inches in diameter. Experimental results on each loudspeaker are presented so that for a given design personal-radio receiver, the most suitable loudspeaker may be selected.

THEORY

A consideration of the limitations imposed upon the loudspeaker by the electrical and acoustical circuits of the radio receiver leads to some interesting results in determining the optimum high- and low-frequency cutoff of the loudspeaker.

Considering the low-frequency cutoff, the mechanical circuit of the

loudspeaker operating under free-field conditions is shown in Figure 1.¹

The total mechanical impedance in mechanical ohms, of the vibrating system at the voice coil is

$$Z_{MT} = r_{MS} + r_{MA} + j\omega m_C + j\omega m_A + \frac{1}{j\omega C_{MS}}$$

where m_C = mass of cone and voice coil,
 C_{MS} = compliance of the suspension system,
 r_{MS} = mechanical resistance of the suspension system,
 m_A = mass of the air load, and
 r_{MA} = mechanical resistance of the air load;

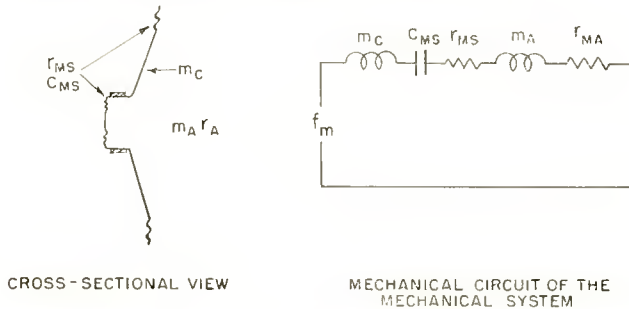


Fig. 1—Cross-sectional view of the loudspeaker in free space. In the mechanical circuit: m_C = mass of cone and voice coil. C_{MS} = compliance of the suspension system. r_{MS} = mechanical resistance of the suspension system. m_A = the mass of the air load. r_{MA} = the mechanical resistance of the air load. f_m = the mechanomotive force in the voice coil.

and at resonance,

$$0 = j\omega m_C + j\omega m_A + \frac{1}{j\omega C_{MS}} \quad \text{mechanical units,}$$

$$0 = \frac{-\omega m_C}{S_C^2} - \frac{\omega m_A}{S_C^2} + \frac{1}{\omega C_{AS}} \quad \text{acoustical units,}$$

C_{AS} = compliance of the suspension system, and

S_C = area of the cone in square centimeters = 25.6.

In the above equation the mass of the cone and the mass of the air load may be determined with a reasonable degree of accuracy. The compliance of the suspension system may then be determined from the

¹ H. F. Olson, *Elements of Acoustical Engineering*, 2nd Edition, D. Van Nostrand, New York, N. Y., 1947.

resonant frequency of the loudspeaker in free space, which is 352 cycles per second.

The mass of the air load, m_a , may be determined as follows: It is found that (Reference (1), page 92)

$$X_A = .273 \text{ acoustical ohm.}$$

For air load on both sides of the cone, $X_A = .546$,

$$\begin{aligned} X_A &= \frac{\omega m_a}{S_C^2} \\ m_a &= \frac{.546}{2\pi \times 352} \times (25.6)^2 \\ &= .16 \text{ gram.} \end{aligned}$$

Mass of the cone and voice coil, $m_C = .390$ gram.

The compliance of the suspension system, C_{AS} , may be determined as follows. At resonance (352 cycles per second)

$$\begin{aligned} 0 &= j\omega m_a + j\omega \frac{m_C}{S_C^2} + \frac{1}{j\omega C_{AS}}, \\ 0 &= -.546 - \frac{2\pi \times 352 \times 390}{655} + \frac{1}{2\pi \times 352 C_{AS}}, \\ C_{AS} &= 2.44 \times 10^{-4} \text{ cm}^5/\text{dyne.} \end{aligned}$$

The mechanical circuit of the loudspeaker mounted in closed case ($4 \times 1 \times 2\frac{1}{16}$ inches) is shown in Figure 2.

The total mechanical impedance in mechanical ohms of the vibrating system at the voice coil is

$$Z_{MT} = r_{MS} + r_{MA} + j\omega m_C + j\omega m_A + \frac{1}{j\omega C_{MS}} + \frac{1}{j\omega C_{MB}},$$

where C_{MB} = the compliance of the receiver case.

At resonance

$$\begin{aligned} 0 &= j\omega m_C + j\omega m_a + \frac{1}{j\omega C_{MS}} + \frac{1}{j\omega C_{MB}} \quad \text{mechanical units,} \\ 0 &= -\frac{\omega m_C}{S_C^2} - \frac{\omega m_a}{S_C^2} + \frac{1}{\omega C_{AS}} + \frac{1}{\omega C_{AB}} \quad \text{acoustical units.} \end{aligned}$$

The acoustical capacitance due to the box,

$$C_{AB} = \frac{V}{\rho C^2},$$

where V = volume, in cubic centimeters,
 ρ = density of air, in grams per cubic centimeter, and
 C = velocity of sound, in centimeters per second.

$$\begin{aligned} C_{AB} &= \frac{176.5}{.0012 \times (34400)^2} \\ &= 1.24 \times 10^{-4} \text{ cm}^5/\text{dyne.} \end{aligned}$$

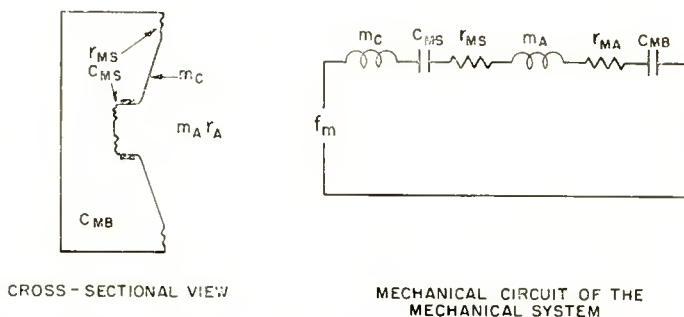


Fig. 2—Cross-sectional view of the loudspeaker in enclosed cabinet. In the mechanical circuit: m_C = mass of cone and voice coil. C_{MS} = compliance of the suspension system. r_{MS} = mechanical resistance of the suspension system. m_A = the mass of the air load. r_{MA} = the mechanical resistance of the air load. C_{MB} = the compliance of the receiver case. f_M = the mechanomotive force in the voice coil.

It is interesting to note that the compliance of the receiver case is approximately one half that of the suspension system, or the stiffness due to receiver case is approximately twice that due to the loudspeaker suspension system.

The mechanical circuit of the loudspeaker mounted in a closed case is shown in Figure 2.

Calculating the resonance of the loudspeaker mounted in the closed case:

$$\begin{aligned} 0 &= j\omega m_C + j\omega m_A + \frac{1}{j\omega C_{MS}} + \frac{1}{j\omega C_{MB}} \quad \text{mechanical units,} \\ 0 &= -\frac{\omega m_C}{S_C^2} - \frac{\omega m_A}{S_C^2} + \frac{1}{\omega C_{AS}} + \frac{1}{\omega C_{AB}} \quad \text{acoustical units.} \end{aligned}$$

$$\omega^2 = \frac{S_c^2}{m_c + m_A} \left(\frac{1}{C_{AS}} + \frac{1}{C_{AB}} \right),$$

where

m_c = mass cone and voice coil = .390 gram,

m_A = mass air load on cone = .16 gram,

C_{AS} = compliance suspension system = 2.44×10^{-4} cm⁵/dyne,

C_{AB} = compliance of receiver case = 1.24×10^{-4} cm⁵/dyne.

$$\omega^2 = \frac{(25.6)^2}{.390 + .16} \left(\frac{10^4}{2.44} + \frac{10^4}{1.24} \right),$$

$$\omega = 3807,$$

$$f = 606 \text{ cycles/sec.}$$

This compares with an experimentally determined resonance of 595 cycles per second when the loudspeaker is mounted in the small receiver case.

If it were possible to increase the compliance of the loudspeaker suspension system, it is interesting to see how much this will lower the resonance of the loudspeaker when it is mounted in the receiver case.

From practical considerations it is difficult to increase the compliance of the loudspeaker suspension; however, let it be assumed this compliance has been increased by a factor of 1.5;

$$C_{AS} = 2.44 \times 10^{-4} \times 1.5 = 3.66 \times 10^{-4} \text{ cm}^5/\text{dyne},$$

$$\omega^2 = \frac{655}{.390 + .16} \left(\frac{10^4}{3.66} + \frac{10^4}{1.24} \right),$$

$$\omega = 3587,$$

$$f = 571 \text{ cycles/sec.}$$

Increasing the compliance of the loudspeaker suspension system by a factor of 1.5 would result in reducing the resonant frequency of the over-all system of about 35 cycles.

If the compliance of the receiver case is now increased by increasing the case volume by a factor of 1.5,

$$C_{AB} = 1.24 \times 10^{-4} \times 1.5 = 1.86 \times 10^{-4} \text{ cm}^5/\text{dyne}.$$

$$\omega^2 = \frac{655}{.390 + .16} \left(\frac{10^4}{2.44} + \frac{10^4}{1.86} \right),$$

$$\omega = 3360,$$

$$f = 535 \text{ cycles/sec.}$$

Increase the compliance of the receiver case by a factor of 1.5 would result in reducing the resonant frequency of the over-all system by about 71 cycles per second.

From the above considerations it is evident that the resonant frequency of the loudspeaker is controlled largely by the compliance of the receiver case, and to a lesser extent by the compliance of the loudspeaker suspension system.

LOUDSPEAKER MOUNTED IN OPEN CASE

If the loudspeaker is mounted in a receiver case, the back of which is perforated so as to be essentially open, it is evident that at very low frequencies the sound from the front and the sound from the back of the loudspeaker are out-of-phase and the effective output is exceedingly low. Where the path difference from front to back is one half wavelength, the sound from the front and back of the loudspeaker is in phase and the response will be increased by 6 decibels.

Since the dimensions of this particular receiver case are small, the path length corresponding to a half wavelength occurs at approximately 1,000 cycles per second. Below this frequency the response falls off at approximately 6 decibels per octave to resonance, at which point it falls off at 18 decibels per octave.

HIGH-FREQUENCY CUTOFF

The high-frequency cutoff of the radio receiver is determined by the i-f transformers, and in general is usually limited to 4,000 to 5,000 cycles per second. It is also desirable that the loudspeaker cut off at approximately 4,000 cycles per second and have very little output at 6,000 cycles per second. This is advantageous in maintaining good receiver selectivity, that is, eliminating annoying interference between stations.

Frequency-response curves and listening tests indicate that the performance of the loudspeaker for this volume enclosure is best when operating in a closed case. This is the result of a uniform response down to 580 cycles per second followed by a sharp cutoff.

When the loudspeaker is completely enclosed, the response is greater in the region of 580 cycles per second. Listening tests indicate this difference in the feeling of more apparent low frequencies.

LOUDSPEAKER DESIGN

Figure 3 shows the general design of the new loudspeaker together

with the over-all dimensions. As shown by Figure 3, the cone and voice-coil assembly are conventional and the front of the loudspeaker cone is the acute angle of the cone. The magnetic structure of the loudspeaker is somewhat unconventional in that the vibrating system and magnetic structure use the same depth.

Table I lists some of the more significant design considerations which may be involved in the production of this loudspeaker. The table also shows the general performance of this type loudspeaker using various designs, that is, varying the over-all diameter of the loudspeaker, the diameter of the magnet and voice coil, the thickness

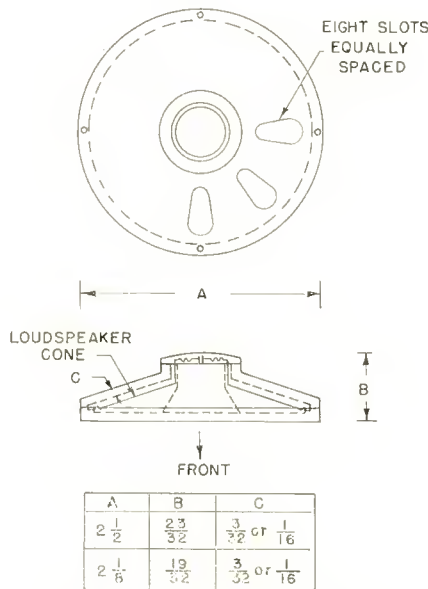


Fig. 3—Loudspeaker assembly.

of the magnetic structure, and the consideration of straight magnet versus tapered magnet. The flux-density figures were, in general, taken from one experimental magnetic structure and, therefore, cannot be taken as absolute since variations in magnet material, assembly techniques, etc., have not been averaged out.

Figure 4 shows a drawing of the two loudspeakers discussed in this paper together with a production loudspeaker, which is referred to in Table I as a comparison with respect to performance. It is readily apparent from Figures 4 and 5 that the new loudspeakers occupy less volume than the production loudspeaker, and that the depth has been

Table I—Loudspeaker Design Considerations and Performance Data

2-Inch Diameter Loudspeaker						
	.566" O.D. Voice Coil 3/32" Return Path		.485" O.D. Voice Coil 3/32" Return Path		Magnetic Return Path .568" V.C. Tapered Magnet	
	Straight Magnet	Tapered Magnet	Straight Magnet	Tapered Magnet	3/32" Thick	1/16" Thick
*Sensitivity DB		0		-1		
Frequency Response		400-4,500		400-4,500		
Flux Density Gauss	7,000	7,500	6,400	6,900	7,500	7,300
Weight—Grams		118		117	118	90

1 1/8-Inch Diameter Loudspeaker				
	.568" O.D. Voice Coil Magnetic Structure Not Shown		.485" O.D. Voice Coil Magnetic Structure Figs. 7, 8	
	Straight Magnet	Tapered Magnet	Straight Magnet	Tapered Magnet
*Sensitivity DB		-2 1/2		-1 1/2
Frequency Response		350-7,000		350-7,000
Flux Density Gauss	6,800	6,750	6,750	6,900
Weight—Grams	69	73	74	77

* Approximate sensitivity using the production loudspeaker as a reference level of 0-DB.

considerably reduced. Figure 5 is a photograph of the same loudspeakers shown in Figure 4 and gives a further indication of relative size. Figure 6 shows the 2 1/2 inch diameter loudspeaker with the top plate removed to reveal construction.

The centering suspension of the loudspeaker may be constructed as shown in Figure 4 or may be modified to extend completely across the air gap. In the latter case the centering suspension will then act as a combination centering suspension and dust screen, to protect the air gap from foreign material such as dirt and small magnetic chips.

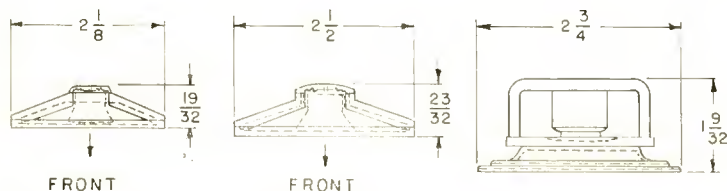


Fig. 4—Relative size of the two experimental loudspeakers and the production loudspeaker discussed in this paper.



Fig. 5—The two experimental loudspeakers and a commercial loudspeaker.



Fig. 6—The 2½ inch diameter loudspeaker with the top plate removed.

ASSEMBLY

The assembly of this loudspeaker varies somewhat from a conventional loudspeaker, but in general does not present any particular problems. First, the voice-coil and cone are cemented together in an appropriate jig; this assembly is then dropped over the magnet and bottom plate, and properly spaced. Next, the cone is cemented to the small step on the bottom plate, the loudspeaker top plate is placed on top of the cone, properly spaced, and screwed to the bottom plate. Finally, the loudspeaker is magnetized and the centering suspension and dust cover are installed.

The straight magnet is preferable from an assembly standpoint in that the lower limit to the motion of the loudspeaker cone is eliminated.

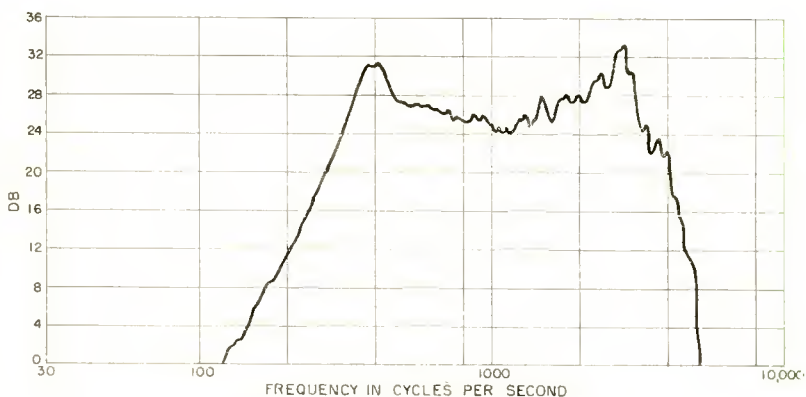


Fig. 7—Production loudspeaker on infinite baffle.

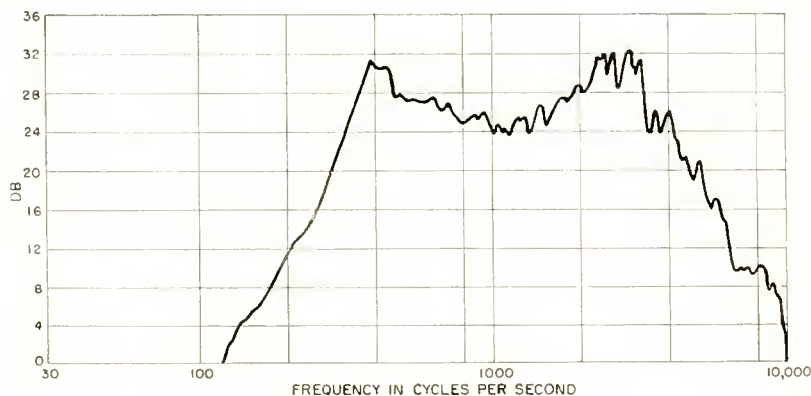


Fig. 8—2½ inch diameter loudspeaker, 0.568 inch diameter voice coil, tapered magnet on infinite baffle.

PERFORMANCE

The frequency response characteristic of the production loudspeaker is shown in Figure 7; this is included as a reference for sensitivity and frequency response. Figures 8 and 9 are frequency-response curves of the new loudspeakers described in this paper; all of these curves were taken using 0.015-watt power input and, in general, are self-explanatory.

As shown by Figures 10 and 11, the 2⅛ inch diameter loudspeaker extends to a higher frequency range than the large loudspeaker. Since, in general, this is not desirable, a lower cutoff frequency may be obtained by increasing the cone-included angle, or by maintaining the same angle, and introducing a compliance at the apex of the cone.

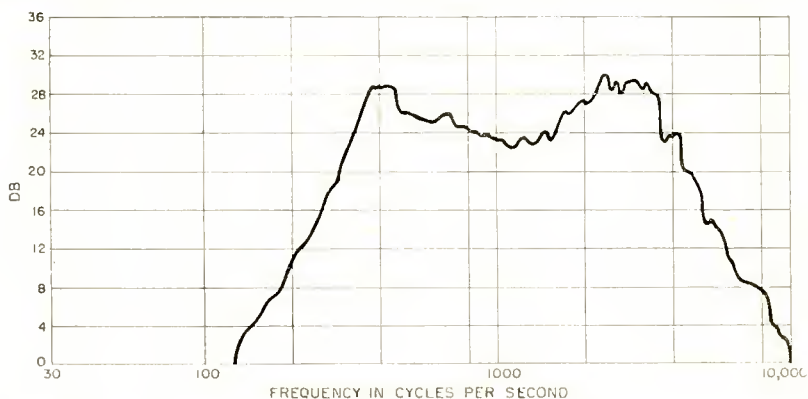


Fig. 9—2½ inch diameter loudspeaker, 0.485 inch diameter voice coil, tapered magnet on infinite baffle.

It is perhaps obvious that where the ultimate in loudspeaker sen-

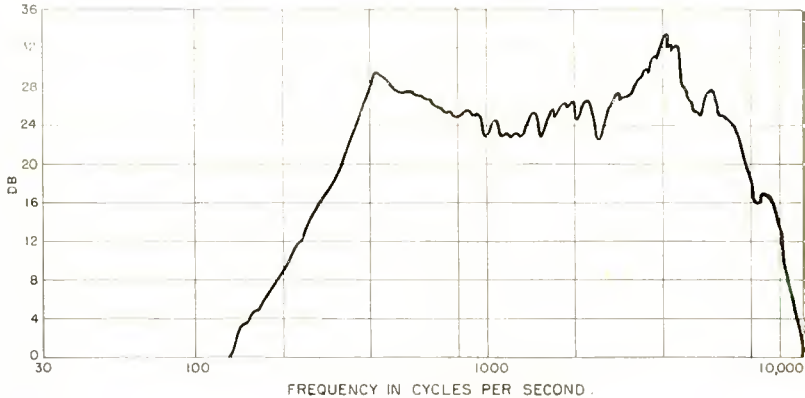


Fig. 10— $2\frac{1}{8}$ inch diameter loudspeaker, 0.485 inch diameter voice coil, tapered magnet on infinite baffle.

sensitivity is required, the larger loudspeaker is desirable; however, where the power output to the loudspeaker is ample, the smaller loudspeaker has the advantages of smaller size and less weight.

CONCLUSIONS

The design and general performance data of two new loudspeakers has been presented. The construction of these loudspeakers is such that they result in a minimum dimension in depth, and when used in a personal radio receiver should allow the over-all size of the radio set to be reduced.

The reduction in size of the loudspeakers presented in this paper has not been accomplished at the expense of the other characteristics of the loudspeaker, that is, sensitivity, frequency response and distortion.

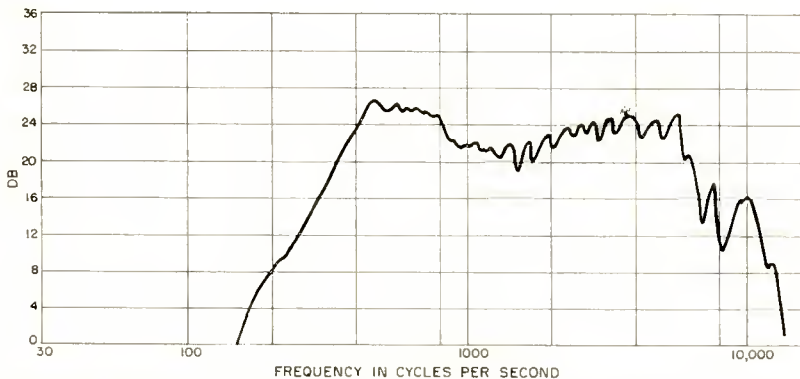


Fig. 11— $2\frac{1}{8}$ inch diameter loudspeaker, 0.568 inch diameter voice coil, tapered magnet on infinite baffle.

A VARIABLE-CAPACITANCE GERMANIUM JUNCTION DIODE FOR UHF†

BY

L. J. GIACOLETTO AND JOHN O'CONNELL

RCA Laboratories,
Princeton, N. J.

Summary—A semiconductor junction when biased in the reverse (nonconducting) direction is a capacitance which can be varied by the bias voltage. Such a voltage-variable capacitance has many possible uses. In particular automatic frequency control (a-f-c) at ultra-high frequencies (UHF) is attractive provided the electrical losses are sufficiently small. In this paper the design, construction, and measurement of a junction diode useful throughout the UHF range are considered. The diode consists of a 0.020-inch dot of indium alloyed on to a 0.002-inch-thick wafer of 0.1 ohm-centimeter *n*-type germanium and mounted with low-inductance connections. It has greater control sensitivity and better electrical characteristics than an electron reactance tube and, in addition, the operating power required by the diode is trivial in comparison with that of an electron tube. Typically, the performance at 6-volt bias is as follows: a capacitance of 38 micromicrofarads; a capacitance change of 3 micromicrofarads per volt; lead inductance of 2.6 millimicrohenries; effective series resistance of 0.5 ohm. Such a variable capacitor has a very high *Q* at the lower radio frequencies, decreasing to $Q = 17$ at 500 megacycles. Only about 1 microwatt of d-c control power is needed. A *Q* of 36 at 500 megacycles was obtained in one of the better units having a series resistance of 0.23 ohm.

GENERAL DISCUSSION

A JUNCTION of two dissimilar semiconductors constitutes, generally, a junction diode with a variety of electrical properties. If the diode is biased in the reverse (nonconducting) direction, the mobile charge carriers are moved away from the junction, leaving uncompensated fixed charges in a region near the junction. The width, and hence the electrical charge, of this region (space-charge layer) depends on the applied voltage giving rise to a junction transition capacitance whose small-signal value is shown as C_s in Figure 1. The variation of a bias voltage is accompanied by a change in current and gives rise to a small-signal conductance, g , across C_s as seen in Figure 1. At frequencies below a few hundred kilocycles, the parallel combination of C_s and g are sufficient to define the small-signal characteristics of the diode. At higher frequencies the inductance of the leads, L_o , and the series resistance of the semiconductors, r_s , become significant. The stray lead capacitance may also be significant, but in the units to be described is small enough to be neglected. Thus, the

† This material was presented at the Conference on Electron Devices, Washington, D. C., October 24-25, 1955.

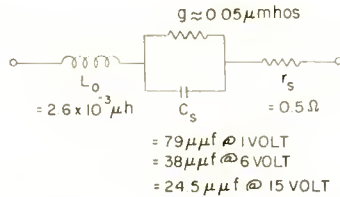


Fig. 1—Diode equivalent circuit.

complete small-signal equivalent circuit of the reverse biased diode applicable from very-low to ultra-high frequencies is as shown in Figure 1.

The factors which must be determined in the design of a diode for ultra-high frequencies are the semiconductor material, its conductivity, the junction area, the height of the semiconductor cylinder between the junction plane and the base plane of the wafer, W (see Figure 2), and the lead length. The semiconductor material is chosen to give the highest Q at high frequencies, and of presently available semiconductors, n-type germanium is well suited. The germanium conductivity should be high to decrease electrical losses but an upper limit is determined by the maximum reverse bias. The desired capacitance for a particular bias voltage determines the area of the junction. The series resistance is determined by the junction area and the dimension W of Figure 2. W should be as small as possible to decrease electrical losses, but a practical minimum value is imposed by the percentage of "short through" rejects during construction of the diodes. The diode leads should have a large diameter and short length to keep the lead inductance to a minimum.

This paper first considers the equations which govern the selection of design factors and which illuminate diode performance. Following this, the construction of a practical diode is described, and its measured

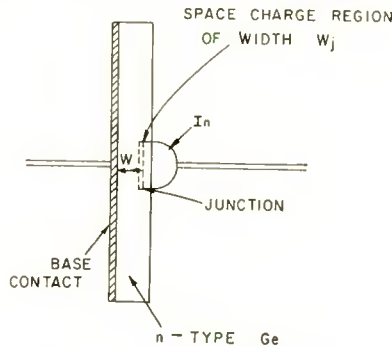


Fig. 2—Diode geometry.

performance is given. An Appendix contains the comparison of measurements with diode theory.

DESIGN RELATIONS

The semiconductor junctions to be considered herein are made by alloying indium (p-impurity) on n-germanium.¹ This process gives an abrupt transition between the p-type indium-enriched germanium and the n-type germanium so that the resulting junction operates in accordance with a theory developed by Schottky.² Similar junctions can be made by alloying n-impurities on p-germanium, or by using a different semiconductor.

Transition Capacitance

The junction diode transition capacitance can be formulated as for a conventional parallel-plane capacitor. Thus

$$C_g = \frac{K \epsilon_0}{W_j} A \quad \text{farads,} \quad (1)$$

where

K = relative permittivity = 16 for germanium,

ϵ_0 = permittivity of free space $\left(\frac{1}{36\pi} \times 10^{-9} \text{ farad/meter} \right)$

A = junction area in square meters, and

W_j = effective width of junction in meters.

The effective junction width is voltage dependent and for the case where the conductivity of the p-type indium enriched germanium is much greater than that of the n-type germanium, is

$$W_j = \sqrt{- (V_0 + V) \frac{2K\epsilon_0\mu_n}{\sigma_n}} \quad \text{meters,} \quad (2)$$

¹ R. R. Law, C. W. Mueller, J. I. Pankove, and L. Armstrong, "A Developmental Germanium P-N-P Junction Transistor," *Proc. I.R.E.*, Vol. 40, pp. 1352-1357, November, 1952.

² For a summary of Schottky's work and complete references, see J. Joffe, "Schottky's Theories of Dry Solid Rectifiers," *Electrical Communication*, Vol. 22, pp. 217-225, 1945. For details of analysis, see W. Shockley, "The Theory of P-N Junctions in Semiconductors and P-N Junction Transistors," *Bell Sys. Tech. Jour.*, Vol. 28, pp. 435-489, July, 1949.

where

$$\mu_n = \text{mobility of electrons in n-germanium in } \frac{\text{meter}^2}{\text{volt sec.}}$$

$$= 0.39 \text{ for intrinsic germanium}$$

$$= 0.30 \text{ for } \sigma_n = 1,000 \text{ mhos per meter germanium used for the present diodes,}^3$$

$$V_0 = \text{contact voltage in volts,}$$

$$V = \text{applied bias voltage in volts measured with n-germanium as reference (negative for reverse bias),}$$

$$\sigma_n = \text{conductivity of n-germanium in mhos per meter}$$

$$= 1,000 \text{ for the germanium used for the present diode.}$$

The change in diode capacitance with temperature will be negligible, provided the diode voltage is constant, since the temperature-dependent quantity in Equation (2), mobility, cancels out for doped germanium where $\sigma_n \propto \mu_n$.

The fractional change in C_s as a function of V can be formulated from Equations (1) and (2) as

$$\frac{\Delta C_s}{C_s} = - \frac{\Delta V}{2(V_0 + V)}. \quad (3)$$

The fractional change in C_s is one half the fractional change of applied voltage and is independent of diode dimensions and material properties, except that at small bias voltages the material properties may be significant in determining the contact voltage, V_0 .

Contact Voltage

The voltage, V_0 , of Equation (2) is an internal contact potential developed between the n- and p-type semiconductors. This voltage will be a few tenths of a volt negative and therefore negligible except at very small applied voltages. The contact voltage can be considered as composed of two parts: a contact voltage of the p-type germanium on intrinsic germanium; and a contact voltage of intrinsic germanium on n-type germanium. Since the p-type germanium conductivity approaches that of a metal, the first part of the contact voltage is very

³ M. B. Prince, "Drift Mobilities in Semiconductors I. Ge," *Phys. Rev.*, Vol. 93, pp. 681-687, November 1, 1953.

nearly half of the germanium voltage gap, namely, -0.36 volt. The second half of the contact voltage can be formulated analytically with the aid of usual junction equations in terms of the properties of the intrinsic and n-type germanium. The net result is a value between zero and -0.36 volt. For the diode herein described, the calculation gives a total contact voltage of -0.54 volt, which is in agreement with measurements (see Appendix).

Series Resistance

The diode series resistance, r_s , is due to the wafer of germanium. When the junction diameter is much larger than W , the distance to the base contact (Figure 2), the series resistance can be rather accurately formulated on the basis of a semiconductor cylinder of area A and height W provided that the diode is biased in the reverse direction. Thus

$$r_s = \frac{W - W_j}{\sigma_n A} \quad \text{ohms.} \quad (4)$$

W_j (Equation 2) will generally be negligible in comparison with W . The temperature dependency of r_s will be that of σ_n and will be generally small.⁴ In the temperature range of ± 100 degrees centigrade, r_s will increase about 0.6 per cent per degree centigrade increase in temperature provided $\sigma_n > 100$ mhos per meter.

The series resistance for the forward biased diode is current dependent and decreases rapidly with increasing current.

Lead Inductance

The diode lead inductance is an important factor which cannot be neglected at ultra-high frequencies. The lead inductance can be computed reasonably accurately from the formula⁵ for a straight length of wire:

$$L_0 = 5.08 l \ln \left(\frac{4l}{d} \right) \quad \text{millimicrohenries,} \quad (5)$$

where l is the length of the wire and d is the wire diameter in inches. Diodes constructed as described in this paper require interpretation in determining appropriate values of l and d , since the wire cross

⁴ P. G. Herkart and J. Kurshan, "Theoretical Resistivity and Hall Coefficient of Impure Germanium Near Room Temperature," *RCA Review*, Vol. 14, pp. 427-440, September, 1953.

⁵ Frederick E. Terman, *Radio Engineers' Handbook*, McGraw-Hill Book Co., New York, N. Y., p. 48, 1943.

section is not uniform. The bulk of the inductance will generally be due to the small wire contacting the diode dot.

Maximum Junction Voltage

The maximum reverse bias (breakdown voltage) which may be applied to a junction is determined by an avalanche breakdown phenomenon which causes a precipitous increase in the junction current. The breakdown voltage, V_B , is a function of the impurity density, N_D (impurities per cubic meter), of the semiconductor material. According to measurements⁶ on n-type germanium

$$V_B = -22 \times 10^{16} (N_D)^{-0.725} \approx -2650 (\sigma_n)^{-0.725} \text{ volts,} \quad (6)$$

where σ_n is in mhos per meter.

Q Figure of Merit

It is common practice to use Q (the ratio of series reactance to series resistance) as a figure of merit for capacitors. The diode Q_d , taking into account both series resistance and shunt conductance, is

$$Q_d = \frac{\omega C_s}{g + r_s (g^2 + \omega^2 C_s^2)}. \quad (7)$$

If the diode parameters are independent of frequency (this is a good assumption particularly in the case of r_s and C_s), Q_d has a maximum when

$$\omega = \frac{1}{C_s} \sqrt{\frac{g}{r_s} (1 + r_s g)}, \quad (8)$$

The maximum Q_d is

$$Q_d (\text{max.}) = \frac{1}{2} \left[r_s g (1 + r_s g) \right]^{-1}. \quad (9)$$

At high frequencies, where the shunt conductance can be neglected, Q_d can be determined from Equations (1), (2), and (4). The result is

$$Q_d = \frac{1}{\omega C_s r_s} = \frac{1}{\omega (W - W_j)} \sqrt{-(V_0 + V) \frac{2\mu_n \sigma_n}{K\epsilon_0}}. \quad (10)$$

⁶ S. L. Miller, "Avalanche Breakdown in Germanium," *Phys. Rev.*, Vol. 99, pp. 1234-1241, August 15, 1955.

From this equation it can be concluded that:

(a) Q_d is independent of junction area and varies inversely with frequency.

(b) For a large Q_d , σ_n should be made as large as possible — the upper limit being determined by the junction breakdown voltage, Equation (6), or by the fact that μ_n decreases as σ_n is made larger. For n-type germanium, the maximum Q_d occurs when σ_n is approximately 10,000 mhos per meter, and for this conductivity, $V_B \approx -3$ volts; W should be as small as construction techniques permit; and a large operating bias should be employed.

(c) Q_d can be increased by selecting a semiconductor material with the largest value of μ/K . Of the two commonly used semiconductor materials (germanium and silicon), n-type germanium has the largest value of μ/K . For this reason the presentation herein has centered around n-type germanium and this material is used in the diode described below.

A loss-free capacitor in series with the diode can be used as an impedance transforming means to increase the effective Q . This series combination decreases the net losses at the expense of the amount of variable capacitance. Placing a capacitor in series with the diode has other advantages such as blocking the d-c bias voltage, limiting a-c voltage across the diode, and eliminating lead inductive reactance at one frequency.

At low frequencies and when the diode is biased in the reverse direction, Q_d is determined by Equations (1) and (2) and the diode conductance, g , which is determined in practice by a leakage conductance. Thus:

$$Q_d = \frac{\omega C_s}{g} = \frac{\omega A}{g} \sqrt{\frac{K \epsilon_0 \sigma_n}{-2\mu_n (V_0 + V)}}. \quad (11)$$

Saturation Current

The saturation current is determined by the geometry and surface and volume recombination of hole-electron pairs. A more exact calculation can be carried out, but with germanium of good quality the contribution from volume recombination is small and may be neglected. Further, the contribution from the base contact surface will outweigh the contributions of the free surfaces because of its higher surface recombination velocity, s , and, also, in a structure designed for UHF, because of its proximity to the junction. The saturation current may be found by formulating an equation for the terminal current, $I = -I_s$, which flows when the diode is biased in the reverse direction.

Under these conditions the hole density at the junction will be zero and will increase approximately linearly to a value p_n at the base contact. Analytically this requires $sW/D_p \gg 1$, where D_p is the diffusion constant of holes in n-type germanium ($D_p = 44 \times 10^{-4}$ square meter per second for intrinsic germanium). It is believed that the s of the metallic base contact is large enough to satisfy the inequality if W is greater than 25 microns (0.001 inch). The actual value of s under these conditions does not enter into the calculation. The saturation current is thus determined by the hole density gradient $p_n/(W - W_j)$ and is

$$I_s = q A D_p \frac{p_n}{W - W_j} = \frac{q^2 n_i^2 \mu_n A D_p}{\sigma_n (W - W_j)} \text{ amperes,} \quad (12)$$

where q is the carrier charge ($q = 1.60 \times 10^{-19}$ coulombs) and n_i is the carrier density in intrinsic material ($n_i = 2.4 \times 10^{19}$ carriers per cubic meter for germanium at room temperature).

The magnitude of I_s together with the bias voltage, V , will determine the amount of bias power required to operate the diode in the reverse direction. I_s will increase rapidly with temperature⁷ (approximately 10 per cent per degree centigrade near room temperature) due primarily to the increase in n_i^2 .

Frequency Effects

The frequency dependencies of r_s and C_s are intimately associated with fundamental properties of the semiconductor⁸ provided the diode is biased in the reverse direction. In this event, r_s and C_s will be frequency independent as long as the semiconductor displacement current proportional to $2\pi f K \epsilon_0$ is much less than the conduction current proportional to σ . For impure germanium as used herein of conductivity, $\sigma_n = 1,000$ mhos per meter, the displacement and conduction currents become equal at $f = 1.1 \times 10^{12}$ cycles. Hence, the formulas for r_s and C_s are valid throughout the present range of interest. At higher frequencies, electrical losses due to skin resistance of the leads may be appreciable, but throughout UHF correction therefor is not required.

In the forward direction the diode performance changes rapidly with frequency and different formulas must be used.⁹

⁷ L. J. Giacoletto, "Power Transistors for Audio Output Circuits," *Electronics*, Vol. 27, pp. 144-148, January, 1954.

⁸ William Shockley, *Electrons and Holes in Semiconductors*, D. Van-Nostrand Co., Inc., New York, N. Y., pp. 199-200.

⁹ W. Shockley, *op. cit.*, pp. 309-318.

Noise

The noise associated with the diode can be determined by introducing into the equivalent circuit of Figure 1 a mean-square voltage generator, $\overline{V^2} = 4kTr_s\Delta f$, in series with r_s and a mean-square current generator, $\overline{I^2} = 2q(I + 2I_s)\Delta f$ in shunt with g . In these formulas, k is Boltzmann's constant (1.38×10^{-23} joules per degree Kelvin) and T is temperature in degrees Kelvin. These noise generators are independent of frequency when the diode is biased in the reverse direction ($I = -I_s$). A $1/f$ type of noise generator may also be significant if diode leakage is appreciable.¹⁰

CONSTRUCTION

The diode for which measurements will be given has a parallel plane geometry with axial leads, and is designed to give good performance through ultra-high frequencies. In accordance with the design relations, n-type germanium is used since this semiconductor gives better performance than p-type germanium or p- or n-type silicon. A minimum germanium resistivity of 0.1 ohm-centimeter was selected to permit operation over a useful range of bias voltages. This resistivity material will permit a bias voltage as large as 18 volts. A junction diameter of 20 mils (area of 20×10^{-6} square centimeters) was selected to achieve the desired range of diode capacitance. Lead inductance is kept small by using short, large diameter lead wires.

The completed diode is shown in the photograph of Figure 3. For comparison purposes, a standard 1N82 (K3E) UHF mixer diode is also shown.

Parts Preparation

The disassembled view of the diode showing the various component parts is shown in Figure 4. The base stud is made of Kovar[†] or Therlo^{*} to match the germanium thermal expansion and is designed so that the diode can be screwed directly to a chassis. A 0.002-inch depression on the top of this stud aids in positioning the base wafer. The depression is covered with about 0.001 inch of high purity tin-lead-antimony solder. The wafers are chemically etched to 0.002 inch thickness. The dots are punched cylinders of indium 0.015 inch by 0.015 inch diameter. The nickel wire has one end balled and coated with indium and the wire is lightly tinned with a low-melting solder. The top stud has a

¹⁰ W. H. Fonger, "A Determination of $1/f$ Noise Sources in Semiconductor Diodes and Triodes," *Transistors I*, RCA Laboratories, Princeton, N. J., 1956, pp. 239-295.

[†] Trademark of the Westinghouse Electric Corp., Pittsburgh, Pa.

^{*} Trademark of the Driver-Harris Co., Harrison, N. J.

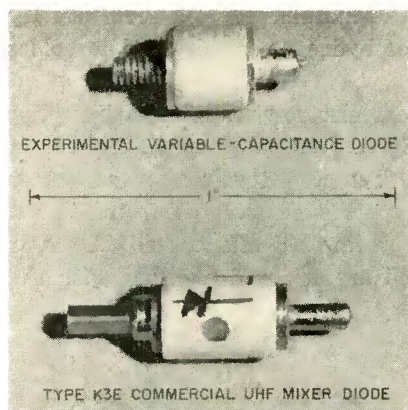


Fig. 3—Photograph of variable capacitance diode and type K3E commercial UHF mixer diode.

0.041-inch-diameter hole through the center, and the inside of this hole is tinned with the same low-melting solder. The top stud is screwed to the ceramic body and bonded in place with Araldite[†] to form a subassembly. The indium dot, germanium wafer, and base stud are also processed as a subassembly. This subassembly is made by mounting the base stud, germanium wafer, and indium dot together with the aid of carbon jigs.¹ The assembled unit is fired for five minutes at 550°C. in an atmosphere of dry hydrogen both to solder the germanium wafer to the stud and to alloy the dot into the germanium.

Assembly

A jig as shown in Figure 5 is used to facilitate assembly and etching. The brass stud ceramic subassembly is inserted and held in place with the set screw. The base stud subassembly is mounted and held in place with a set screw made of insulating material. The wire is inserted through the jig hole, adjusted so that the indium coated balled

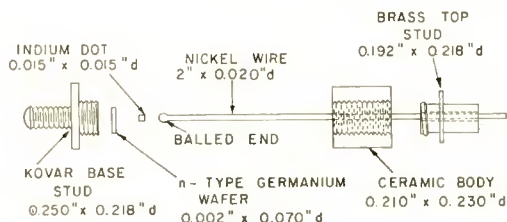


Fig. 4—Disassembled drawing of diode.

[†] Trademark of Ciba Inc., New York, N. Y.

end is contacting the indium dot, and then held in place with the set screw. A hot jet of hydrogen gas is used to solder the wire and dot together.

The diode is next electrolytically etched by dipping the base stud end only of the jig into the electrolyte. After etching, the diode is washed, dried, and then coated with a protective coating. The threads of the base stud are next coated with Araldite and the brass stud ceramic subassembly lowered and threaded onto the base stud. The wire and brass stud are soldered together with the same low-melting

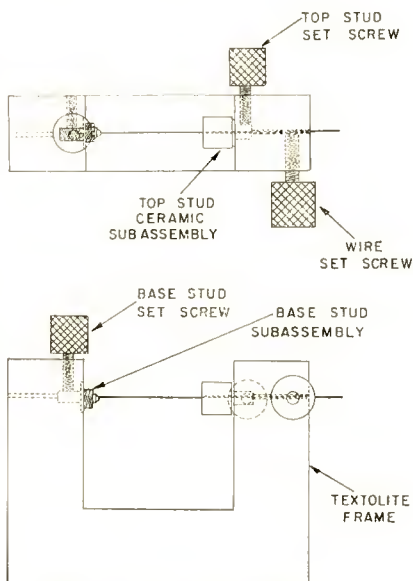


Fig. 5—Diode fabrication jig.

solder used to tin these parts. At this point, the diode is a completed unit and may be removed from the jig.

MEASURED RESULTS ON A TYPICAL UNIT

As a variable reactance device, the characteristics of greatest interest are the capacitance versus reverse bias voltage (measured at low frequencies), the total reactance with variation of bias voltage and frequency, and the loss. Figure 6 shows measured data at 1 and 2 megacycles where lead inductance and loss resistance are negligible. The solid curve was computed from the design formulas and agrees with the data. At the nominal bias of -6 volts, the capacitance is 38

micromicrofarads, and the slope is about 3 micromicrofarads per volt. Over the useful range, up to -16 volts, the capacitance varies inversely with the square root of the bias voltage from about 160 to 25 micromicrofarads.

The terminal reactance as a function of frequency, with the bias as a parameter, is plotted in Figure 7. The measured points agree with the solid curves which were calculated from the theoretical junction capacitance (see Equations 1 and 2) and a lead inductance

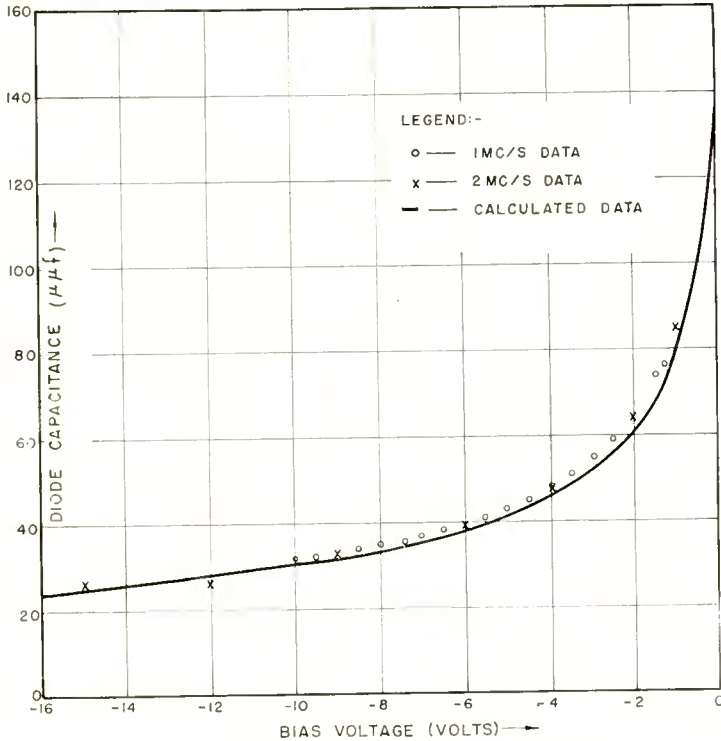


Fig. 6—Diode capacitance versus bias voltage.

of 2.6 millimicrohenries. It is seen that the diode is useful as a controllable reactance well into the UHF range.

The loss resistance was measured in equipment specially designed for the purpose and was found to be approximately constant with frequency and bias variations. Typical measured results correspond to a series resistance of about 0.5 ohm, and the Q at 500 megacycles, with -6 volts bias, is about 17. Since all the data confirms the type of equivalent circuit shown in Figure 1, it is possible to compute the

diode behavior over a wide range of frequencies and operating conditions.

Since the units described in the paper are experimental units, some variation was encountered between units, particularly in the series resistance. In one of the better units, the series resistance was 0.23 ohm resulting in a Q of 36 at 500 megacycles.

In the Appendix, comparison of the measured results with the theoretical design relations is discussed in more detail.

CONCLUSIONS

A junction diode has been described which has attractive operating

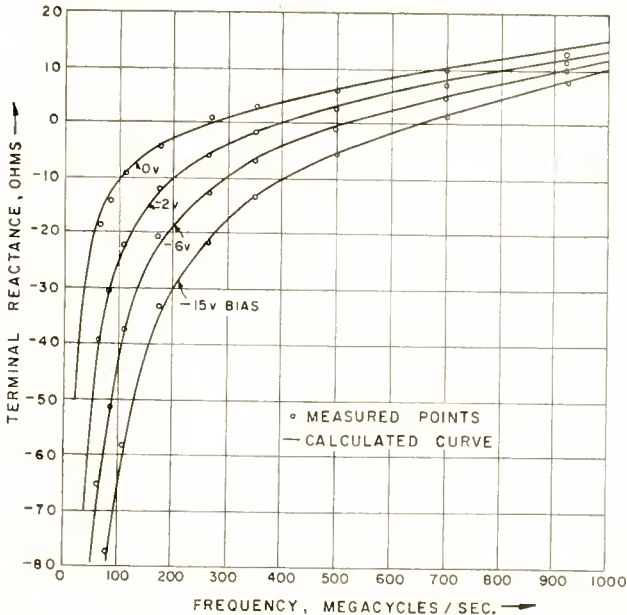


Fig. 7—Terminal reactance versus frequency.

characteristics over a wide range of frequencies including ultra-high frequencies. Diodes of the type described can be used for automatic frequency control,¹¹ frequency selection, mixing, voltage-controlled tuning, frequency modulation, and as dielectric amplifiers. It is found that the diodes follow theory very closely so that the design relations can be used for designing diodes for various applications.

ACKNOWLEDGMENT

The writers would like to acknowledge the following contributions

¹¹ W. Y. Pan and O. Romanis, "Automatic-Frequency Control of Television Receivers using Junction Diodes," *Transistors I*, RCA Laboratories, Princeton, N. J., 1956, pp. 598-608.

by their colleagues: I. Sochard* assisted in the assembly of the diodes and carried out most of the measurements. R. Braden helped considerably on measurement problems and built the special equipment required for measuring the series resistance. B. Goldstein provided the 1-megacycle data in Figure 6.

APPENDIX—COMPARISON OF MEASUREMENTS WITH DIODE THEORY

It is of interest to compare the junction theory with measured data. The agreement in general is exceptionally good.

Consider first the forward volt-ampere characteristics of the diode. The current flow in an ideal diode is given by

$$I = I_s (e^{\Lambda V} - 1), \quad (13)$$

where Λ is q/kT (equal to 38.8 volts⁻¹ at 25° C). In many conventional diodes, the series ohmic resistance is not negligible and the theoretical exponential diode equation is not found. Figure 8 shows the measured forward characteristics of one of the present diodes. This figure indicates that the characteristics follow rather exactly the ideal diode Equation (13) with the slope indicating an exponential factor $\Lambda = 37.3$, rather than the theoretical value of 38.8 at $T = 25^\circ \text{C}$. In accordance with Equation (13) the zero voltage intercept of the straight line on Figure 8 is the saturation current, $I_s = 0.15$ microampere.

Another method of determining I_s is to evaluate¹² the diode conductance, $g_0 = \Lambda I_s$, at zero bias voltage and current. From the measured $g_0 = 7.2$ micromhos, $I_s = 0.186$ microampere is computed using $\Lambda = 38.8$ for room temperature, $T = 25^\circ \text{C}$. A third method of determining I_s is to measure the diode current for a reverse bias. By this means $I_s = 0.17$ microampere was measured at $V = -1$ volt. The last two methods of measuring I_s include current flow due to any leakage across the junction; this current is not included in the first method of evaluating I_s . Therefore the difference between these values of I_s can be used as a rough estimate of the leakage conductance, which is about 1 micromho by this method. The value is in reasonable agreement with direct measurement of diode conductance with reverse bias which

* Now with the National Bureau of Standards.

¹² L. J. Giacoletto, "Equipments for Measuring Junction Transistor Admittance Parameters for a Wide Range of Frequencies," *RCA Review*, Vol. 14, pp. 269-296, June, 1953.

ranges from 1 to 0.03 micromho for bias voltages ranging from -1 to -6 volts.

With aid of Equation (13), the diode conductance, g , is

$$g = \frac{\partial I}{\partial V} = \Lambda (I + I_s) + \frac{I}{I_s} \frac{\partial I_s}{\partial V}. \quad (14)$$

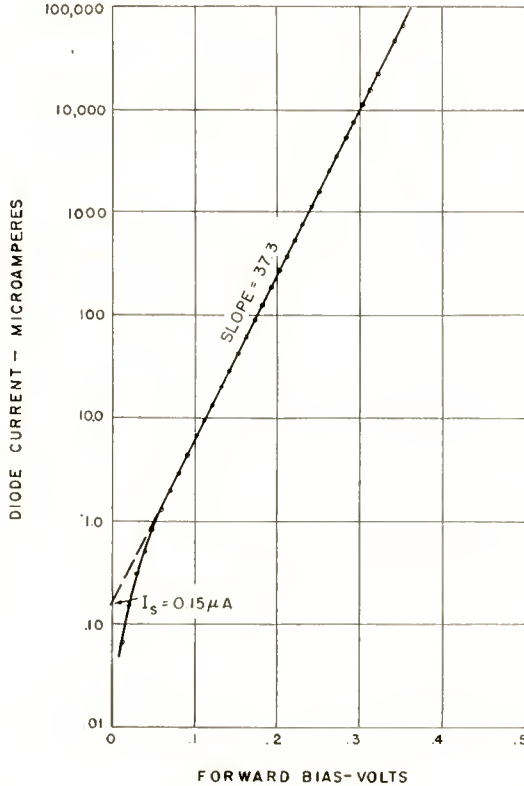


Fig. 8—Diode current versus forward bias voltage.

In the forward direction, the diode conductance is dominated by the first term in Equation (14); in the reverse direction, provided $-V$ is greater than a few tenths of a volt, $I = -I_s$, and g is given by the second term in Equation (6). The formulation of the second term can be carried out with the aid of Equations (2) and (12). When this formulation is carried out and evaluated it is found that the resulting conductance is about an order of magnitude smaller than measured conductances. It is therefore concluded that the measured conductance is due to a leakage conductance, g_l . The diode conductance is of rela-

tively minor importance which is fortunate since g_i is not a designable constant.

When the diode bias is smaller than a few tenths of a volt in the reverse direction or when the diode is biased in the forward direction, a diode diffusion capacitance, C_d , must be added to the transition capacitance (Equations (1) and (2)) to obtain the total junction capacitance. The diode diffusion capacitance when W is small compared with the diffusion length of minority carriers is

$$C_d = \Lambda (I + I_s) \frac{W^2}{2D_p} \text{ farads.} \tag{15}$$

This diffusion capacitance relation is useful to determine the value W , i.e., the thickness of the semiconductor between junction and soldered connection. For example, on the present diode, $C_d = 2120$ micromicrofarads at $I = 285$ microamperes was measured, and $W = 4.1 \times 10^{-5}$ meter is obtained. This value of W agrees reasonably well with 4.6×10^{-5} meter calculated from a resistance measurement (see below).

A plot of diode transition capacitance with bias voltage is shown in Figure 9. The data of this figure is the same as for Figure 6 but has been replotted to indicate that the transition capacitance obeys exactly the formulation of Equations (1) and (2). The slope of the line should,

according to theory, be $\frac{2\mu_n}{A^2 K \epsilon_0 \sigma_n} = -1.06 \times 10^{-4} (\mu\mu\text{f})^{-2} V^{-1}$. This

can be compared with a measured slope of $-1.0 \times 10^{-4} (\mu\mu\text{f})^{-2} V^{-1}$.

The intercept on the voltage axis in Figure 9 gives the contact voltage, $V_0 = -0.5$ volt. This value can be compared with the computed value, -0.54 volt, obtained using the equation

$$V_0 = -0.36 - \frac{1}{\Lambda} \ln \frac{N_d}{n_i} \text{ volt.} \tag{16}$$

N_d is the impurity density in the doped n semiconductor and can be determined from the approximate expression, $\sigma_n \approx q \mu_n N_d$.

The frequencies used for the data of Figure 9 were low enough that lead inductive reactance is negligible. At higher frequencies the lead inductive reactance cannot be neglected. A plot of the type shown in Figure 10 can be used in determining the lead inductance. Here, the intercept at zero net bias voltage corresponding essentially

with zero diode impedance gives the lead inductive reactance. Due to small measurement errors the intercepts do not all give the same lead inductance. An average of the several inductance values indicates $L_0 = 2.6$ millimicrohenries. According to theory this inductance for a wire diameter of 0.020 inch would correspond with a wire length of 0.15 inch. This wire length corresponds closely with the best estimate for the geometry employed. Also, the straight-line plots of Figure 10 indicate that stray capacitance is negligible for the range of operation considered here.

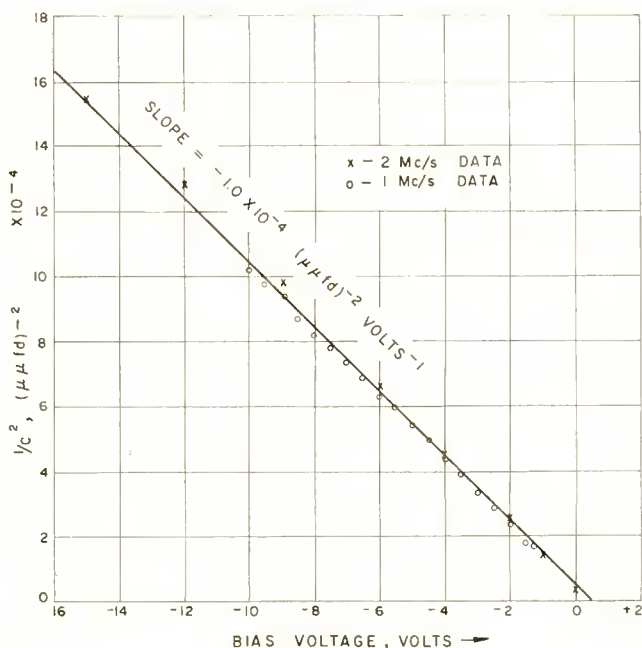


Fig. 9— $1/C^2$ versus bias voltage.

Using the measured value of the series resistance for this particular unit, i.e., $r_s = 0.23$ ohm, Equation (4) indicates that $W = 4.6 \times 10^{-5}$ meter. From the original wafer thickness of 5.1×10^{-5} meter, a penetration during alloying of 0.5×10^{-5} meter (0.2 mil) is indicated. This amount of penetration is somewhat less than expected on the bases of alloying temperature and dot geometry.¹³ Other diodes had series resistance values that were larger than could be explained by Equation (4). Thus it appears that there is an extraneous variable contribution to the series resistance. This is believed to be a contact resistance.

¹³ L. Pensak, "Calculations of Alloying Depth of Indium in Germanium," *Transistor I*, RCA Laboratories, Princeton, N. J., 1956, pp. 112-120.

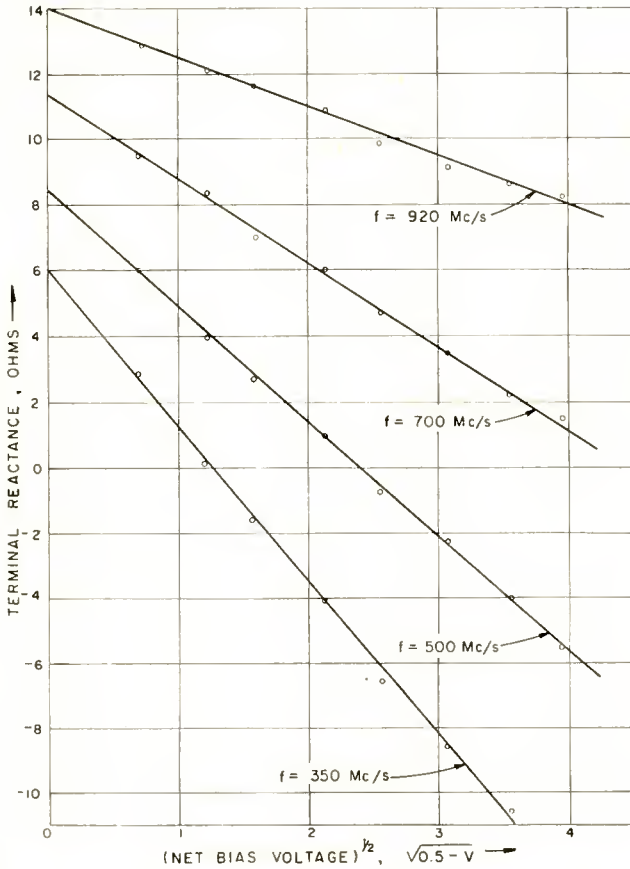


Fig. 10—Terminal reactance versus (net bias voltage)^{1/2}.

Calculations of diode Q (Equation 7) using $r_s = 0.23$ ohm, $C_s = 38$ micromicrofarads and $g = 0.03 \times 10^{-6}$ mho corresponding to -6 volts bias indicate values of $Q_d = 175, 36,$ and 18 at $100, 500,$ and $1,000$ megacycles. Equations (8) and (9) indicate a maximum Q of $6,015$ at $f = 1.5$ megacycles.

PHASE ANGLE DISTORTION IN TRAVELING-WAVE TUBES

BY

W. R. BEAM[†] AND D. J. BLATTNER[‡]

Summary—Using Pierce's first-order traveling-wave-tube theory, expressions are derived for the change in phase shift through the tube which should accompany various changes in operating conditions and signal level. Excellent verification of the theoretical values is obtained from measurements on a developmental low-noise traveling-wave tube.

INTRODUCTION

THE purpose of an amplifier* is to produce an output signal which is an accurate enlarged reproduction of the input signal. There is, however, no amplifier which will amplify high-frequency signals with no amplitude or phase distortion. Amplitude distortion is usually the result of nonlinear processes, while phase distortion is usually linked to the variation of internal reactances with frequency. At low signal levels, a traveling-wave tube is remarkably good from both points of view. The interaction between beam and circuit is essentially linear; and the circuit, being a broadband transmission line, has a phase angle which is very nearly constant despite variation in the operating conditions of the tube.

In some applications of traveling-wave tubes, however, e.g., microwave relays and certain types of radar systems, where a frequency- or phase-modulated signal is to be amplified, even very small phase distortion can be of importance. The total phase angle through a traveling-wave tube is dependent upon the helix and gun electrode potentials, and upon the signal level. If the electron beam is focused with an electromagnet, the magnetic field strength will influence the total phase angle to some extent. Reflections at the output transformer may cause increased phase angle. The object of this investigation was to compute the magnitude of these phase shifts and to compare the theoretical results with measured actual changes. Nonlinear amplification of the signal will not be considered since this occurs at higher signal levels than those which are of interest here.

The interaction circuit of a traveling-wave tube is usually ten or more wavelengths long. With a total phase shift of $3,600^\circ$ or more, it

[†] RCA Laboratories, Princeton, N. J.

[‡] RCA Tube Division, Harrison, N. J.

* The term "amplifier" without further specification is used with the meaning of "linear amplifier."

requires a very slight change in operation to alter this shift by a few degrees. In Pierce's¹ traveling-wave-tube terminology, the quantity of importance is the variation of the phase velocity, v , of the wave along the interacting circuit. The phase shift in radians per unit length is $\beta = \omega/v$, where ω represents the operating frequency. The total phase angle through the tube is β times the circuit length.

The next section includes a theoretical study of the variation of β with change of:

1. Supply voltages,
2. Signal level,
3. Matching conditions.

Simple formulas for the resulting phase shifts are derived.

In the third section, experimental results are discussed. Experiments were carried out on a 3,000-megacycle low-noise traveling-wave tube in which the relation of output to input phase was measured to better than one degree accuracy. The independent variables were

1. Helix voltage,
2. First-anode voltage (beam current),
3. Second-anode voltage,
4. Magnetic focusing field current,
5. Signal level,
6. Output matching.

In each case, the quantity was varied only over the range in which the phase shift variations were essentially linear, as the variations expected in practical operation will be well within the linear regions.

DERIVATION OF THEORETICAL RELATIONS

The entire first-order phase shift theory presented here is based upon Pierce's small-signal theory of the traveling-wave tube.¹ Pierce defines the phase constant of the wave traveling along the delay line circuit under operating conditions as

$$\beta = \beta_e (1 - Cy), \quad (1)$$

¹J. R. Pierce, *Traveling-Wave Tubes*, D. Van Nostrand, New York, N. Y., 1950.

where

$$\beta_e = \frac{\omega}{v_e},$$

v_e = electron-beam velocity,

C = Pierce's gain parameter (proportional to the cube root of the beam current),

y = a dimensionless parameter defined by Equation (1).

The unperturbed helix wave phase constant, β_1 , is defined by Pierce as

$$\beta_1 = \beta_e (1 + Cb), \quad (2)$$

where b is another dimensionless parameter. The parameter C is determined by the beam diameter, voltage, and current, and the circuit geometry. Pierce gives curves relating y and b (Chapter 8, pp. 120-126) as a function of the parameter QC . Q is given by beam and circuit geometry alone. We thus have all that is needed to relate changes of β to changes in β_e (helix voltage), C (first anode voltage, beam current) and QC (beam diameter). Pierce's loss parameter, d , has been assumed to be zero. Its effect is usually minor; in addition, it cannot be controlled by tube operating conditions, but is determined by construction of the slow-wave circuit.

Variation of Helix Voltage²

Let the helix voltage V_0 change by an amount ΔV_0 . Then the beam velocity v_e will change by an amount Δv given by

$$\frac{\Delta v}{\Delta V_0} = -\frac{1}{2} \frac{v_e}{V_0}.$$

Then, since β_e and v_e are reciprocally related,

$$\frac{\Delta \beta_e}{\beta_e} = -\frac{1}{2} \frac{\Delta V_0}{V_0}.$$

From Equation (2) since β_1 is a constant, $\Delta \beta_1$ must be zero and, assuming C to be constant,

² W. J. Bray, "The Traveling Wave Valve as a Microwave Phase-Modulator and Frequency-Mixer," *Proceedings of the Institute of Electrical Engineering*, Vol. 99, part III, p. 28, 1953.

$$\Delta\beta_1 = 0 = \Delta\beta_e (1 + Cb) + \beta_e (C\Delta b), \quad (3)$$

$$\frac{\Delta\beta_e}{\beta_e} = -\frac{C\Delta b}{1 + Cb}. \quad (4)$$

Therefore,

$$\frac{C\Delta b}{1 + Cb} = \frac{1}{2} \frac{\Delta V_0}{V_0}. \quad (5)$$

A linear approximation to Pierce's curves relating y and b is

$$y = -(0.42 + 0.07 QC) b - (0.5 + 0.5 QC), \quad (3)$$

$$\Delta y = -(0.42 + 0.07 QC) \Delta b, \quad (6a)$$

where Δy and Δb represent small changes in y and b .

Taking differentials of Equation (1),

$$\Delta\beta = \Delta\beta_e (1 - Cy) + \beta_e (-C\Delta y). \quad (7)$$

Equations (5), (6a), and (7) can be combined to give

$$\Delta\beta = \frac{\Delta V_0}{2V_0} \beta_e ([1 + bC] [0.42 + 0.07 QC] + Cy - 1). \quad (3)$$

The change in total phase angle, $\Delta\phi$, is found by multiplying $\Delta\beta$ by the circuit length L .

$$\Delta\phi = \Delta\beta L$$

$$\Delta\phi = \frac{\Delta V_0}{V_0} \pi ([1 + bC] [0.42 + 0.07 QC] + Cy - 1) \times N \text{ radians.} \quad (3)$$

N is the circuit length in wavelengths. We are often interested in tubes with low C and QC . In the case of tubes with low C and QC , Equation (9) reduces to the approximate form

$$\Delta\phi \approx -0.58 \pi \frac{\Delta V_0}{V_0} N \text{ radians,} \quad (11)$$

$$\Delta\phi \approx -105 \frac{\Delta V_0}{V_0} N \text{ degrees.}$$

Variation of First-Anode Voltage, V_1

If first-anode voltage changes, causing change of beam current following Child's law,

$$I = kV_1^{3/2}; \quad (11)$$

then

$$\frac{\Delta I}{I} = \frac{3}{2} \frac{\Delta V_1}{V_1}. \quad (12)$$

Since C is proportional to $I^{1/3}$,

$$\frac{\Delta C}{C} = \frac{1}{3} \frac{\Delta I}{I},$$

and

$$\frac{\Delta C}{C} = \frac{1}{2} \frac{\Delta V_1}{V_1}. \quad (13)$$

Taking differentials of Equations (1) and (2) again, allowing C , b , and y (but not β_e and β_1) to vary,

$$\begin{aligned} \Delta\beta &= (-C\Delta y - y\Delta C) \beta_e, \\ 0 &= (C\Delta b + b\Delta C) \beta_e. \end{aligned} \quad (14)$$

By reduction, and use of Equation (6),

$$\Delta\beta = -\frac{\beta_e \Delta V_1}{2V_1} C (y + [0.42 + 0.07 QC] b). \quad (15)$$

From Equation (6) it is seen that the quantity in parentheses is very nearly $-(0.5 + 0.5 QC)$, so to this approximation,

$$\Delta\phi = 90 \frac{\Delta V_1}{V_1} C (1 + QC) N \quad \text{degrees.} \quad (16)$$

Phase Shift as a Function of Signal Level

As the signal level increases, the power extraction from the beam increases. This power represents a loss in beam velocity, and is equivalent to a helix voltage which drops near the output end. There is produced a phase shift which is not uniform along the circuit. It is, therefore, necessary to integrate $\Delta\beta dz$ to find the change of phase angle.

It is assumed that the power level in the tube varies exponentially (signal levels which lead to saturation in the power output are excluded) and that this power is extracted directly from the d-c beam power. If G is the gain in decibels per unit axial length, the power in the wave as a function of distance from the output z can be written as

$$P_{(z)} = P_2 e^{-0.2303 G z},$$

where P_2 is output power. Assuming the electron energy at the input is V_0 electron volts, the electron energy at z is

$$V_{(z)} = V_0 - \frac{P_2}{I_0} e^{-0.2303 G z}.$$

The total energy loss is, therefore,

$$\Delta V_0 = -\frac{P_2}{I_0} e^{-0.2303 G z}.$$

From Equation (8),

$$\Delta\phi = -\int_{z_0}^0 dz \frac{P_2}{2V_0 I_0} e^{-0.2303 G z} \beta_e ([1 + bC] [0.42 + 0.07 QC] + Cy - 1).$$

The limit z_0 may be taken as the input of the tube, but this is unrealistic, since the power does not, in general, vary exponentially near the input. It will usually be satisfactory to let $z_0 = \infty$. The presence of an attenuator may change the power versus distance, but if the power level is 14 decibels down from the output power at the lumped attenuation, the error will be about 10 per cent, which is far less than some other sources of error. Letting $z_0 = \infty$,

$$\Delta\phi = -\frac{4.343}{G} \frac{P_2}{2V_0 I_0} \beta_e ([1 + bC] [0.42 + 0.07 QC] + Cy - 1) \text{ radians.} \quad (19)$$

The maximum value of G is given in Pierce's notation as

$$\frac{BC \beta_e}{2\pi}.$$

Therefore,

$$\Delta\phi_{\min} = -\frac{13.7 P_2}{V_0 I_0} \times \frac{[1 + bC] [0.42 + 0.07 QC] + Cy - 1}{BC} \quad \text{radians.} \quad (20)$$

If the numerator of the right-hand factor is approximated, as earlier, by -0.58 and the low Q approximation is used with $B = 47.3$,

$$\Delta\phi_{\min} \approx 9.6 \frac{P_{\text{out}}}{P_{\text{beam}}} \times \frac{1}{C} \quad \text{degrees,} \quad (21)$$

where $P_{\text{beam}} = V_0 I_0$ and $P_2 = P_{\text{out}}$, the power at the tube output.

Effect of Poor Output Matching³

In the analysis above, the power that has been extracted from the beam when it reaches the output terminal, P_2 , has been assumed equal to the output power, P_{out} . If the output match is not perfect, some power will be reflected and absorbed by the attenuator. This power will increase the power extracted from the beam, and hence the P_2 in Equations (20) and (21) must be replaced by $P_2 = (P_{\text{out}} + P_{\text{reflected}})$. $P_{\text{reflected}} = K^2 (P_{\text{out}} + P_{\text{reflected}})$ where K is the magnitude of the reflection coefficient given in terms of voltage-standing-wave ratio, R , by $K = (R - 1)/(R + 1)$. The total power extracted from the beam is now

$$P_2 = P_{\text{out}} \frac{(R + 1)^2}{4R}.$$

As an example, if the voltage-standing-wave ratio is 1.5, the total power extracted from the beam is $1.04 P_{\text{out}}$; if the voltage-standing-wave ratio is 3, the extracted power is $1.33 P_{\text{out}}$, and the phase shift will be 33 per cent more sensitive to power than in the case of a perfect match.

EXPERIMENTAL EVIDENCE AND CONCLUSIONS

The low-noise traveling-wave tube tested was a developmental type having the following nominal operating conditions:

frequency	3,000 megacycles,
gain	25 decibels,
noise factor	9 decibels,

³ L. Brück, "Phasenverzerrungen bei der Verstärkung mit Lauffeldrohren," *Archiv der Elektrischen Übertragung*, Vol. 7, p. 28, 1953.

helix voltage	575 volts,
beam current	0.3 milliampere,
focusing field	500 gaussess,
saturation level	10 milliwatts.

The system used to measure the phase shift through the amplifier is shown in Figure 1. It is one of several methods suggested by R. A. Braden of these Laboratories. The movable probe was adjusted to give a null or minimum in the receiver for each value of the independent variable and the difference in probe positions measured and converted into degrees of phase shift.

In the tests, electrode voltages and focusing magnet current were varied about their nominal operating values, and the resulting phase

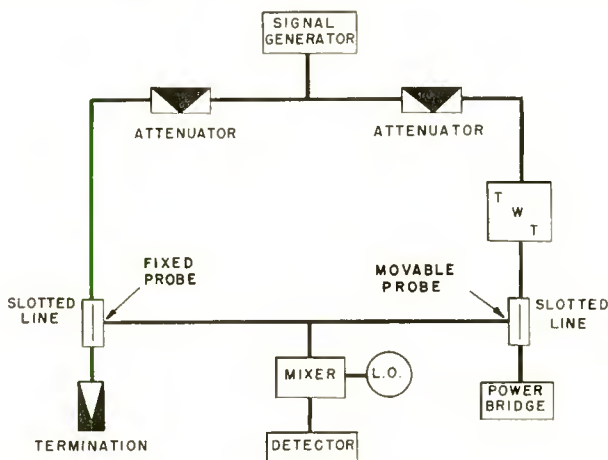


Fig. 1—The circuit used for phase-shift measurements.

shifts measured. In the variable power level test, the difference in phase shift at a power output of 1.4 milliwatts and at negligibly low power output was measured.

Phase Shift versus Helix Voltage

In Figure 2 the experimental results are compared with a point-by-point computation from Pierce's equation 8.14 and with the simple linear theory of Equation (21). The agreement is good.

The requirement on a power supply to keep phase modulation of the signal below 1° is a ripple of less than .02 per cent, which can be obtained by electronic voltage regulation. The phase shift due to helix voltage, as seen from Equation (9), is principally dependent on the length of the circuit in wavelengths. A tube with a large C will be

less sensitive to helix voltage variations than a tube with a small C because such a tube is shorter for the same gain.

Phase Shift versus First-Anode Voltage or Beam Current

Figure 3 illustrates data taken over a range of beam currents by changing the first anode voltage. The agreement with theory here is not very good, which may be due in part to the fact that changing the first-anode voltage may make the "average" diameter of the scalloped beam greater than if the beam were in parallel flow. From Equation

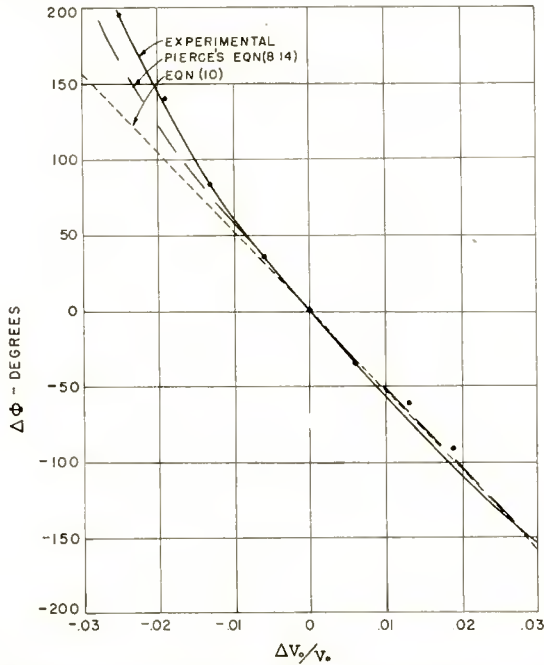


Fig. 2—Change in phase angle through tube as helix voltage, V_0 , is changed from its maximum gain value of 575 volts. $I_0 = 300$ microamperes.

(16) it will be noted that a large C will accentuate this phase shift variation. This phase shift is less serious than that caused by helix voltage changes because it takes .5 per cent change in first anode voltage to cause a shift of 1° .

Phase Shift versus Magnet Current

If the beam size is changed by altered focusing conditions, both the gain parameter C and the space charge factor Q can be expected to change. These changes, and their effect on the total phase angle of the tube, can be calculated if it is assumed that the electron beam has a uniform diameter determined by the magnetic field. But as has been

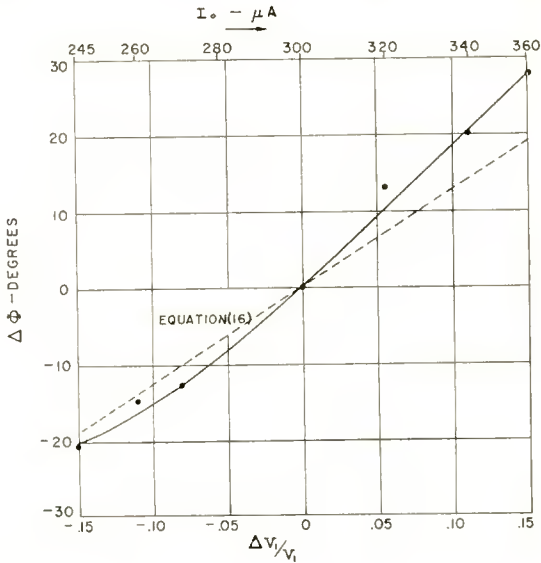


Fig. 3—The change of a phase angle through the tube as first-anode voltage, V_1 , is changed about a center value of 36.5 volts. The values of beam current corresponding to V_1 are shown on top.

noted, the beam is actually scalloped, and the effect of the change in magnetic field is to change the scalloping much more than it is to change the average diameter. This behavior of the beam geometry as a function of magnetic field is not well known, so no quantitative theory is attempted.

Figure 4 presents experimental results. It is seen that, from a practical point of view, ripple in the focusing magnet current would be of minor importance. Permanent magnets eliminate it entirely.

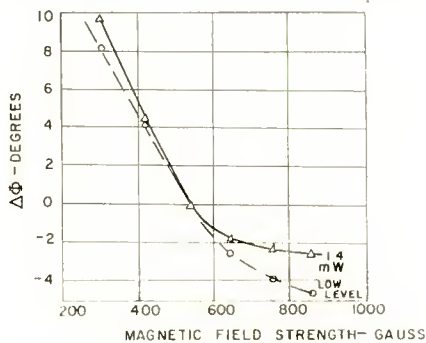


Fig. 4—Change in total phase angle through tube when magnetic focussing field is changed.

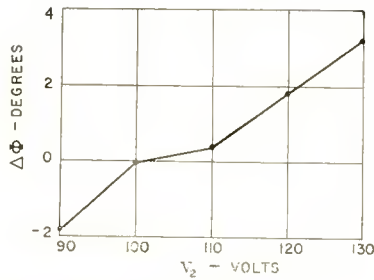


Fig. 5—Change in phase angle through tube as second-anode voltage is changed.

Phase Shift versus Second Anode Voltage

There is a slight effect here, of negligible size compared to other sources. The best way to explain it is in terms of the beam geometry; this electrode will cause slight changes in beam scalloping. A 1° phase shift requires 5 per cent or more change in this voltage. Figure 5 illustrates the measured results.

Phase Shift versus Output Power

In Figure 6 the linear nature of this effect is illustrated. Since the

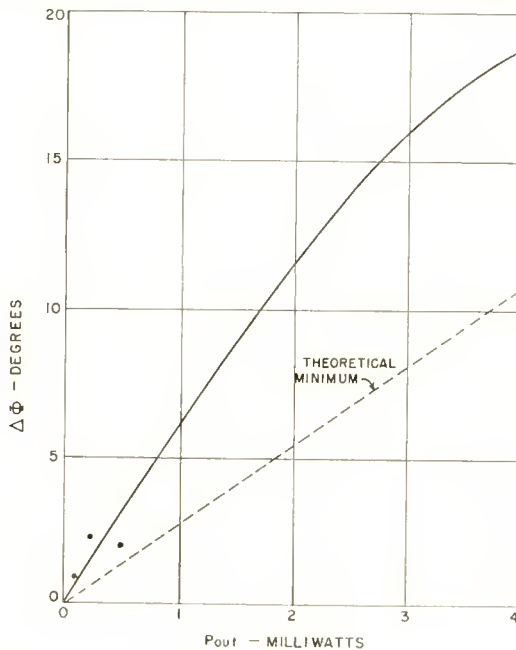


Fig. 6—Change in phase angle of tube as a function of power output, $I_0 = 300$ microamperes, $V_0 = 580$ volts.

values plotted were not taken at the helix voltage giving maximum gain, they do not agree with Equation (21). The phase shift versus power curve departs from a straight line at high powers where saturation effects set in. It is approximately linear, however, over the entire region of interest.

Of considerable importance is the manner in which phase shift versus power behaves at different helix voltages. We know that gain is a maximum at a particular helix voltage and less on either side. It follows that the phase shift will have a minimum. If the curve y versus b^* were actually a straight line, the minimum phase error would fall

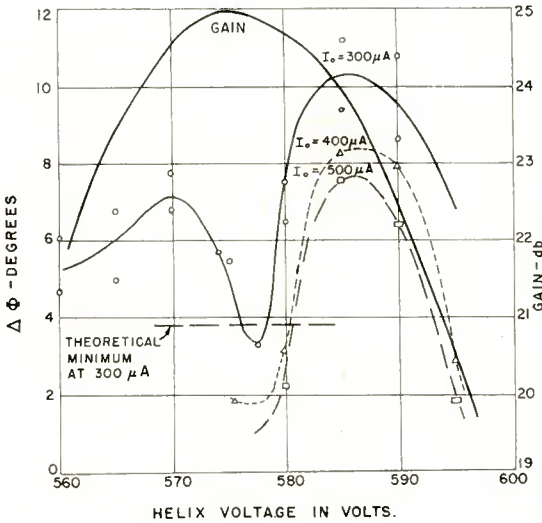


Fig. 7—The difference between the phase shift at low level and the phase shift at 1.4 milliwatts output, as a function of helix voltage and beam current.

at the maximum gain point. Since this relation (y versus b) is slightly curved, the phase shift will be minimum at a helix voltage slightly higher than the one producing maximum gain (which was 575 volts for $I_0 = 300$ microamperes). The curves of Figure 7 show good agreement with expectations. The maxima at each side of the central minimum result from the change of y versus b to flatter slopes at the ends of the gain band. The curves for 400 and 500 microamperes illustrate the fact that as C increases, the minimum phase shift decreases. These curves could not be completed, for oscillation set in at lower voltages when beam current was above 300 microamperes.

* See Reference (1), Figure 8.1.

Mismatch at Output

In the final experiment, the output transformer was deliberately mismatched. The difference in phase shift in the tube at low output and at 1.4 milliwatts output was measured as before. As the match deteriorated, it became necessary to increase the input power to establish 1.4 milliwatts output as abscissa. The fact that all the points lie on a line through the origin fully corroborates the thesis that the reflected power is absorbed by the attenuator, and that the beam behaves just as if all the power were extracted from the wave. This demonstrates the need for good matching if minimum phase shift is desired.

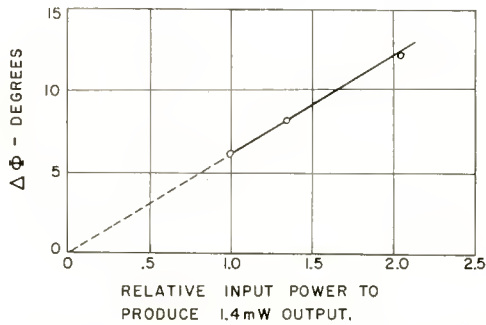


Fig. 8—The effect of mismatch at the output of the traveling-wave tube.

CONCLUSIONS

Sufficient data has been taken to show that the first-order theory agrees with experiments to better than order-of-magnitude accuracy. Specifically, the sensitivity of total phase shift in the tube to operating conditions may be summarized, for this particular tube under the previously specified operating conditions. The output phase shifts

- (1) 50° for 1 per cent change in helix voltage,
- (2) 2° for 1 per cent change in first-anode voltage,
- (3) about .1° for 1 per cent change in magnet current,
- (4) 6° for each milliwatt increase of output power,
- (5) 6° for each milliwatt of power lost by reflection at the output coupler.

In a system where it is impossible to keep ripple to a sufficiently low value, it is possible to use dynamic compensation, for example, by applying a controlled ripple signal to the first anode. If it is necessary to make phase shift independent of signal amplitude, the detected signal

could be fed back as a small helix voltage variation, thus compensating at least partially.

In the direction of decreasing sensitivity to all the disturbing factors, the greatest improvement could be brought about by an increase of beam current, which would at once make C greater and allow a shorter tube. Insensitivity to focusing conditions is favored by the "confined flow" method of focusing used in the tube tested over the so-called "Brillouin flow" condition where the gun is magnetically shielded. In power tubes operating with the latter, more critical beam focusing changes in anode voltages and magnetic field will be very important.

A good output match will minimize the phase shift. A voltage-standing-wave of 1.5, however, represents a power loss of only 4 per cent; any further improvement in matching, therefore, will have little effect on phase shift reduction.

The best way to eliminate phase distortion at high power levels is to make the power-handling capacity so great that the maximum output power will be much less than 1 per cent of the beam power.

THE ELECTRON-VOLTAIC EFFECT IN GERMANIUM AND SILICON P-N JUNCTIONS*

BY

P. RAPPAPORT, J. J. LOFERSKI, AND E. G. LINDER

RCA Laboratories,
Princeton, N. J.

Summary—The electron voltaic effect is analyzed to show how the properties of the semiconductor (energy gap, minority carrier diffusion length, surface recombination velocity and the temperature) and of the impinging electrons (average energy, density, maximum energy) affect the usefulness of the electron-voltaic effect as a means of converting the energy of beta rays into electricity. Experiments on germanium and silicon p-n junctions are described. It is shown that the maximum conversion efficiency using silicon p-n junctions will probably not exceed about 5 per cent. Measurements on such junctions show a maximum efficiency of 2.5 per cent, with an open-circuit voltage of .35 volt and short-circuit current of 20 microamperes under irradiation by 50 millicuries of Sr90-Y90. With such a source, beta particle multiplications of approximately 2.5×10^5 have been observed. These correspond to an average cost in energy per electron-hole pair of about 4.2 electron volts in silicon and 4.4 electron volts in germanium. Experiments with monoenergetic beta particles are also described. The effect of radiation damage is discussed.

INTRODUCTION

WHEN beta particles are absorbed by a semiconductor they dissipate most of their energy by ionizing the atoms of the solid. The carriers generated in this fashion are in excess of the number permitted by thermodynamic equilibrium and if they diffuse to the vicinity of a rectifying junction they induce a voltage across the junction. This phenomenon, which has been termed the electron-voltaic effect (EVE) is the subject of this investigation. It has been briefly described for selenium and CuO by Ehrenberg et al.¹ and by one of the present authors for germanium and silicon.² Pfann

* Much of the work described in this paper was performed under contract with the Components and Systems Laboratory, Wright Air Development Center, Air Research and Development Command, U. S. Air Force, and it is described in the Final Report Contract No. AF33(038)-23686 issued in November 1953.

¹ W. Ehrenberg, Chi-Sai Lang, and R. West, "The Electron Voltaic Effect," *The Proceedings of the Physical Society*, Vol. 64, p. 424, April, 1951.

² P. Rappaport, "The Electron-Voltaic Effect in p-n Junctions Induced by Beta-Particle Bombardment," *Phys. Rev.*, Vol. 93, p. 246, January, 1954.

and van Roosbroeck³ have published an analysis of the effect and have given some experimental results for germanium and silicon.

At these laboratories the effect was studied as a possible source of electrical power since it permits the direct conversion of the energy of the beta rays emitted by a radioactive material into electricity. Consequently the work described here emphasizes the total power and the maximum efficiency of energy transformation which can be realized by this process. In the discussion, because of the application that was intended, the EVE is compared with other methods of direct conversion which have been proposed and described in the literature.⁴⁻⁷

To illustrate the nature of the EVE, Figure 1a shows a cross section of a p-n junction irradiated by electrons, while Figures 1b and 1c show the configuration of the bands across the junction in equilibrium and during irradiation, respectively. At equilibrium, the Fermi level must be continuous across the junction so that the discontinuous change in the nature of the impurities (from p-type to n-type) produces an internal electrostatic potential difference. Its height is equal to the difference between the location of the Fermi level on the n and p sides at a large distance from the junction. If the junction is irradiated, it acquires a forward bias, as shown in Figure 1c. If the impedance is infinite, the current is zero and the voltage has its maximum value, V_{max} . As the impedance is decreased there is a net flow of current in the load until, when a short circuit is placed across the junction, the maximum current, I_s , will flow through it, and $V = 0$.

The EVE is one of a class of phenomena (the best known is the photovoltaic effect) in which a radiation capable of producing ionization in a solid interacts with a rectifying junction. Other forms of electromagnetic radiation (γ -rays, X-rays) as well as other particles (α particles, protons) are possible sources of such ionization, and the analysis presented here can be applied to these other radiations. Beta rays were chosen as the primary source for direct conversion because their specific ionization is higher than that of γ -rays. They are there-

³ W. G. Pfann and W. van Roosbroeck, "Radioactive and Photoelectric p-n Junction Power Sources," *Jour. Appl. Phys.*, Vol. 25, p. 1422, November, 1954.

⁴ E. G. Linder and S. M. Christian, "The Use of Radioactive Material for the Generation of High Voltage," *Jour. Appl. Phys.*, Vol. 23, p. 1213, November, 1952.

⁵ P. Rappaport and E. G. Linder, "Radioactive Charging Effects With a Dielectric Medium," *Jour. Appl. Phys.*, Vol. 24, p. 1110, September, 1953.

⁶ P. E. Ohmart, "A Method of Producing an Electric Current From Radioactivity," *Jour. Appl. Phys.*, Vol. 22, p. 1504, December, 1951.

⁷ K. C. Jordan and J. G. Birden, Mound Laboratory Report MLM-984, October, 1954.

fore absorbed in a reasonable thickness of semiconductor and they can be shielded more easily. They were preferred over α particles because they are emitted by radioisotope by-products of the fission process and because their smaller weight produces less radiation damage.

Table I lists the properties of some long half-life pure beta emitters. It includes the current per curie, I_B , the maximum energy, V_{Bmax} , the average energy, \bar{V}_B , the half life, t_H , and the specific activity, G , which is computed on the assumption that every atom is radioactive.

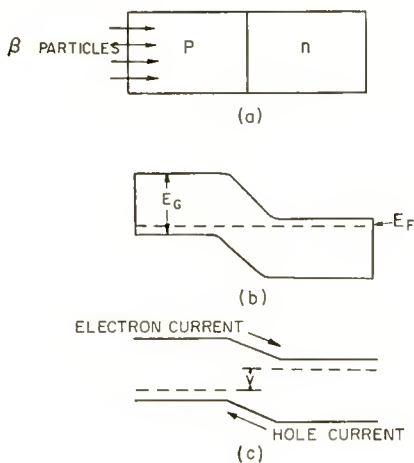


Fig. 1—Energy-band configuration in a p-n junction at equilibrium and under bombardment.

Table I—Properties of Beta-Emitting Radioisotopes

Isotope	I_B (amperes per curie)	V_{Bmax} (electron volts)	\bar{V}_B (electron volts)	t_H (years)	G
Sr90-Y90	5.9×10^{-9}	2.2×10^6	$.54 \times 10^6$	20	400 curies/gm
H-3	5.9×10^{-9}	$.019 \times 10^6$	$.006 \times 10^6$	12.4	2.63 curies/cc
Pm-147	5.9×10^{-9}	$.23 \times 10^6$	$.073 \times 10^6$	2.6	950 curies/gm
Ni-63	5.9×10^{-9}	$.063 \times 10^6$	$.021 \times 10^6$	80	72 curies/gm

ANALYSIS OF THE EVE AND ITS MAXIMUM EFFICIENCY

The equations governing the EVE can be most simply deduced from the equivalent circuit of an irradiated rectifying junction which is shown in Figure 2a. The circuit consists of a constant-current

generator delivering a current I_s into a network of impedances, which include the nonlinear impedance of the junction, R_j , an intrinsic series resistance, r_s , an intrinsic shunt resistance, r_{sh} , and the load resistance, R_L . The origin of the first two circuit elements is described as follows:

(a) The ionizing radiation which shall be represented hereafter by a current of particles I_B having an average energy \bar{V}_B , by interacting with the solid generates the constant current I_s . This combination is represented by the constant-current generator of Figure 2.

(b) The junction has a current-voltage characteristic of the form

$$I_j = I_o (e^{\lambda V} - 1), \tag{1}$$

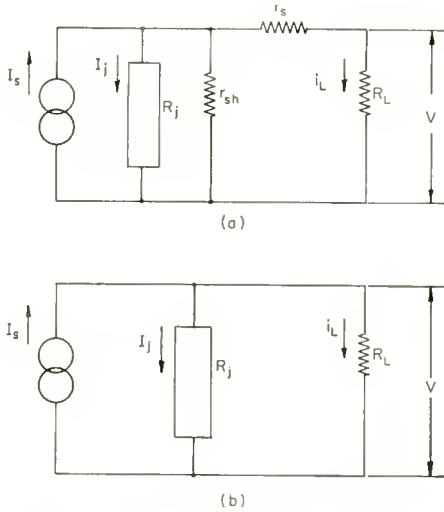


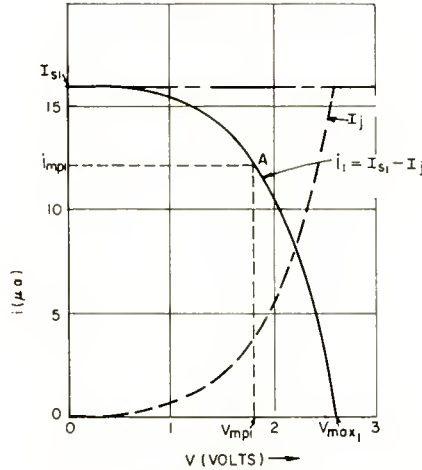
Fig. 2—Equivalent circuit of an irradiated p-n junction power source.

where I_j is the current through the junction, I_o is the reverse saturation current of the diode, V is the voltage across it, and $\lambda \equiv q/kT$. Its effective impedance is given by

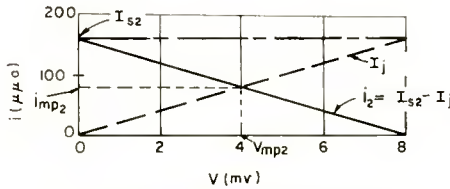
$$R_j \equiv \frac{\partial V}{\partial i} = \frac{e^{-\lambda V}}{\lambda I_o}. \tag{2}$$

The circuit and the analysis can be simplified by noting that when the maximum power is transferred to the load resistance, R_L , then $R_L \ll r_{sh}$ and $R_L \gg r_s$. The first condition is easy to attain since generally $r_{sh} > 10^4$ ohms. Low values of r_{sh} would make the device a poor rectifier

but they would not affect its operation as a voltaic cell. The second condition can be realized in practice by using a geometry in the device which will reduce r_s to the desired range. The simplified circuit is shown in Figure 2b. It is evident from this diagram that the current passing through the load impedance, R_L , is the difference between the generated current, I_s , and the current which flows through the junction, I_j , i.e.,



(a) $i-V$ CHARACTERISTIC FOR $I_{s1}/I_0 \gg 1$



(b) $i-V$ CHARACTERISTIC FOR $I_{s2}/I_0 < 1$

Fig. 3—Theoretical $i-V$ diagram for an irradiated p-n junction.

$$i = I_s - I_0 (e^{\lambda V} - 1). \tag{3}$$

A current-voltage diagram which illustrates this relation is shown in Figure 3. It represents the constant current generator by the line I_{s1} , the junction $i-V$ characteristic (Equation (1)) by the I_j curve and i_1 by the difference between these two.

Three parameters which are readily accessible to experimental measurement are also shown in Figure 3. They are the open-circuit voltage, V_{max} , the short-circuit current, I_s , and I_0 which can be determined from the slope of the $i-V$ diagram at $V = 0$, i.e.,

$$-\frac{\partial i}{\partial V} \Big|_{V=0} = -\lambda I_o. \quad (4)$$

From Equation (3), it is evident that

$$\lambda V_{\max} = \ln (I_s/I_o + 1). \quad (5)$$

In terms of these parameters, the voltage and current at maximum power (V_{mp} and i_{mp} , respectively) can be determined by equating the load impedance to the impedance of the junction as given by Equation (2), i.e.,

$$R_{mp} = \frac{V_{mp}}{i_{mp}} = \frac{e^{-\lambda V_{mp}}}{\lambda I_o}. \quad (6)$$

By combining Equations (3) and (6) and comparing to Equation (5), one finds that

$$e^{\lambda V_{mp}} (1 + \lambda V_{mp}) = \frac{I_s}{I_o} + 1 = e^{\lambda V_{\max}}. \quad (7)$$

Appropriate substitutions yield the following expressions for the current at maximum power, and for the maximum power dissipated in the load, respectively:

$$i_{mp} = \frac{\lambda V_{mp}}{(1 + \lambda V_{mp})} \left(1 + \frac{I_o}{I_s} \right) I_s, \quad (8)$$

$$P_{\max} = I_o \lambda V_{mp}^2 e^{\lambda V_{mp}}. \quad (9)$$

The maximum efficiency, η_{\max} , is the ratio of P_{\max} to the input power, $P_i = I_B \bar{V}_B/q$, so that

$$\eta_{\max} = \left(1 + \frac{I_o}{I_s} \right) \frac{\lambda V_{mp}}{(1 + \lambda V_{mp})} \frac{q V_{mp} I_s}{\bar{V}_B I_B}. \quad (10)$$

Equation (10) can be simplified by introducing the concept of electron multiplication, i.e., we define a multiplication m by the equation

$$I_s = m I_B, \quad (11)$$

which says that on the average a primary particle generates m hole-electron pairs in the solid. In terms of the average energy of the beta particles, \overline{V}_B , and the average energy expended in creating a hole-electron pair, w , the multiplication can be defined as

$$m \equiv \frac{\overline{V}_B}{w}. \quad (12)$$

w , which is analogous to an ionization energy, can be related to the energy gap of the semiconductor, E_G by the definition

$$w = f E_G, \quad (13)$$

where $f \geq 1$. The actual value of f varies among semiconductors. Thus McKay reports $f = 1.7$ in diamond,⁸ $f = 3.2$ in silicon, and $f = 4.1$ in germanium.⁹

Substituting these relations into Equation (10),

$$\eta_{\max} = \left(1 + \frac{I_o}{I_s} \right) \frac{\lambda V_{mp}}{(1 + \lambda V_{mp})} \frac{q V_{mp}}{f E_G}. \quad (14)$$

From Equation (7) it is evident that if $I_s/I_o \gg 10^5$, then $\lambda V_{mp} \gg 1$, and

$$\eta_{\max} \doteq \frac{q V_{mp}}{f E_G} = \frac{q V_{mp}}{w}. \quad (15)$$

This relation states simply that for large values of V_{mp} the maximum efficiency approaches the ratio of the voltage at which electrons are delivered to the load to the average energy spent in freeing an electron. It implies that most of the liberated electrons flow through R_L . This can be demonstrated from Equation (8) which shows that if $\lambda V_{mp} \gg 1$, i_{mp} approaches I_s . Furthermore, Equation (7) shows that if $\lambda V_{mp} \gg 1$, $V_{mp} \approx V_{\max}$. These characteristics of the device are latent in the nonlinear i - V diagram, which is illustrated in Figure 3. Large values of I_s (e.g., I_{s1} of Figure 3a) yield the ratio $I_s/I_o \gg 1$ and the curve becomes nonlinear. For the operating point (A) the rectangular area $i_{mp1} V_{mp1}$ represents power delivered to R_L , while the remaining (smaller) area

⁸ K. G. McKay, "Electron-Hole Production in Germanium by Alpha-Particles," *Phys. Rev.*, Vol. 84, p. 829, November, 1951.

⁹ K. G. McKay and K. B. McAfee, "Electron Multiplication in Silicon and Germanium," *Phys. Rev.*, Vol. 91, p. 1079, September, 1953.

under the i - V curve represents the power lost in the junction. If, however, $I_s < I_o$ (e.g., I_{s2} of Figure 3b) then the i - V characteristic is linear. Under these conditions only half the power is available to the load, i.e.,

$$I_{mp2} = I_{s2}/2, \quad V_{mp2} = V_{\max2}/2, \quad \text{so that } \eta_{\max2} = V_{\max2}/(4W).$$

To establish how E_G affects η_{\max} , it is necessary to determine how the ratio I_s/I_o depends on E_G . The relation between I_s and E_G is given by combining Equations (11), (12), and (13), i.e.,

$$I_s = \frac{\bar{V}_B I_B}{f E_G}. \quad (16)$$

The dependence of I_o on E_G and the other semiconductor parameters as derived by Shockley¹⁰ is given by

$$I_o = \frac{b}{(1+b)^2} \frac{\sigma_i^2}{\lambda} \left(\frac{1}{\sigma_n L_p} + \frac{1}{\sigma_p L_n} \right) = \text{constant} \times e^{-\frac{E_G}{kT}}, \quad (17)$$

where b is the mobility ratio, σ_i is the intrinsic conductivity, σ_n and σ_p are the conductivities, and L_n and L_p are the minority carrier diffusion lengths of the n and p sides of the junction, respectively. It has been found empirically however, that I_o does not necessarily follow Equation (17), although it can usually be written as

$$I_o = A e^{\frac{-E_G}{BkT}} \quad (18)$$

where A is a constant characteristic of each material and B is a constant ≥ 1 . If we consider only the case of large input flux, i.e., $I_s/I_o \gg 1$, we can approximate $V_{mp} \sim V_{\max}$ and combining Equations (5), (15), (16), and (18), it is found that

$$\eta_{\max} \sim \frac{1}{Bf} \frac{\ln\left(\frac{AfE_G}{I_B \bar{V}_B}\right)}{\lambda f E_G}. \quad (19)$$

¹⁰ W. Shockley, *Electrons and Holes in Semiconductors*, D. Von Nostrand Co., New York, N. Y., 1950, p. 315.

The second term decreases with increasing E_G , so that there is a slight advantage gained by using a semiconductor with large E_G . The importance of low values for B and f is obvious; they determine the limiting value of η_{\max} . Since neither of these constants has been studied extensively in semiconductors, it is not possible at this time to recommend materials which might be superior to silicon in this respect.

COMPUTATION OF I_s AND THE OVER-ALL EFFICIENCY

To compute I_s and the over-all efficiency it is necessary to consider all possible losses of potential carriers. These include the following: (a) self-absorption of primary particles in the radioactive isotope, (b) reflection of these particles at the interface between the isotope and the semiconductor, (c) transmission of some of these particles through the semiconductor and, (d) the loss of minority carriers by recombination within the semiconductor before they arrive at the junction.

When all these factors have been considered, the expression for I_s assumes the form

$$I_s = Q (1 - r) (1 - e^{-\alpha l}) (1 - e^{-\alpha_0 d}) \frac{V_B i_{\max}}{w}. \quad (20)$$

In these equations, Q is the collection efficiency defined as the ratio of the rate of carrier flow across the junction to the total rate of carrier generation in the solid, r is the reflection coefficient for β particles, α is the absorption constant for β particles in the solid, l is the thickness of the absorbing semiconductor, α_0 is the self-absorption constant of the radioisotope, d is the thickness of the radioactive layer, and i_{\max} is the current leaving the surface of a radioactive layer with $d = \infty$.

In deriving Equation (20), the following assumptions were made:

(1) In their passage through matter, β particles are attenuated according to the empirical relation

$$\frac{I_R(x)}{I_R(0)} = e^{-\alpha x}, \quad (21)$$

where $I_R(x)$ and $I_R(0)$ are the β particle currents at x and $x = 0$. The absorption constant is given by another empirical relation

$$\alpha = \frac{22}{V_{B\max}^{1.33}}, \quad (22)$$

where α is the density of the absorber and $V_{B\max}$ is the maximum energy in β spectrum.

(2) In computing the current emitted by a layer of radioactive material the non-isotropic character of β emission was neglected. Under these conditions it is found that the current out of each face of the layer is given by

$$I_B(d) = \frac{qN_c G \rho A}{2 \alpha_0} (1 - e^{-\alpha_0 d}) = i_{\max} (1 - e^{-\alpha_0 d}), \quad (23)$$

where N_c is the number of disintegrations per curie, G is the specific activity in curies per gram, ρ is the density, and A is the area of the layer. The other parameters have been identified above. Table II shows the values of i_{\max} , α/ρ , α_0 , $I_{s\max} = (V_B/w) i_{\max}$, and of the maximum input power $P_{\max} = 2 i_{\max} \overline{V}_B$ which includes the power output from each side of the layer.

Table II—Properties of Layers of Some β -Emitting Radioisotopes;
 $w = 3.5$ electron volts per pair

Isotope	Specific Activity, G (Curies/gm)	i_{\max} (amp/cm ²)	Max. Input Power, P_{\max} (watts/cm ²)	$I_{s\max}$ (amp/cm ²)	α/ρ (cm ² /gm)	Self-absorption const. α_0 (cm ⁻¹)
H3	9,720	2.4×10^{-9}	0.028×10^{-3}	3.4×10^{-6}	4,110	0.36
Ni63	72	2.5×10^{-10}	0.010×10^{-3}	1.43×10^{-6}	860	7,650
Sr90-Y90	400	1.54×10^{-7}	166×10^{-3}	2.4×10^{-2}	7.7	20
Pm147	950	1.7×10^{-8}	2.5×10^{-3}	3.5×10^{-4}	165	1,300

The magnitudes of the factors in Equation (20) can be summarized as follows:

(a) Q , which is discussed in detail in the appendix, cannot be expected to exceed about 0.70 for Sr90-Y90 although it could be between 0.9 and 1.0 for other radioisotopes, such as Pm147.

(b) The reflection coefficient, r , is about 0.1 for silicon for β particles in the energy range of interest here.⁵

(c) The transmission loss, $e^{-\alpha d}$, depends on the radioisotope used. It would be negligible for Pm147 but is about 0.60 for Sr90-Y90 and a wafer of a thickness of about .020-inch. This loss would be reduced in batteries which consisted of cells placed back to back.

(d) The thickness of the radioisotope layer would have to be chosen to keep the self absorption loss $e^{-\alpha_0 d}$ at about 0.1.

In terms of the same parameters the over-all efficiency, η'_{\max} , can be shown to be

$$\eta'_{\max} = Q(1-r)(1-e^{-\alpha_0 d}) \frac{(1-e^{-\alpha_0 d})}{\alpha_0 d} \eta_{\max}, \quad (24)$$

where η_{\max} is computed from Equation (14), using Equation (20) for I_s . There exists an optimum value of η'_{\max} associated with the thickness of the radioisotope layer, since I_s increases with d whereas $\eta'_{\max} \propto 1/d$. It can be shown that this optimum occurs when $\alpha_0 d \sim 0.15$ so that the optimum d changes with the radioisotope. If, however, power output is the main consideration, a radioisotope layer whose thickness is greater than the optimum value can be used. This is shown in Figure 4 where η'_{\max} and P_{\max} are plotted against the thickness of a Pm 147 layer.

EXPERIMENTAL RESULTS

Devices Investigated

Large-area (0.25 square centimeter) alloy type p-n junctions¹¹ were made by alloying indium or lead antimony into germanium, and gold antimony into silicon. Ohmic contacts were made to the semiconductor wafers which were usually 1.5 diffusion lengths thick (see appendix) and 0.38 inch in diameter. A typical fabrication schedule consisted of firing at 550°C for ten minutes followed by a 20-second etch in CP-4.¹² All the experimental results were obtained on units whose surfaces were exposed to air. The resistivity of the semiconductor was chosen to be as low as possible consistent with high lifetime, so that the potential barrier was high and therefore I_0 was low. Values of I_0 in the range between 10^{-7} and 10^{-9} ampere per square centimeter were measured for silicon devices. Resistivities of the wafers were usually in the range of 1 to 10 ohm-centimeters.

Figure 5 shows the experimental arrangement used for bombarding the p-n junctions. By varying the load resistance, R_L , and observing the voltage, it was possible to determine I_s , V_{\max} , R_{mp} , P_{\max} , η_{\max} , and m of the electron-voltaic cells.

¹¹ R. R. Law, C. W. Mueller, J. I. Pankove, and L. D. Armstrong, "A Developmental Germanium P-N-P Junction Transistor," *Proc. I.R.E.*, Vol. 40, p. 1352, November, 1952.

¹² J. R. Haynes and W. Shockley, "The Mobility and Life of Injected Holes and Electrons in Germanium," *Phys. Rev.*, Vol. 81, p. 835, March, 1951.

Radioactive Source

The source of beta particles was a specially constructed¹³ Sr90-Y90 medical applicator. The total activity contained in the applicator was 0.25 curie, although the measured β current, I_β , which penetrated the 12-mil aluminum and stainless steel protective windows corresponded to the emission from 0.05 curie. Thus the total electron current from the source as measured by a Faraday cage was 3.2×10^{-10} ampere. The beta spectrum¹⁴ of this source as a function of aluminum absorber thickness is shown in Figure 6. The average beta energy from this

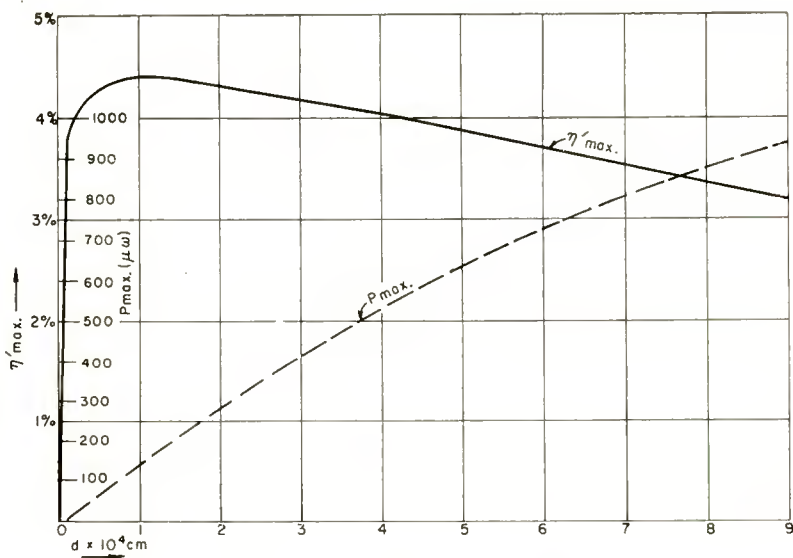


Fig. 4— η'_{\max} and P_{\max} versus thickness of radioisotope layer for Pm147; $w = 5$ electron volts per pair.

spectrum, \bar{V}_β , with no added absorber was found to be 1.05×10^6 electron volts, which high value is due to the absorption of the low-energy beta particles by the protective window of the medical applicator. Therefore, the total available radiated power from the applicator is $I_\beta \bar{V}_\beta / q = 336$ microwatts. Figure 7 shows the absorption of the beta current as a function of silicon thickness. Note that 22 per cent of the total current is absorbed by 10 mils of silicon, which is the wafer thickness of most devices tested. Thus the total power absorbed in

¹³ The medical applicators were manufactured by Tracerlab, Inc., Boston, Massachusetts.

¹⁴ The beta spectrum of the source was determined by Dr. L. N. Russell of the Mound Laboratory, operated by the Monsanto Chemical Company, Miamisburg, Ohio.

the device is about 63 microwatts. The data in Figure 7 can be used for germanium if the silicon thickness is multiplied by the ratio of densities for germanium and silicon, i.e., by 2.3.

i-V Characteristics

Figure 8 shows a current-versus-voltage curve for a typical germanium p-n junction bombarded by the source described above. The

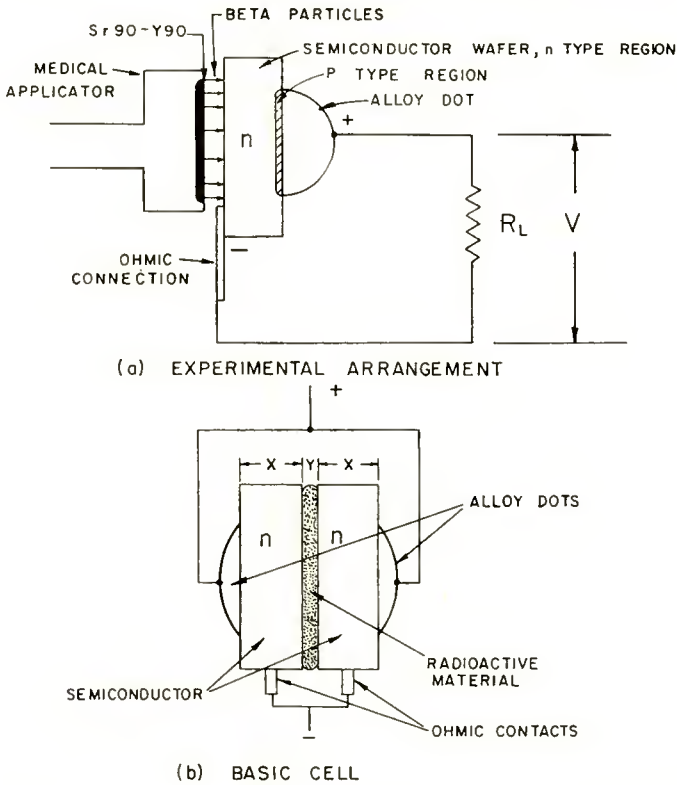


Fig. 5—Experimental arrangement for EVE measurements and a proposed basic cell.

i-V curve is linear as predicted by the theory for the small-voltage approximation. Here $V_{\max} \approx 10$ millivolts. A measurement of the slope gives a value of 770 ohms for R_{mp} , while calculation from the expression $R_{mp} = 1/\lambda I_o$ yields about 830 ohms, indicating satisfactory agreement. As a further check of the theory, V_{\max} , when it is computed from the relation $V_{\max} = I_s/\lambda I_o$ using the measured values of I_o , which was 3×10^{-5} ampere, and I_s , which was 1.35×10^{-5} ampere, is found to be 10.4 millivolts compared to the experimental value of 10.5 millivolts.

Figure 9 shows i - V characteristics of three silicon p-n junctions under bombardment. The linear approximation is no longer valid, since $\lambda V_{\max} \gg 1$, so that the general expression (Equation (3)) must be used. The result is the nonlinear i - V characteristic of the figure, which resembles that shown in Figure 3. Comparisons with theory on silicon units are difficult because neither λ nor I_0 as measured experimentally agree with theoretical values. However, if V_{\max} and V_{mp} are experi-

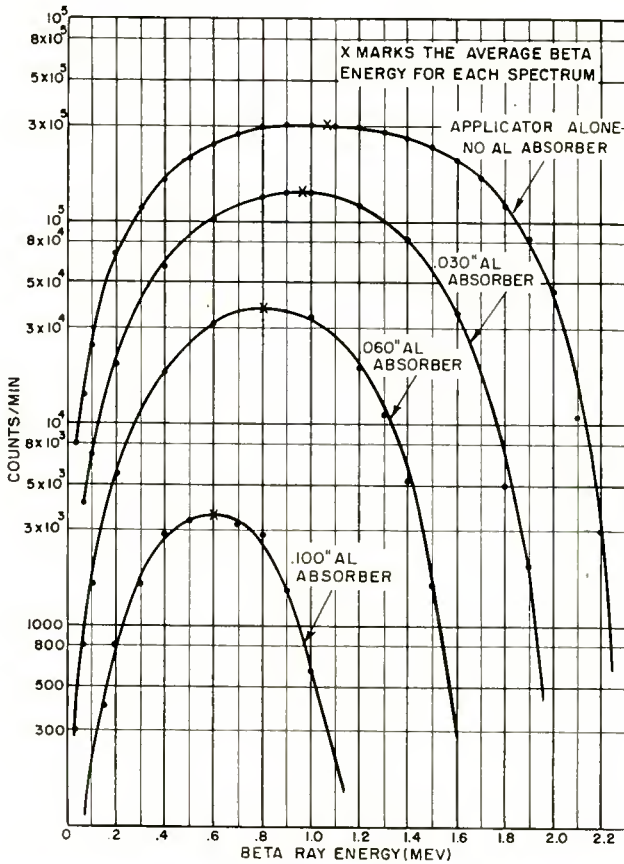


Fig. 6—Sr90-Y90 spectrum for different thickness of aluminum absorber.

mentally determined then Equation (7) yields an experimental value for λ . Knowing λ and I_s , I_0 can then be calculated using Equation (5). R_{mp} can in turn be calculated by using Equation (6) and can be compared to the measured R_{mp} . Table III shows the results of such a comparison for the three units shown in Figure 9. The calculated values of λ and I_0 are reasonable, and the agreement between the values of R_{mp} is good.

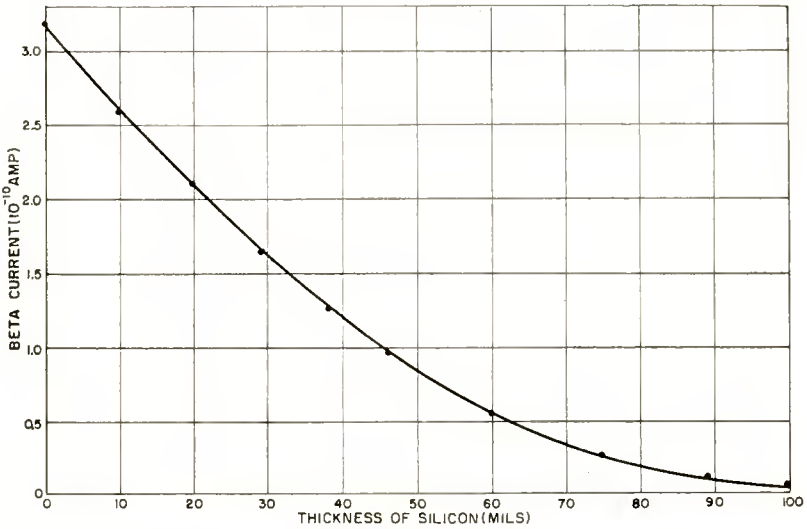


Fig. 7—Absorption of Sr90-Y90 beta radiation versus thickness for silicon absorber.

Experiments with low-energy electrons (≤ 100 kilovolts) also have been performed and the results have been compared with theory. Observations consisted of measuring the bombardment-induced current I_s and V_{max} in a large-area germanium junction. Using Equation (5), I_o was computed for each value of I_B . The average value of I_o was then combined with the measured I_s to compute V_{max} from Equation (5).

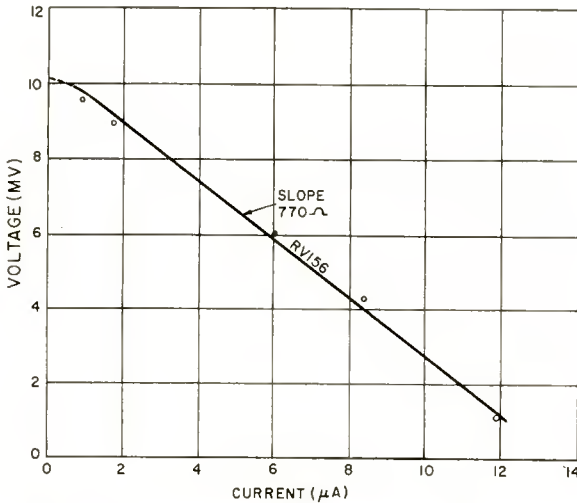


Fig. 8— i - V characteristic for germanium EVE device.

Table III

Unit	Experimental Values				Calculated Values		
	I_s (amperes)	V_{max} (volts)	V_{mp} (volts)	R_{mp} (ohms)	λ	I_0 (amperes)	R_{mp} (ohms)
SAB12	5×10^{-6}	0.354	0.285	6.6×10^4	34	2.93×10^{-11}	6.2×10^4
SAB85	7×10^{-6}	0.320	0.250	4.1×10^4	33	1.85×10^{-11}	4.3×10^4
SAB109	7.5×10^{-6}	0.312	0.240	3.58×10^4	29	3.8×10^{-10}	3.65×10^5

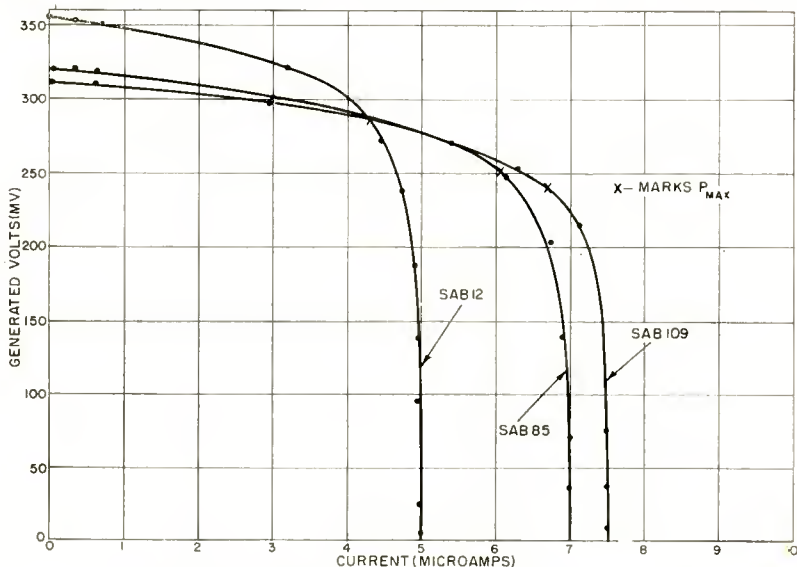


Fig. 9— i - V characteristics for silicon EVE devices.

The results are shown in Figure 10 where V_{max} is plotted as a function of I_s . The measured values of V_{max} are plotted as the experimental points.

Table IV lists the parameters and typical experimental values that have been obtained from the i - V curve for various germanium and silicon devices. P_{max} can be determined by calculating the power output which is equal to the iV product for each point on the curve. The crosses on the curves in Figure 9 indicate the maximum power point for the three units shown. R_{mp} can be computed from i_{mp} and V_{mp} . The maximum efficiency, η_{max} , is then determined from the ratio of P_{max} to the primary radioactive power absorbed in the semiconductor wafer.

Maximum Voltage

V_{max} depends on the input flux I_B and on the characteristics of the

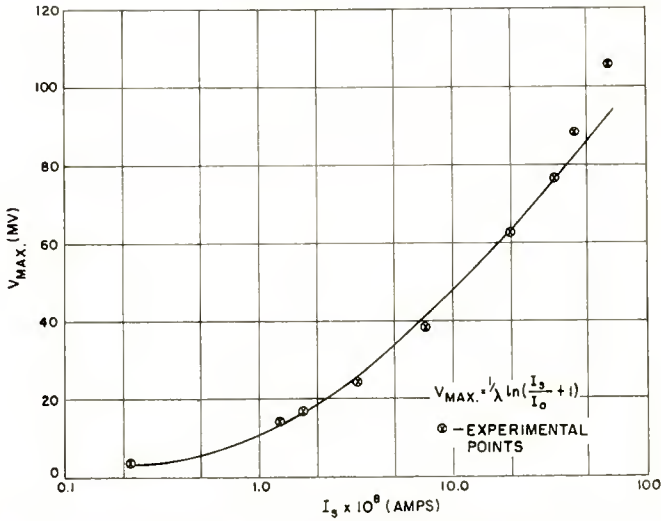


Fig. 10—Comparison between theoretical expression for V_{max} and experimental values of I_s for germanium.

semiconductor that determine I_0 . For a particular semiconductor, maximum doping in both the p and n region would give the highest values of V_{max} . For the p - n junction discussed here and using the 50-millicurie

Table IV—Properties of p - n Junction Electron-Voltaic Devices (50-millicurie Sr90-Y90 Source)

Unit	Silicon			
	V_{max} (millivolts)	I_s (microamperes)	R_{mp} (ohms)	P_{max} (microwatts)
SAB12	354	5	5×10^4	1.23
SAB85	320	7.0	4×10^4	1.51
SAB109	312	7.5	4×10^4	1.58
SAB113	318	7.8	4×10^4	1.53
SAB1006	221	19	10^4	1.41
SAB1009	233	17.4	10^4	1.56
SAB1006 + 1009 Stacked	450	9.2	5×10^4	1.92
Germanium				
RV168	25	4	2×10^3	.08
RV156	10.2	14	8×10^2	.03
RV174	20	20	1.2×10^3	.09
Ge403N-1	44	22	1600	.3

beta source, V_{\max} was as high as 354 and 44 millivolts for silicon and germanium units, respectively, as shown in Table IV.

The difference (by a factor of almost 10) between silicon and germanium was probably due to the difference in I_o , which can be shown to be about 10^4 times greater in germanium than in silicon. Such a difference in I_o could account for the factor of 10 in V_{\max} . There is some uncertainty about this factor because neither λ nor I_o behave as would be theoretically expected in silicon.

Short-Circuit Current

The measured values of I_s in Table IV fall between 5 and 19 microamperes for silicon and 4 and 22 microamperes for germanium. Since I_s is a measure of the total number of carriers generated in the solid by the incoming radiation, m and w can be calculated. The highest values of I_s that have been observed during this study were 22.0 microamperes for germanium and 19 microamperes for silicon. The wafer thicknesses were 7 mils and 14 mils respectively, and from Figure 7 this corresponds to an absorption of beta current in germanium of 9.0×10^{-11} ampere and in silicon of 8.0×10^{-11} ampere. From these figures the computed value of m in germanium is 2.5×10^5 and in silicon, 2.4×10^5 . This yields a value for w in germanium of 4.2 electron volts per pair and in silicon of 4.4 electron volts per pair. These values should also be corrected for collection efficiency, Q , which should be about 0.6 for these junctions so that the corrected value of w would be about 2.5 electron volts per pair for germanium and 2.6 electron volts per pair for silicon. More accurate determinations of w in germanium were made by measuring I_s during bombardment by monoenergetic electron beams produced by a Van de Graaf accelerator. A value of w in germanium as low as 3.0 electron volts per pair has been observed. These values may be compared to those given by McKay and McAfee⁹ for α particle bombardment, namely, 3.60 electron volts per pair in silicon and 2.94 electron volts per pair in germanium. The fact that the value of w measured by electron bombardment corresponds closely to these results indicates that the short circuit current that has been obtained by beta bombardment is as high as can be expected.

By making use of an electron-gun source, in the low-energy range, the electron multiplication was measured in an attempt to show that w is independent of the energy of the incident particles, and of the current in the bombarding beam. The bombardment was done in vacuum. The apparatus permitted the use of only three values of bombarding voltage. Table V lists these values of V_B , I_B , V_{\max} , I_s , m , and w . It is evident from the table that for the values of V_B used

there is no significant variation in w . The values of w listed in Table V corresponds to approximately $6 E_G$, where E_G is the gap width of germanium. This figure is large, because no attempt has been made to correct for collection efficiency which was probably low, since the ratio of electron range to sample thickness was not greater than 0.2 for any of the tabulated values of V_B .

Table V—Electron Multiplication versus V_B

V_B (electron volts)	I_B (amperes)	I_s (amperes)	V_{max} (millivolts)	m	w (electron volts per electron)
50×10^3	7.5×10^{-9}	6.6×10^{-5}	45	8.8×10^3	5.7
80×10^3	14.0×10^{-9}	26.0×10^{-5}	82	1.9×10^4	4.3
100×10^3	19.0×10^{-9}	36.0×10^{-5}	89	1.9×10^4	5.3

Using low-energy beams, I_s has been measured on germanium diodes as a function of the electron beam current, I_B , which was permitted to vary over almost three decades. The results indicate a linear relationship between I_s and I_B within the experimental error. Similar experiments on other junction devices using electrons from a Van de Graaf machine have confirmed the fact that the electron multiplication, m , is independent of I_B , over at least four orders of magnitude, i.e., from 10^{-10} to 10^{-6} ampere per square centimeter.

Maximum Power and Efficiency

Table IV shows the experimental values of P_{max} as obtained from the i - V curve for various silicon and germanium junctions. The highest power from a single-wafer silicon device (.010 inch thick) was 1.58 microwatts and for a germanium device (.007 inch thick) was 0.3 microwatt.

The efficiency of those devices can be expressed either as the ratio of the maximum power output delivered by the device to (a) the total beta power bombarding the semiconductor (336 microwatts) or (b) the total beta power absorbed by the semiconductor (63 microwatts for silicon, and 94.5 microwatts for germanium). Considering the best units in Table IV the efficiencies of germanium and silicon are shown in Table VI, where methods (a) and (b) refer to the methods of computation discussed above. The principal difference between these methods of calculation is the loss of primary particles by transmission through the semiconductor. This loss would be eliminated if the wafer

thickness were increased to absorb most of the beta particles. However, such a solution is not possible at this time because the technology of these semiconductors does not permit the attainment of diffusion lengths sufficiently large to collect the carriers in thicker wafers.

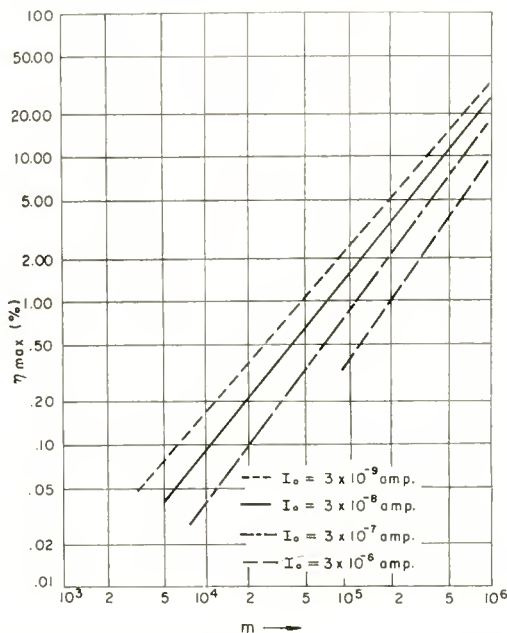


Fig. 11—Maximum efficiency, η_{max} , versus multiplication, m , for different values of I_0 .

Table VI

Method of Computation	Ge	Si
	η_{max}	η_{max}
Method (a)	.09%	0.47%
Method (b)	0.32%	2.5%

These values of η_{max} can be compared with theory by reference to Figure 11, where η_{max} is plotted against multiplication, m . In this case m is defined as the ratio of the experimentally measured I_s to the current absorbed by the wafer irradiated by the 50-millicurie Sr90-Y90 source. Such a calculation does not include reflection, transmission, and self-absorption losses. The lines in Figure 11 are computed for different plausible values of I_0 . If the best measured values of I_0 and m are used for germanium ($I_0 = 10^{-6}$ ampere and $m = 2.5 \times 10^5$) and silicon ($I_0 = 10^{-8}$ ampere and $m = 2.5 \times 10^5$) then the predicted theo-

retical values of η_{\max} are about 0.5 per cent for germanium and 3 per cent for silicon, in good agreement with the experimental results summarized in Table VI.

Finally it should be noted that η_{\max} increases with increasing I_B so that by using larger amounts of radioisotopes it can be expected that η_{\max} would increase beyond the values shown in Table VI.

Combining Units in Series and Parallel

A single radioactive source emitting penetrating radiation could activate simultaneously a number of wafers containing p-n junctions. The maximum number which can be thus used depends on the thickness of the wafers. The junctions can, of course, be electrically connected in series or parallel. Table IV includes an example of two silicon junctions stacked and connected in series. Here it is evident that the voltages add together as expected. The short-circuit current, however, is seen to be lower than in either of the two single units, which was not expected. The explanation for the latter deviation lies in the differences in R_{mp} for each of the units, since they are being irradiated by differing amounts of primary flux.

As an example of the feasibility of connecting electron-voltaic units powered by separate radioactive sources, an eight-microwatt battery energized by four separate sources was built. Each source, about the size of a dime, emitted about 3×10^{-10} ampere of Sr90-Y90 beta radiation from each face. An alloy junction was energized by radiation from each face of each of the sources. The four junctions on a given side of the sources were connected in parallel, and the two banks of four junctions were connected in series. The resulting battery had a maximum power of 8 microwatts, V_{\max} of .615 volt, I_s of 23.2 microamperes, R_{mp} of 2×10^4 ohms, V_{mp} of .404 volt. Such a battery was able to operate a three-stage superregenerative transistor earphone radio receiver.

Life of Devices

Radiation damage by high-energy electrons can limit the life of electron-voltaic devices to a shorter period than the half-life of the radioactive material.

The damage process appears to be the production of Frenkel defects by beta particles of sufficient energy. Such defects act as bulk recombination centers and reduce the minority carrier lifetime, τ , which can change by an order of magnitude¹⁵ if the defect density is increased by an order of magnitude from 10^{10} to 10^{11} per cubic centimeter.

¹⁵ P. Rappaport, "Minority Carrier Lifetime in Semiconductors as a Sensitive Indicator of Radiation Damage," *Phys. Rev.*, Vol. 94, p. 1409, June, 1954.

Figure 12 shows the behavior under bombardment of a typical silicon electron-voltaic device. V_{max} , I_s , and P_{max} are plotted versus time of bombardment using the previously described beta source. It takes about 14 hours for the power to decay by one half. The half-power decay time is a function of resistivity of the wafer. For example, a half-power point of 43 hours was observed in a device made of 450 ohm-centimeter p-type silicon.

The data of Figure 12 when replotted shows conformance to a simple theory which predicts the following relationships, where t is the time of bombardment:

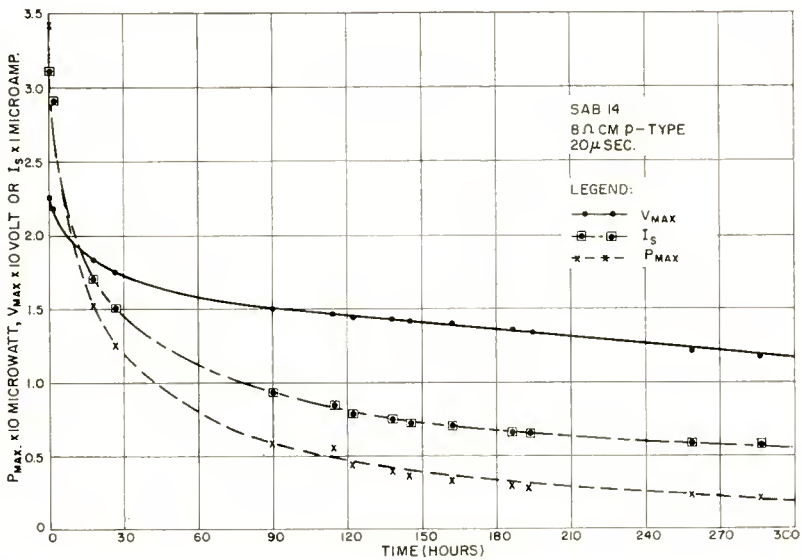


Fig. 12—Decay of V_{max} , I_s , and P_{max} with bombardment time, t , for a silicon p-n junction bombarded by a 50-millicurie Sr90-Y90 source.

$$V_{max} \propto \ln(1/t) \tag{25}$$

$$I_s^2 \propto 1/t \tag{26}$$

$$P_{max} \propto t^{-1/2} \ln(1/t). \tag{27}$$

Two factors are fundamentally important in determining the severity of the radiation damage, namely, the energy of the beta particles and the mass of the semiconductor atom. Recent experiments with monoenergetic electrons show that the electron damage threshold is 325×10^3 electron volts for germanium and 145×10^3 electron volts

for silicon.^{16,17} Therefore, in order to eliminate damage a beta source with maximum energy less than these values would be required. This would suggest a beta emitter such as Pm147. Since $V_{\beta\max}$ in the Pm147 spectrum is above the silicon threshold, it would preferably be used with a semiconductor of higher atomic weight such as CdTe.

Radiation damage cannot be effectively reduced by the use of absorbers to decrease the energy of the beta particles. This is demonstrated in Figure 6. Only 0.5 per cent of the beta current is transmitted when a .100-inch aluminum absorber is employed while the average energy is reduced from 1.05×10^6 to 0.58×10^6 electron volts, still above the damage threshold.

Effect of Temperature

A phenomenon which depends on the properties of a semiconductor such as germanium or silicon should exhibit considerable sensitivity to temperature, and the EVE is no exception. The theory of the EVE shows that the highest efficiency is realized when the rate of radioactive generation of carriers is much larger than the rate of thermal generation, i.e., $(I_s/I_o) \gg 1$. This ratio decreases rapidly as temperature increases, so that the output decreases.

Measurements of the photovoltaic effect in germanium and the electron-voltaic effect in silicon were made as a function of temperature in the range -60°C to 80°C . It was found that in the vicinity of 27°C , V_{\max} varies with the temperature with a slope of -1.5 millivolts per $^\circ\text{C}$ in germanium and -1 millivolt per $^\circ\text{C}$ in silicon. The curves in Figure 13 show a series of i - V characteristics as a function of temperature for silicon. The maximum power delivered (marked X on each curve) at -68°C is 24 times that delivered at 23°C , thus indicating the expected increased output from such devices at low temperatures.

DISCUSSION

Design of a Basic Cell

The ultimate potentialities of EVE beta energy converters can be illustrated by considering the properties of a basic cell such as that shown in Figure 5. For high collection efficiency the thickness of the wafers (X in Figure 5) should not exceed one diffusion length which,

¹⁶ J. J. Loferski and P. Rappaport, "Electron Voltaic Study of Electron Bombardment Damage and Its Thresholds in Ge and Si," *Phys. Rev.*, Vol. 98, p. 1861, June, 1955.

¹⁷ P. Rappaport and J. J. Loferski, "Thresholds for Electron Bombardment Induced Lattice Displacements in Si and Ge," *Phys. Rev.*, Vol. 100, p. 1261, November, 1955.

for low resistivity silicon, is about 0.05 centimeter. The thickness of the radioactive layer (*Y* in Figure 5) is chosen so that the current out of each face of the layer is 90 per cent of i_{\max} (defined in the section on self-absorption). Table VII shows the results of such a calculation. The isotopes are assumed to have the highest possible specific activities and the value of pertinent parameters shown in Tables I and II have

Table VII—Properties of a Basic Cell (Area = 1 square centimeter)

Isotope	<i>X</i> (centi- meters)	<i>Y</i> (centi- meters)	<i>I_s</i> (amperes)	<i>P_{max}</i> (milli- watts)	η_{\max} Method (b)	η'_{\max}	Total Activity (curies)
Sr90–Y90	.05	.11	1.1×10^{-2}	9.9	5.9%	2.4%	11 μ
Pm147	.005	.002	2.6×10^{-4}	0.18	7.1%	2.8%	1 μ

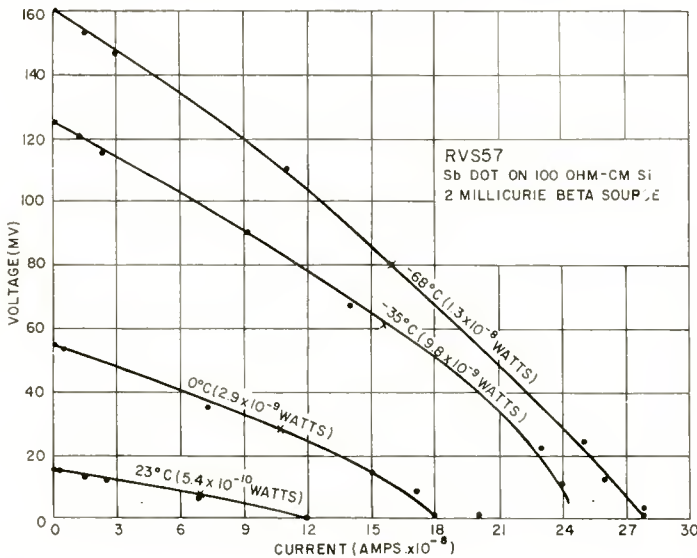


Fig. 13—*i-V* characteristics versus temperature for a bombarded silicon p-n junction.

been used to compute η'_{\max} , the over-all efficiency. Table VII also shows the maximum efficiency excluding self-absorption in the isotope, i.e., the ratio of power output from the junction to the power input at its front face which is η_{\max} of Method (b) above. The following values were used in arriving at Table VII: $I_0 = 10^{-9}$ ampere per square centimeter; $\lambda^{-1} = 30$ volts; $Q = 0.9$; $w = 3.5$ electron volts per pair; and $r = 0.1$.

From the data in Table VII one can also compute the power available per unit volume. The figure for Sr90-Y90 is .050 watt per cubic centimeter and for Pm147 it is 0.017 watt per cubic centimeter. This figure for Sr90-Y90 is somewhat low because the values in the table include a 60 per cent transmission loss. Part of this loss would be recovered in a battery containing many basic cells packed together so that each cell utilizes some radiation from adjacent cells.

Comparison with Other Direct Conversion Methods

Finally it is interesting to compare the EVE as a method of direct conversion of radioactivity to the other methods appearing in the literature.¹⁸ Table VIII shows the results. Because of the high multiplication accompanying the absorption of beta particles in the semiconductor, the EVE gives a high current and lower impedance than any of the other methods for a radioactive source of specified intensity. The problem of direct conversion of radioactive energy can be viewed as that of transforming the high impedance of the source to a practical value, without an undue loss of energy during the transformation. Thus for the .05 curie Sr90-Y90 source used for most of the experiments, the source impedance is $Z_s = V/i = 10^6/10^{-10} = 10^{16}$ ohms. The impedances after conversion are listed in Table VIII. Here it is evident that the EVE is superior to the other effects listed, since the relatively low impedance offers many practical advantages.

Table VIII

Method	Voltage (volts)	Current (amperes)	Impedance (ohms)	Eff.
High-vacuum charger	to 350,000	10^{-9}	10^{15}	25%
Dielectric charger	to 10,000	10^{-11}	10^{13}	up to 1%
Contact potential	1 per cell	10^{-11}	10^8-10^{11}	$10^{-2}\%$
Electron-voltaic device	.3 per cell	10^{-5}	10^2-10^4	2.5%

The EVE devices and the contact potential device possess an advantage over the vacuum and dielectric chargers because the latter do not have any current multiplication mechanisms. To reduce their impedance their operating voltage must be reduced, and since their efficiency is given by

¹⁸ E. G. Linder, P. Rappaport, and J. J. Loferski, "The Direct Conversion of Radiation into Electrical Energy," to appear in the Proceedings of the International Conference on the Peaceful Uses of Atomic Energy, June, 1955.

$$\eta = \frac{qV}{2\bar{V}_B}, \quad (28)$$

where V is the maximum voltage attained by the device; the efficiency is decreased by the same factor as the voltage.

The EVE yields higher efficiencies than the contact potential device for two reasons: (1) The ionization energy for a solid is 1/10 of that for a gas, i.e., it takes about 3 electron volts to yield a pair of charge carriers in a semiconductor whereas in a gas about 30 electron volts is required. (2) The specific ionization is greater in a solid than in a gas so that it becomes difficult to absorb all the energy of the radioactive particles in a contact potential device.

ACKNOWLEDGMENTS

It is with pleasure that the authors acknowledge the encouragement and interest displayed by I. Wolff and E. W. Herold. For informative discussions and helpful suggestions we are indebted to many of our colleagues at the RCA Laboratories, especially to D. O. North, A. R. Moore, and W. M. Webster, and to Professor M. G. White of Princeton University.

APPENDIX—CALCULATION OF Q

All the minority carriers which are generated in the solid by the radiation do not contribute to the power developed in the load since some of them recombine with majority carriers either inside the volume or at the surface, thus reducing I_s and η_{\max} . For the general case it is convenient to define a collection efficiency, Q , which is the ratio of the carriers passing through the circuit (i.e., the experimentally measured short circuit current, I_s) to the total number of carriers generated in the solid per unit time; thus

$$Q = \frac{I_s}{(1-R)(1-\epsilon^{-\alpha l})m i_{\max}(1-\epsilon^{-\alpha_0 d})}. \quad (29)$$

Q can be computed for plane geometry which approximates the experimental units under investigation. We consider the case of an infinite plane p-n junction at $x=l$ with the n region extending from $x=0$ to $x=l$. The surface at $x=0$ is irradiated by N_0 particles per second. Minority carrier generation in the p region has been neglected since for alloy-type junctions the recrystallized p region is very thin, and most of the contribution to the EVE comes from the n-type material.

Under equilibrium conditions the net rate of generation of minority carriers (the discussion is centered on holes as minority carriers) in a volume dV is equal to the loss of carriers by recombination in the bulk and the diffusion into the volume so that

$$\alpha N_o e^{-\alpha x} = \frac{p}{\tau_p} - D_p \frac{\partial^2 p}{\partial x^2}. \quad (30)$$

To calculate Q we must determine the diffusion current across the junction at $x = l$;

$$\left. \frac{\partial p}{\partial x} \right|_{x=l}, \quad (31)$$

so that Equation (30) must be solved subject to appropriate boundary conditions, which in this case are as follows:

$$\left. \frac{\partial p}{\partial x} \right|_{x=0} = \frac{s_s}{D_p}, \quad (32)$$

$$p(l) = 0, \quad \text{i.e., } s|_{x=l} = \infty. \quad (33)$$

Thus the surface at $x = 0$ is represented by a recombination velocity s , and the junction at $x = l$ by an infinite recombination velocity. Then

$$Q = \frac{D_p \left. \frac{\partial p}{\partial x} \right|_{x=l}}{\alpha N_o (1 - e^{-\alpha l})}, \quad (34)$$

where the denominator is the total minority carrier current generated in the n region between $x = 0$ and $x = l$. The solution of the problem finally takes the form

$$Q = \frac{\beta v e^{\nu l} - \gamma v e^{-\nu l} - \alpha e^{-\alpha l}}{(1 - e^{-\alpha l}) \left(1 - \frac{\nu^2}{\alpha^2} \right)}, \quad (35)$$

$$\text{where } \beta \Delta = e^{-\nu l} (h + \alpha) - e^{-\alpha l} (\nu + h), \quad (36)$$

$$\gamma \Delta = e^{-\alpha l} (h - \nu) - e^{\nu l} (h + \alpha), \quad (37)$$

$$\Delta = e^{-\nu l} (\nu - h) + e^{\nu l} (\nu + h). \quad (38)$$

The symbols used above are defined as follows:

$$v = \frac{1}{L_p}, \quad (39)$$

$$h = \frac{s}{D_p}, \quad (40)$$

s = surface recombination velocity,

D_p = diffusion constant,

and the other symbols are as defined in the text.

Values of Q computed from the above equations are plotted in Figure 14 where Q versus the ratio l/L_p for values of α and s appro-

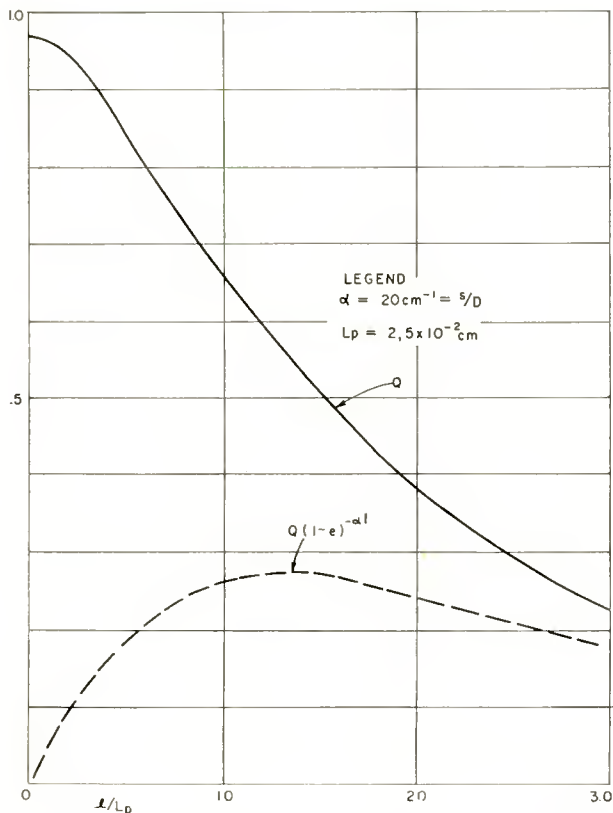


Fig. 14—Collection efficiency, Q , and $Q(1 - e^{-\alpha l})$ showing existence of an optimum value of l at $l = 1.5 L_p$.

priate to Sr90-Y90 and silicon is computed. The following conclusions can be made concerning the interrelation among the parameters affecting Q :

(a) Smaller values of s yield larger values of Q .

(b) For a given value of s , α , and l , Q increases with increasing L_p until it saturates at a value which is a function of s , α , and l .

(c) Although neither of these figures illustrates this fact directly, Q increases for fixed s , L_p , and l as α decreases.

(d) There is a close relation between Q and transmission losses, i.e., if s , α , and L_p are fixed, then Q increases as l decreases, but the fraction of incident particles which are lost by transmission increases. If these two parameters are considered simultaneously the product $Q(1 - e^{-\alpha l})$ which appears in the expression for the over-all efficiency, η'_{\max} passes through a maximum value. This behavior is shown in Figure 14, where it is seen that with values of α characteristic of Sr90-Y90 and silicon with characteristic L_p and s , the optimum η'_{\max} occurs for $l/L_p = 1.5$.

If surface losses are neglected and a uniform generation rate, g , is assumed, then all the minority carriers within a diffusion length of the junction will flow across it, and Q can be shown to be given by

$$Q = g (L_p + L_n). \quad (41)$$

RCA TECHNICAL PAPERS†

Fourth Quarter, 1955

Any request for copies of papers listed herein should be addressed to the publications to which credited.*‡

- "An Accurate Electronic Multiplier," S. Sternberg, *RCA Review* (December) 1955
- "Analogue Computers," A. W. Vance, E. C. Hutter, J. Lehmann, and M. L. Wadlin, Chapter of *Advances in Electronics and Electron Physics*, Vol. VII, Edited by L. Marton, Academic Press, New York, N. Y. 1955
- "Application of Carbon Microphones to Narrow-Band Speech Transmission, R. M. Carrell, *RCA Engineer* (October-November) .. 1955
- "Applications of Ferrites to Deflection Components, B. V. Vonderschmitt and W. H. Barkow, *RCA Engineer* (December-January) 1955
- "Audio-Standard Generator," P. Koustas, *Electronics* (December) .. 1955
- "Automatic Chroma Control Circuitry," W. W. Cook, *Service* (November) 1955
- "Blower Requirements for RCA Forced-Air-Cooled Tubes," *RCA Application Note AN-161*, RCA Tube Division, Harrison, N. J. (October) 1955
- "Broadcast and Communications Equipment Withstands Atom Blast," E. C. Bill, *Broadcast News* (October) 1955
- "Calculations of Alloying Depth of Indium in Germanium," L. Pensak, *RCA Industry Service Laboratory Research Bulletin RB-23* (December 12) 1955
- "Chemistry of Color Television," D. J. Donahue, *RCA Engineer* (October-November) 1955
- "Class B Operation of Transistors III—Hybrid Radio," K. E. Loofbourrow, *Electronic Design* (October) 1955
- "Color Television," V. K. Zworykin, Technical Bulletin, *Comite International de TV* (France) 1955
- "Color Television IF Amplifiers," B. Fisher, *RCA Industry Service Laboratory Bulletin LB-998* (October 20) 1955
- "Colour Television in the U.S.A.," C. G. Mayer, *Electronic Engineering* (November) 1955
- "Control of Light Intensity in Television Projectors," K. Sadashige and B. F. Melchioni, *Broadcast News* (October) 1955
- "Corrections to the Theory of the Grounded-Grid Triode," W. A. Harris, *IRE Convention Record* 1955
- "Cross-Modulation in Transistor RF Amplifiers," D. D. Holmes, *RCA Industry Service Laboratory Bulletin LB-1008* (November 28) 1955
- "Crystal Selection in Stabilized Frequency Control," E. M. Washburn and R. R. Bigler, *RCA Engineer* (December-January) 1955
- "Cyclotron Resonance in Ge-Si Alloys," S. M. Christian, (co-author), *Phys. Rev.* (Letter to the Editor) (November 15) 1955

† Report all corrections or additions to RCA Review, RCA Laboratories, Princeton, N. J.

* *RCA Industry Service Laboratory Bulletins* are not published and are issued only as a service to licensees of the Radio Corporation of America.

‡ *The RCA Engineer* is published exclusively for the use of RCA engineers and is not available for outside distribution.

- "A DC Stabilized Color Difference Amplifier," C. B. Oakley, *RCA Industry Service Laboratory Bulletin LB-999* (October 20) .. 1955
- "Development of the 'Candelabra' Antenna System," L. J. Wolf, *Broadcast News* (October) 1955
- "Directly Heated Hum-Free Cathode for Cathode-Ray Tubes," F. H. Nicoll, *Rev. Sci. Instr.* (December) 1955
- "A Double-Corona Charging Unit and Its Utilization in the Electrofax Process," E. C. Giaimo, Jr., *RCA Industry Service Laboratory Bulletin LB-1009* (December 12) 1955
- "Edge Electroluminescence from ZnS Single Crystals," R. W. Smith, *Phys. Rev.* (Letter to the Editor) (October 15) 1955
- "Edge Emission from ZnS Single Crystals," R. W. Smith, *RCA Industry Service Laboratory Research Bulletin RB-16* (October 25) 1955
- "Electrofax—A New Tool for the Graphic Arts," M. L. Sugarman, Jr., *The American Pressman* (November) 1955
- "'Electrofax'—A New Tool for the Graphic Arts," M. L. Sugarman, Jr., *RCA Industry Service Laboratory Bulletin LB-1006* (November 1) 1955
- "An Electroluminescent Light-Amplifying Picture Panel," B. Kazan and F. H. Nicoll, *Proc. I.R.E.* (December) 1955
- "An Electroluminescent Light-Amplifying Picture Panel," F. H. Nicoll and B. Kazan, *RCA Industry Service Laboratory Research Bulletin RB-14* (October 14) 1955
- "Electrolytic Etching at Small-Angle Grain Boundaries in Germanium," S. G. Ellis, *Phys. Rev.* (November 15) 1955
- "Electron and Ion Motion in Oxide Cathodes," L. S. Nergaard, *RCA Industry Service Laboratory Research Bulletin RB-21* (November 26) 1955
- "The Electronic Energy Band Structure of Silicon and Germanium," F. Herman, *Proc. I.R.E.* (December) 1955
- "The Electronic Energy Band Structure of Silicon and Germanium," F. Herman, *RCA Industry Service Laboratory Research Bulletin RB-27* (December 26) 1955
- "Electron Optics," E. G. Ramberg, Chapter in book—*Fundamental Formulas of Physics*, Edited by Donald Menzel, D. Van Nostrand 1955
- "Engineering the RCA Bizmac System," J. W. Leas, *RCA Engineer* (December-January) 1955
- "Experimental High-Transconductance Gun for Cathode-Ray Tubes," F. H. Nicoll, *RCA Industry Service Laboratory Bulletin LB-1003* (October 24) 1955
- "Experimental High-Transconductance Gun for Kinescopes," F. H. Nicoll, *RCA Review* (December) 1955
- "Forward Scattering of Radio Waves by Anisotropic Turbulence," H. Staras, *Proc. I.R.E.* (October) 1955
- "Grounded-Green-Grid Kinescope Adding System," A. Macovski, *RCA Industry Service Laboratory Bulletin LB-992* (October 20) .. 1955
- "A Hermetic Enclosure for Power Transistors," M. W. Green, *RCA Industry Service Laboratory Bulletin LB-1011* (December 14) 1955
- "High-Emitter-Efficiency Alloy Materials for P-N-P Transistors," C. L. Carlson and L. D. Armstrong, *RCA Industry Service Laboratory Bulletin LB-1013* (December 16) 1955
- "High-Gain Transistor Amplifier," J. J. Davidson, *Audio* (October) 1955
- "A High-Gain Video-Amplifier Peaking Circuit," L. Schupak, *RCA Industry Service Laboratory Bulletin LB-996* (October 20) .. 1955
- "High-Level Triode Demodulator Design Considerations," R. L. Pickholtz, *RCA Industry Service Laboratory Bulletin LB-997* (October 20) 1955

“High-Speed Electronic Fault Protection for Power Tubes and Their Circuitry,” W. N. Parker and M. V. Hoover, <i>IRE Convention Record</i>	1955
“Image Gradation, Graininess and Sharpness in Television and Motion-Picture Systems, Part IV, A & B: Image Analysis in Photographic and Television Systems (Definition and Sharpness),” O. H. Schade, <i>Jour. S.M.P.T.E.</i> (November)	1955
“Improvement in Color Kinescopes Through Optical Analogy,” P. E. Kaus, D. D. VanOrmer, and D. W. Epstein, <i>RCA Industry Service Laboratory Bulletin LB-1002</i> (October 25)	1955
“Improvement in Color Kinescopes Through Optical Analogy,” D. W. Epstein, P. Kaus, and D. D. VanOrmer, <i>RCA Review</i> (December)	1955
“Instantaneous Light Output and Build-Up Effects in Electroluminescent Phosphors,” A. J. Pressley, <i>RCA Industry Service Laboratory Research Bulletin RB-24</i> (December 19)	1955
“Interception Noise in Electron Beams at Microwave Frequencies,” W. R. Beam, <i>RCA Review</i> (December)	1955
“Junction Transistor Designed for Iterative Operation at Low Frequencies,” L. J. Giacioletto, <i>RCA Industry Service Laboratory Bulletin LB-1016</i> (December 30)	1955
“Land-Mobile Communications,” J. R. Neubauer, <i>RCA Engineer</i> (October-November)	1955
“A Locked-Oscillator Quadrature-Grid FM Sound Detector,” J. Avins and T. J. Brady, <i>RCA Review</i> (December)	1955
“Looking Ahead in Research on Gaseous Conduction Processes,” Edward O. Johnson, <i>RCA Engineer</i> (October-November) ...	1955
“A Low-Cost Sound Detector for Television Receivers,” T. J. Brady and J. Avins, <i>RCA Industry Service Laboratory Bulletin LB-1000</i> (October 20)	1955
“Low-Noise Traveling-Wave Tubes,” A. J. Bianculli, R. M. Collins, E. W. Kinaman, and G. Novak, <i>RCA Engineer</i> (October-November)	1955
“Magnetoresistance of Germanium-Silicon Alloys,” M. Glicksman, <i>Phys. Rev.</i> (November 15)	1955
“A Method for Salvaging Components of Brazed Assemblies,” M. B. Lemeshka, <i>RCA Industry Service Laboratory Bulletin LB-1015</i> (December 27)	1955
“Miniature Loudspeakers for Personal Radio Receivers,” J. C. Bleazey, E. G. May, and J. Preston, <i>RCA Industry Service Laboratory Bulletin LB-1004</i> (October 31)	1955
“The Need for Some Standards in Electron Microscopy,” J. Hillier, <i>Scientific Instrument News</i> , Vol. 1, No. 1	1955
“New Alignment and Constructional Techniques for the Bode Linear Phase Shift Filter,” G. L. Fredendall, <i>RCA Industry Service Laboratory Research Bulletin RB-25</i> (December 20)	1955
“New Dual-Channel Consolette,” E. J. Meehan, <i>Broadcast News</i> (December)	1955
“A New Low-Power Single-Sideband Communication System,” E. A. Laport and K. L. Neumann, <i>RCA Review</i> (December)	1955
“A Noise-Clipping AGC Circuit for High-Gain Video Amplifiers,” A. Macovski, <i>RCA Industry Service Laboratory Bulletin LB-993</i> (October 20)	1955
“Noise Considerations for P-N-P Junction Transistors,” J. W. Englund, <i>RCA Industry Service Laboratory Research Bulletin RB-20</i> (November 26)	1955
“Nomographs for Determining Significant Differences,” C. H. Li, <i>Metal Progress</i> (November)	1955
“Nomographs for Determining Significant Differences,” C. H. Li, <i>RCA Engineer</i> (December-January)	1955

"Nylon for Test-Socket Covers Increases Efficiency," I. Weiss, <i>RCA Engineer</i> (December-January)	1955
"Optical Factors in the Photoemission of Thin Films," E. G. Ramberg, <i>RCA Industry Service Laboratory Research Bulletin RB-22</i> (December 12)	1955
"Opto-Electronic Devices and Networks," E. E. Loebner, <i>Proc. I.R.E.</i> (December)	1955
"A Parabolic Tubeless Convergence Circuit for the RCA 21-Inch Color Kinescope," M. D. Nelson, <i>RCA Industry Service Laboratory Bulletin LB-995</i> (October 20)	1955
"Peak Brightness Considerations in Color Television Receivers," R. N. Rhodes, <i>RCA Industry Service Laboratory Bulletin LB-1001</i> (October 20)	1955
"Performance of Photoconductors," A. Rose, <i>Proc. I.R.E.</i> (December)	1955
"Photoconduction in Germanium and Silicon," M. L. Schultz and G. A. Morton, <i>Proc. I.R.E.</i> (December)	1955
"Photoconduction in Germanium and Silicon," M. L. Schultz and G. A. Morton, <i>RCA Industry Service Laboratory Research Bulletin RB-19</i> (November 21)	1955
"Photoconductivity of the Sulfide, Selenide, and Telluride of Zinc or Cadmium," R. H. Bube, <i>Proc. I.R.E.</i> (December)	1955
"Planning TV Microwave Systems," <i>Broadcast News</i> (December).	1955
"A Portable Transmitter-Receiver for 148 Mc.," J. F. Sterner, <i>Rad. and Tele. News</i> (November)	1955
"Preparation, Properties, and Applications of a New Oxide Permanent Magnet Material," I. Gordon and H. L. Donley, <i>RCA Industry Service Laboratory Research Bulletin RB-18</i> (November 18)	1955
"Printed Deflection Yoke Design," H. J. Benzuly, <i>Tele-Tech</i> (December)	1955
"Problems of Producing Low-Noise Electron Beams," R. W. Peter, <i>Proceedings of the Symposium on Modern Advances in Microwave Techniques</i> (November 9, 1954)	1955
"Progress in Experimental High-Frequency Transistors," Harwick Johnson, <i>RCA Engineer</i> (December-January)	1955
"The RCA Bizmac Electronic Accounting System," W. K. Halstead, <i>RCA Engineer</i> (December-January)	1955
"RCA Demonstrates Color TV for Medical Use," E. T. Griffith, <i>Broadcast News</i> (October)	1955
"RCA Test Points," J. A. May, <i>Rad. and Tele. News</i> (November) ..	1955
"Recent Advances in Power Junction Transistors," B. N. Slade, <i>RCA Industry Service Laboratory Bulletin LB-1010</i> (December 14)	1955
"A Secondary Frequency Standard," R. M. Mendelson, <i>RCA Ham Tips</i> (December)	1955
"Single-Ended Class-C Amplifier Design," C. A. West, <i>RCA Ham Tips</i> (October)	1955
"Some Problems Associated with Television AGC Circuits," L. P. Thomas, <i>RCA Engineer</i> (October-November)	1955
"Space-Control Production Area," S. Cornberg, <i>Broadcast News</i> (December)	1955
"Stability Considerations in Transistor IF Amplifiers," T. O. Stanley and D. D. Holmes, <i>RCA Industry Service Laboratory Bulletin LB-1014</i> (December 20)	1955
"The Structure and Development of the Cell Wall in Nitella," G. B. Chapman and P. B. Green, <i>American Journal of Botany</i> (October)	1955
"Studies of Externally Heated Hot Cathode Arcs," Edward O. Johnson, <i>RCA Review</i> (December)	1955

"A Study of the Etching Rate of Single-Crystal Germanium," P. R. Camp, <i>Journal of the Electrochemical Society</i> (October)	1955
"Symmetry Properties of the Energy Bands of the Zinc Blende Structure," R. H. Parmenter, <i>Phys. Rev.</i> (October 15)	1955
"A Synchronous Color Killer and Balanced Phase Detector," A. Macovski, <i>RCA Industry Service Laboratory Bulletin LB-994</i> (October 20)	1955
"Technical Standards for Color Television," J. W. Wentworth, <i>RCA Engineer</i> (October-November)	1955
"Television Vertical Aperture Compensation," A. C. Schroeder and W. G. Gibson, <i>Jour. S.M.P.T.E.</i> (December)	1955
"Television Vertical Aperture Compensation," W. G. Gibson and A. C. Schroeder, <i>RCA Industry Service Laboratory Research Bulletin RB-17</i> (November 14)	1955
"Test Equipment for Color-TV Receivers," E. R. Klingeman and S. Wlasuk, <i>Service</i> (November)	1955
"Thresholds for Electron Bombardment Induced Lattice Displacements in Si and Ge," P. Rappaport and J. J. Loferski, <i>Phys. Rev.</i> (November 15)	1955
"Transient Response of Detectors in Symmetric and Asymmetric Sideband Systems," T. Murakami and R. W. Sonnenfeldt, <i>RCA Review</i> (December)	1955
"Transistor Electronics," A. W. Lo, R. O. Endres, J. Zawels, F. D. Waldhauer, and C. C. Cheng, Prentice-Hall, Inc., Englewood Cliffs, New Jersey	1955
"Transistor Video Amplifiers," M. C. Kidd, <i>RCA Engineer</i> (December-January)	1955
"A Transistorized Output Meter," J. J. Lawler and J. D. Hodge, <i>RCA Engineer</i> (December-January)	1955
"Transistorized Sync Separator Circuits for Television Receivers," H. C. Goodrich, <i>RCA Review</i> (December)	1955
"Two Bridged-T Equivalents of the Bode Low-Pass Lattice Filter," G. L. Fredendall, <i>RCA Industry Service Laboratory Research Bulletin RB-26</i> (December 20)	1955
"Underwriters' Laboratories—Their Importance to the Design Engineer," J. W. Fulmer, <i>RCA Engineer</i> (October-November)	1955
"The Use of Concentric-Line Transformers in UHF Measurements," W. A. Harris and J. J. Thompson, <i>IRE Transactions on Instrumentation</i> (PGI-4) (October)	1955
"Vapor Pressure Data on Metals and Alloys," E. Goldman, <i>RCA Industry Service Laboratory Research Bulletin RB-15</i> (October 24)	1955
"A Variable-Capacitance Germanium Junction Diode for UHF," J. O'Connell and L. J. Giacoletto, <i>RCA Industry Service Laboratory Bulletin LB-1005</i> (November 1)	1955
"Variation of Junction-Transistor Current-Amplification Factor with Emitter Current," L. J. Giacoletto, <i>Proc. I.R.E.</i> (Letter to the Editor) (October)	1955
"A 20-Watt Transistor Audio Amplifier," H. C. Lin, <i>RCA Industry Service Laboratory Bulletin LB-1012</i> (December 14)	1955
"The 21-Inch Tricolor Picture Tube," W. W. Lenz, Jr., <i>Service</i> (November)	1955
"35mm Intermittent Motion Picture Projector for Color TV," W. R. Isom and W. F. Fisher, <i>Broadcast News</i> (October)	1955
"35mm Intermittent Motion-Picture Projector for Color Television," W. F. Fisher and W. R. Isom, <i>Jour. S.M.P.T.E.</i> (December)	1955

Correction:

In the paper entitled "A Locked-Oscillator Quadrature-Grid FM Sound Detector," by Jack Avins and Thomas Brady, which appears on pages 648-655 of the December 1955 issue, the strip of 3 oscilloscope traces which make up Figure 5, page 652, has been reversed. The trace at the right actually shows an undamped input with a scope gain of unity, and the trace at the left shows a damped input with a scope gain of 10. The center trace is properly identified.

AUTHORS



L. D. ARMSTRONG received the B.A. degree from the University of Saskatchewan, Canada in 1938, and the M.A. and Ph.D. degrees in Physics from the University of Toronto in 1940 and 1949, respectively. He was employed as a physicist at the National Research Laboratories in Ottawa, Canada from 1942 to 1947. After receiving his Ph.D. degree in 1949, he joined the Radio Corporation of America at the David Sarnoff Research Center in Princeton, N. J. His work at the Laboratories was concerned primarily with ceramic-to-metal seals and semiconductor devices. In 1954, he transferred

to the Semiconductor Division at Harrison, N. J., where he is working on the development of commercial transistors. Dr. Armstrong is a Member of the Institute of Radio Engineers.

WALTER R. BEAM received the B.S. degree in Electrical Engineering from the University of Maryland. He pursued graduate work while serving as Instructor in Electrical Engineering at the same university, and received the M.S. degree in 1950. During part of this period he was also engaged in development of radio sounding instruments at Washington Institute of Technology. He joined the Microwave Tube group at RCA Laboratories in 1952. In 1953 he was awarded the Ph.D. degree from the University of Maryland. Since joining RCA he has been engaged in research on microwave amplifiers and electron guns. Dr. Beam is a member of Institute of Radio Engineers, Tau Beta Pi, and Sigma Xi, and is a licensed Professional Engineer.



MICHAEL BENTIVEGNA received the B.S. degree in Electrical Engineering from the Newark College of Engineering in 1952. After graduation, he joined the Tube Division of the Radio Corporation of America in Harrison, N. J. as a design and development engineer in the Receiving-Tube Advanced Development activity. He worked principally on the development of semiconductor devices, and became a member of the Semiconductor Development Shop when the new Semiconductor Division was organized. He was concerned with the design of commercial and military transistors. In 1955 he joined CBS-Hytron in Danvers, Mass.

D. J. BLATTNER received the B.S. degree in Electrical Engineering from Columbia University while a student in the Navy college-training program. After active duty in the Navy, he returned to Columbia to receive the M.A. degree in Physics and do research in solid-state devices. He also served as an assistant and lecturer in physics. He joined the RCA Laboratories at Princeton, N. J. in 1953, and worked on traveling-wave-tube problems. In 1955, he transferred to the Microwave-Tube Advanced Development activity of the Tube Division in Harrison, N. J. Mr. Blattner is a member of Sigma Xi and the Institute of Radio Engineers.



JOHN C. BLEAZEY received the B.S. degree in Electrical Engineering from the Drexel Institute of Technology in 1940. In 1941 he was commissioned in the U.S. Army Signal Corps. While in the Army, he was promoted to the rank of Captain and commanded a Radar Maintenance Unit in the European Theatre till the end of the war. In 1945 he joined the RCA Laboratories Division, Princeton, N. J. and has been engaged in research in acoustics. Mr. Bleazey is a member of the Acoustical Society of America.

CARL L. CARLSON received the B.S. degree in Physics and Mathematics from Upsala College, East Orange, N. J. During 1948 and 1949, he did graduate work in Physics at Brooklyn Polytechnic Institute, N. Y. He was employed as a physicist at the Research Laboratories of Tung Sol Electric Company in Bloomfield, N. J. from 1948 to 1952. He joined the Tube Division of the Radio Corporation of America in Harrison, N. J. in 1952 as a research and development engineer in the Chemical and Physical Laboratory. Shortly thereafter, he transferred to the Advanced Materials activity of the Semiconductor Division, where he is concerned with the development of quality materials for use in commercial transistors.



NORMAN DITRICK received the B.S. and M.S. degrees in Physics from Ohio State University in 1952. He joined RCA as a specialized trainee in July of 1952, and was later assigned to the Receiving-Tube Advanced Development Activity of the Tube Division. He was transferred to the Semiconductor Advanced Devices Development Activity in April of 1953 and, since that time, has been working principally on high-frequency transistor development. Mr. Ditrick is a member of Sigma Pi Sigma, Tau Beta Pi, and the Institute of Radio Engineers.

L. J. GIACOLETTO received the B.S. degree in Electrical Engineering from Rose Polytechnic Institute, Terre Haute, Indiana, in 1938, and the M.S. degree in Physics from the State University of Iowa in 1939. From 1939 to 1941, while a Teaching Fellow in the department of Electrical Engineering at the University of Michigan, he engaged in frequency-modulation research. He received the Ph.D. degree in Electrical Engineering from the University of Michigan in 1952. He was associated with the Collins Radio Company during the summers of 1937 and 1938, and with the Bell Telephone Laboratories in 1940. From 1941 to 1945 he served with the Signal Corps and returned to inactive status as a major in the Signal Corps Reserve in May, 1946. Since June, 1946, he has been serving as a research engineer at RCA Laboratories, Princeton, N. J. Dr. Giacoletto is a member of the American Association for the Advancement of Science, Gamma Alpha, Iota Alpha, Phi Kappa Phi, Tau Beta Pi, and Sigma Xi.





JAMES J. GIBSON received the civilingenjörsexamen at the Royal Institute of Technology in Stockholm, Sweden, in 1947. During 1946 he served with the Swedish Airforce, working on UHF antennas and circuits. From 1947 to 1952 he was a research engineer at the Research Institute of National Defence, Stockholm, Sweden, doing research work on antennas, microwave circuits and pulse circuitry. Simultaneously he took graduate studies at the Royal Institute of Technology. From October 1952 to April 1954 he was an Honorary Fellow of the American Scandinavian Foundation as a trainee at RCA Laboratories Division, Princeton, N. J., where he was engaged with research work on UHF antennas and transistor circuits. He is now with the Division of Radio Engineering of the Royal Institute of Technology, Stockholm, Sweden, where he is doing research work on transistor circuits. Mr. Gibson is an Associate Member of the Institute of Radio Engineers.

ERNEST G. LINDER received the B.A. and M.S. degrees from the University of Iowa in 1925 and 1927, and the Ph.D. degree from Cornell University in 1931. He was an instructor at California Institute of Technology 1927-1928, and a Detroit Edison Research Associate at Cornell University 1928-1932. In 1932 he joined the RCA Manufacturing Company, and in 1941 transferred to RCA Laboratories. He has worked in the fields of thermoelectricity, photoelectricity, crystals, electrical discharges in gases, mass spectrography, microwave tubes, microwave propagation, electron physics, radar, and the electron and photovoltaic effects. Dr. Linder is a Fellow of the Institute of Radio Engineers, and a member of the American Physical Society and Sigma Xi.



JOSEPH J. LOFERSKI received the B.S. degree from the University of Scranton in 1948, and M.S. and Ph.D. degrees in Physics from the University of Pennsylvania in 1949 and 1953, respectively. He was a Research Associate at the University of Pennsylvania during 1952-1953. He joined RCA Laboratories Division in July 1952, where he has been engaged in research on semiconductor radiation converters. Dr. Loferski is a member of Sigma Xi, American Physical Society, and the American Association for the Advancement of Science.

EVERETT G. MAY attended Kansas Wesleyan University and Kansas State College. In 1941 he was employed by Bendix Aviation Ltd. in North Hollywood, California. Trojan Powder Company was his employer from late 1941 to 1943 at Sandusky, Ohio, in the Plum Brook Ordnance Works. Returning to Kansas State College, he received the B.S. degree in Electrical Engineering in 1945. In 1945 he joined RCA Laboratories, Princeton, N. J., as a research engineer in the Acoustical Laboratory. He received the M.S. degree in Electrical Engineering from Princeton University in 1947. Mr. May is a member of the Acoustical Society of America, Sigma Tau, Eta Kappa Nu, Pi Mu Epsilon, and Sigma Xi.





A. R. MOORE received the B.S. degree in Chemistry in 1942 from the Polytechnic Institute of Brooklyn. He worked on phototube and thyratron development at RCA Victor in Harrison, N. J. and Lancaster, Pa. from 1942 to 1945. In 1945 he entered Cornell University and received the Ph.D. in Physics in 1949, specializing in physics of solids. During his last two years at Cornell he was an RCA Fellow. He joined RCA Laboratories at Princeton, N. J., in 1949, where he has worked on semiconductor physics.

CHARLES W. MUELLER received the B.S. degree in Electrical Engineering from the University of Notre Dame in 1934, the S.M. degree in Electrical Engineering in 1936 from the Massachusetts Institute of Technology, and the degree of Sc.D. in Physics from M.I.T. in 1942. From 1936 to 1938 he was associated with the Raytheon Production Corporation, first in the engineering supervision of factory production of receiving tubes, and then in the development of gas-tube voltage regulators and cold-cathode thyratrons. From 1938 to 1942 he worked at M.I.T. on the development of gas-filled special-purpose tubes for counting operations. Since 1942 he has been a member of the technical staff of RCA Laboratories Division in Princeton, N. J. where he has been engaged in research on high-frequency receiving tubes, secondary electron emission phenomena, and solid-state devices. Dr. Mueller is a member of the American Physical Society and Sigma Xi and a Senior Member of the Institute of Radio Engineers.



HERBERT NELSON received the B.S. degree from Hamline University in 1927 and the M.S. degree in Physics from the University of Minnesota in 1929. From 1929 to 1930 he was an engineer with the Westinghouse Lamp Company in Bloomfield, New Jersey. He transferred to RCA in 1930 and was engaged in electronic research and development at the Tube Plant in Harrison, N. J. until 1953 when he joined the semiconductor activity at the RCA Laboratories in Princeton. Mr. Nelson is a member of Sigma Xi and of the American Physical Society.

JOHN H. O'CONNELL received the B.S. degree in Electrical Engineering in 1954 from Fournier Institute of Technology, Lemont, Illinois. In the same year he joined RCA Laboratories and spent a year on a training program. Upon completion of his training program he joined the Industry Service Laboratory group in Princeton and he is now working on transistor circuit applications. Mr. O'Connell is an Associate Member of the Institute of Radio Engineers.





JOHN PRESTON received his education in England, attended Manchester Scientific Institute taking courses in Mechanical Engineering. He then joined the engineering staff of the Bolton Power and Electrical Company. He became a member of Radio Corporation of America in 1929 and was associated with the Research Department of RCA Victor from 1930 to 1935; the Research Department of RCA Manufacturing Company from 1935 to 1941, and RCA Laboratories Division from 1941 to date. His work has been in the field of acoustics since joining Radio Corporation of America. Mr. Preston is a member

of the Acoustical Society of America and of Sigma Xi and a Fellow of the Audio Engineering Society.

PAUL RAPPAPORT studied chemistry at Temple University, Philadelphia, Pa. before entering the U. S. Navy as an electronic technician in 1944. As a civilian in 1946 he worked nine months at the Naval Air Experimental Station in Philadelphia in the capacity of Physicist. He received the B.S. and M.S. degrees in solid state physics in 1948 and 1949 at Carnegie Institute of Technology where he was a graduate teaching assistant from 1948 to 1949. He joined RCA Laboratories in 1949, where he has worked in the fields of secondary electron emission, direct conversion of radiation into electricity, and radiation damage in semiconductors. Mr. Rappaport is a member of the American Physical Society, Pi Mu Epsilon, and Sigma Xi.



OAKLEY M. WOODWARD, JR. received the degree of Bachelor of Science in Electrical Engineering from the University of Oklahoma in 1938. He joined the Seismograph Service Corporation of Tulsa, Oklahoma, after graduation. During 1941, he was a research engineer at the RCA Manufacturing Company, Camden, N. J. Since January 1942, he has been with RCA Laboratories Division, Princeton, N. J. Mr. Woodward is a Member of Sigma Xi, and a Senior Member of the Institute of Radio Engineers.